Eur. Phys. J. C (2023) 83:628
https://doi.org/10.1140/epjc/s10052-023-11631-7

THE EUROPEAN PHYSICAL JOURNAL C

Regular Article - Experimental Physics

Measurement of the mass dependence of the transverse momentum of lepton pairs in Drell–Yan production in proton–proton collisions at $\sqrt{s} = 13$ TeV

CMS Collaboration*

CERN, 1211 Geneva 23, Switzerland

Received: 10 May 2022 / Accepted: 29 September 2022 / Published online: 17 July 2023

Abstract The double differential cross sections of the Drell–Yan lepton pair ($\ell^+\ell^-$, dielectron or dimuon) production are measured as functions of the invariant mass $m_{\ell\ell}$, transverse momentum $p_{\mathrm{T}}(\ell\ell)$, and φ^*_η. The φ^*_η observable, derived from angular measurements of the leptons and highly correlated with $p_{\mathrm{T}}(\ell\ell)$, is used to probe the low-$p_{\mathrm{T}}(\ell\ell)$ region in a complementary way. Dilepton masses up to 1 TeV are investigated. Additionally, a measurement is performed requiring at least one jet in the final state. To benefit from partial cancellation of the systematic uncertainty, the ratios of the differential cross sections for various $m_{\ell\ell}$ ranges to those in the Z mass peak interval are presented. The collected data correspond to an integrated luminosity of 36.3 fb^{-1} of proton–proton collisions recorded with the CMS detector at the LHC at a centre-of-mass energy of 13 TeV. Measurements are compared with predictions based on perturbative quantum chromodynamics, including soft-gluon resummation.

1 Introduction

The Drell–Yan (DY) production of charged-lepton pairs in hadronic collisions [1] provides important insights into the partonic structure of hadrons and the evolution of the parton distribution functions (PDFs). At leading order (LO) in perturbative quantum chromodynamics (pQCD), the DY process is described in terms of an s-channel Z/γ^* exchange process convolved with collinear quark and antiquark parton distribution functions of the proton. At LO, the lepton pair transverse momentum $p_{\mathrm{T}}(\ell\ell)$, corresponding to the exchanged boson transverse momentum, is equal to zero. At higher orders, initial-state QCD radiation gives rise to a sizable $p_{\mathrm{T}}(\ell\ell)$. Whereas the spectrum for large $p_{\mathrm{T}}(\ell\ell)$ values is expected to be described through fixed-order calculations in pQCD, at small values ($p_{\mathrm{T}} < \mathcal{O}(m_{\ell\ell})$), where $m_{\ell\ell}$ is the invariant mass of the lepton pair, soft-gluon resummation to all orders is required [2,3]. In addition, the low-$p_{\mathrm{T}}(\ell\ell)$ region also includes the effects of the intrinsic transverse motion of the partons in the colliding hadrons that has to be extracted from data and parameterized. The resummation functions are universal and obey renormalisation group equations, predicting a simple scale dependence in the leading logarithmic approximation, where the scale is given by $m_{\ell\ell}$. Therefore, measuring the $p_{\mathrm{T}}(\ell\ell)$ spectrum in a wide $m_{\ell\ell}$ range tests the validity of the resummation approach and the precision of different predictions. Calculations for inclusive DY production as a function of $m_{\ell\ell}$ and $p_{\mathrm{T}}(\ell\ell)$ are available up to next-to-next-to-leading order (NNLO) in pQCD [4–7]. Soft-gluon resummation can be computed analytically, either in transverse momentum dependent parton distributions (TMD) or in parton showers of Monte Carlo (MC) event generators matched with matrix element calculations [8–15].

The $p_{\mathrm{T}}(\ell\ell)$ resolution is dominated by the uncertainties in the magnitude of the transverse momenta of the leptons, whereas the measurement precision of the lepton angle does not contribute significantly. The kinematic quantity φ^*_η [16–18], derived from these lepton angles, is defined by the equation:

$$\varphi^*_\eta \equiv \tan\left(\frac{\pi - \Delta\varphi}{2}\right) \sin(\theta^*_\eta). \tag{1}$$

The variable $\Delta\varphi$ is the opening angle between the leptons in the plane transverse to the beam axis. The variable θ^*_η is the scattering angle of the dileptons with respect to the beam in the longitudinally boosted frame where the leptons are back to back. It is related to the pseudorapidities of the oppositely charged leptons by the relation $\cos(\theta^*_\eta) = \tanh\left[(\eta^- - \eta^+)/2\right]$. The variable φ^*_η, by construction greater than zero, is closely related to the normalized transverse momentum $p_{\mathrm{T}}(\ell\ell)/m_{\ell\ell}$ [16]. Since φ^*_η depends only on angular variables, its resolution is significantly better than that of the transverse momentum, especially at low-$p_{\mathrm{T}}(\ell\ell)$ values, but its interpretation in terms of initial-state radiation (ISR) is not as direct as that of $p_{\mathrm{T}}(\ell\ell)$.

* e-mail: cms-publication-committee-chair@cern.ch (corresponding author)

The DY process in the presence of one jet is a complementary way to investigate the initial-state QCD radiations. The requirement of a minimal transverse momentum associated with this jet is reflected in the $p_{\mathrm{T}}(\ell\ell)$ distribution by momentum conservation. When more hadronic activity than a single jet is present in the events, the transverse momentum balance between the leading jet and the lepton pair has a broad distribution. As a consequence, the full $p_{\mathrm{T}}(\ell\ell)$ spectrum in the presence of jets brings additional information, since at small values it is sensitive to numerous hard QCD radiations. Furthermore, DY production in association with at least one jet also brings up contributions where virtual partons acquire transverse momentum, whose collinear radiations will have a significant angle with respect to the beam, which contributes as a component of the final $p_{\mathrm{T}}(\ell\ell)$.

This paper presents a DY differential cross section measurement in bins of $m_{\ell\ell}$, over the range of 50 GeV to 1 TeV, as functions of $p_{\mathrm{T}}(\ell\ell)$ and φ^*_η for inclusive DY production, and in events with at least one jet as a function of $p_{\mathrm{T}}(\ell\ell)$. The data were collected in 2016 with the CMS detector at the CERN LHC, corresponding to an integrated luminosity of 36.3 fb^{-1} of proton–proton (pp) collisions at a centre-of-mass energy of $\sqrt{s} = 13$ TeV. To reduce the uncertainties, the measured cross sections combine measurements of separately extracted cross sections for the electron and the muon channels. The measurements presented in this paper are extensively discussed in Ref. [19].

Complementary measurements of the DY process have been performed recently by the CMS, ATLAS, and LHCb Collaborations at the CERN LHC [20–38] and by the CDF and D0 Collaborations at the Fermilab Tevatron [39–45]. The cross section measurements presented in this paper extend the mass range below and above the Z boson resonance with respect to the previous CMS measurements of $p_{\mathrm{T}}(\ell\ell)$ dependence.

The outline of this paper is the following: in Sect. 2 a brief description of the CMS detector is given. In Sect. 3 the selection criteria of the measurement are described. The simulation samples used in the measurement are described in Sect. 4. Section 5 explains the details of the unfolding procedure and the systematic uncertainties are given in Sect. 6. Theory predictions used for comparison with the measurements are described in Sect. 7. The results are presented in Sect. 8 and a summary of the paper is given in Sect. 9.

2 The CMS detector

The central feature of the CMS apparatus is a superconducting solenoid of 6 m internal diameter, providing a magnetic field of 3.8 T. Within the solenoid volume are a silicon pixel and strip tracker, a lead tungstate crystal electromagnetic calorimeter (ECAL), and a brass and scintillator hadron calorimeter (HCAL), each composed of a barrel and two endcap sections. Forward calorimeters extend the η coverage provided by the barrel and endcap detectors. Muons are detected in gas-ionization chambers made of detection planes using three technologies: drift tubes, cathode strip chambers, and resistive plate chambers, embedded in the steel flux-return yoke outside the solenoid.

The global event reconstruction (also called particle-flow event reconstruction [46]) reconstructs and identifies each individual particle in an event, with an optimized combination of all subdetector information. In this process, the identification of the particle type (photon, electron, muon, charged or neutral hadron) plays an important role in the determination of the particle direction and energy.

Electrons are identified as a primary charged particle track and potentially many ECAL energy clusters corresponding to this track extrapolation to the ECAL and to possible bremsstrahlung photons emitted along the way. The electron momenta are estimated by combining energy measurements in the ECAL with momentum measurements in the tracker [47]. The momentum resolution for electrons with $p_{\mathrm{T}} \approx 45$ GeV from $\mathrm{Z} \to \mathrm{ee}$ decays ranges from 1.7 to 4.5%. It is better in the barrel region than in the endcaps, and also depends on the bremsstrahlung energy emitted by the electron as it traverses the material in front of the ECAL.

Muons are identified as tracks in the central tracker consistent with either a track or several hits in the muon system, and associated with calorimeter deposits compatible with the muon hypothesis. The reconstructed muon global track, for muons with $20 < p_{\mathrm{T}} < 100$ GeV, has a relative transverse momentum resolution of 1.3–2.0% in the barrel and better than 6% in the endcaps. The p_{T} resolution in the barrel is better than 10% for muons with p_{T} up to 1 TeV [48]. The resolution is further improved with corrections derived from the Z mass distribution [49].

Charged hadrons are identified as charged particle tracks not identified as electrons or as muons. Finally, neutral hadrons are identified as HCAL energy clusters not linked to any charged-hadron trajectory, or as a combined ECAL and HCAL energy excess with respect to the expected charged-hadron energy deposit. For each event, hadronic jets are clustered from these reconstructed particles using the infrared- and collinear-safe anti-k_{T} algorithm [50,51] with a distance parameter of 0.4. Jet momentum is determined as the vectorial sum of all particle momenta in the jet, typically within 5–10% of the true momentum over the entire p_{T} spectrum and detector acceptance.

The primary vertex (PV) is taken to be the vertex corresponding to the hardest scattering in the event, evaluated using tracking information alone, as described in Section 9.4.1 of Ref. [52].

Events of interest are selected using a two-tiered trigger system. The first level (L1), composed of custom hardware

processors, uses information from the calorimeters and muon detectors to select events at a rate of around 100 kHz within a fixed latency of about 4 μs [53]. The second level, known as the high-level trigger, consists of a farm of processors running a version of the full event reconstruction software optimized for fast processing, and reduces the event rate to around 1 kHz before data storage [54].

A more detailed description of the CMS detector is reported in Ref. [55], together with a definition of the coordinate system used and the relevant kinematic variables.

3 Event selection

The initial event selection requires a dielectron trigger with a p_{T} threshold of 23 and 12 GeV on the two leading electrons in the electron channel. In the muon channel we require a dimuon trigger with p_{T} thresholds of 18 and 7 GeV or a single-muon trigger with a p_{T} threshold of 24 GeV. The final selection is restricted to the region where the triggers are fully efficient: $p_{\mathrm{T}} > 25$ GeV for the leading lepton, $p_{\mathrm{T}} > 20$ GeV for the subleading lepton and $|\eta| < 2.4$ for both channels.

An event must contain exactly two isolated leptons of the same flavour (with the isolation criteria as detailed in Ref. [26]). In addition the two leptons must have opposite charges. Events with a third lepton with p_{T} greater than 10 GeV and $|\eta| < 2.4$ are vetoed.

Due to the high instantaneous luminosity of the LHC, additional proton–proton interactions occur during the same bunch crossing (pileup) that contribute additional overlapping tracks and energy deposits in the event, and result in an apparent increase of jet momenta. To mitigate this effect, tracks identified as originating from pileup vertices are discarded and an offset correction is applied to correct for the remaining neutral pileup contributions [56]. The two identified leptons can be reconstructed as jets. Those jets are disregarded by requiring a separation, $\Delta R = \sqrt{(\Delta\eta)^2 + (\Delta\phi)^2}$, between the reconstructed jets and these lepton candidates to be larger than 0.4.

To suppress the contamination of jets coming from pileup, a multivariate discriminant is used. The pileup contamination is also reduced by the choice of the final selection: jets are required to have a minimum transverse momentum of 30 GeV and, to ensure high-quality track information, they are limited to a rapidity range of $|y| < 2.4$.

To reduce the $\mathrm{t\bar{t}}$ background, events containing one or more b tagged jets are vetoed. The medium discrimination working point of the combined secondary vertex b tagging algorithm [57] is used. The effect on the signal is small and is corrected for in the unfolding procedure.

The effects of finite detector resolution and selection efficiency are corrected by using the unfolding procedure described in Sect. 5. Scale factors are applied to the simulation used for the unfolding, to correct for differences with respect to the data in the efficiencies of the different selections: trigger, lepton identification, lepton isolation, and b-tagged jet veto. For the trigger, the factor is given as a function of $|\eta|$ of the two leptons and is applied once per lepton pair. The value of the scale factor is close to one. When dealing with the identification and isolation efficiencies, the scale factor is given per lepton as a function of its p_{T} and $|\eta|$, and applied to each of the two selected leptons [26].

4 Simulated samples and backgrounds

For the simulation of the Z/γ^* process (including the $\tau^+\tau^-$ background), a sample is generated with MadGraph5_*a*mc@nlo[58] version 5.2.2.2 (shortened to mg5_amc) using the FxFx jet merging scheme [59]. The parton shower, hadronization, and QED final-state radiation (FSR) are calculated with pythia 8.212 [60] using the CUETP8M1 tune [61]. The matrix element calculations include $\mathrm{Z}/\gamma^* + 0, 1, 2$ jets at next-to-leading order (NLO), giving an LO accuracy for $\mathrm{Z}/\gamma^* + 3$ jets. The NLO NNPDF 3.0 [62] is used for the matrix element calculation. In control plots and when comparing to the measurement, this prediction is normalized to the cross section obtained directly from the generator, 1977 pb per lepton channel (for $m_{\ell\ell} > 50$ GeV).

Other processes that can give a final state with two oppositely charged same-flavour leptons are WW, WZ, ZZ, $\gamma\gamma$, $\mathrm{t\bar{t}}$ pairs, and single top quark production. The $\mathrm{t\bar{t}}$ and single top backgrounds are generated at NLO using the powheg version 2 [63–66] interfaced to pythia 8. Background samples corresponding to diboson electroweak production (denoted VV in the figure legends) [67] are generated at NLO with powheg interfaced to pythia 8 (WW) or at LO with pythia 8 alone (WZ and ZZ). These samples are generated using NLO NNPDF 3.0 for the matrix element calculation. The $\gamma\gamma$ background process leading to two charged leptons in the final state, $\gamma\gamma \to \ell^+\ell^-$, is simulated using lpair [68,69] interfaced with pythia 6 and using the default γ-PDF of Suri–Yennie [70]. This contribution is split into three components, since the interaction at each proton vertex process can be elastic or inelastic.

The total cross sections of WZ and ZZ diboson samples are normalized to the NLO prediction calculated with mcfm v6.6 [71], whereas the cross sections of the WW samples are normalized to the NNLO prediction [72]. The total cross section of the $\mathrm{t\bar{t}}$ production is normalized to the prediction with NNLO accuracy in QCD and next-to-next-to-leading logarithmic (NNLL) accuracy in soft gluon resummation calculated with Top++ 2.0 [73]. The single top and $\gamma\gamma$ background

distributions are normalized to the cross sections calculated by their respective event generators.

It is possible for hadrons to mimic the signature of an electron in the detector. The main processes that contribute to this background are W + jet production, when the W decays leptonically, and QCD multijet events. Such backgrounds are nonnegligible only in the electron channel.

The contamination of the signal region by events containing hadrons misidentified as electrons is estimated using a control region where two electrons of the same sign are required. This control region mainly contains events with hadrons misidentified as electrons and events originating from the DY process when the charge of one electron is incorrectly attributed. The probability of charge misidentification is obtained as a function of p_{T} and η of each electron in the Z peak region ($81 < m_{\ell\ell} < 101$ GeV), where the hadron contamination is negligible even in the control region. These probabilities are then used to estimate the charge misidentification rate for other values of $m_{\ell\ell}$. The difference between the observed number of events in the control region and the estimated charge misidentification rate is assumed to be the contamination from hadron background. We observe that the numbers of misidentified-lepton events in the same-sign electron sample and in the signal (opposite-sign electron) sample are compatible.

The number of events at the reconstructed level is compared with the sum of the contributions from signal and backgrounds. In Fig. 1, the dilepton mass spectrum is shown for both the electron and and the muon channels, whereas Fig. 2 shows the $p_{\mathrm{T}}(\ell\ell)$ distributions in various $m_{\ell\ell}$ bins for the electron channel only. Globally, the background contamination is lower than 1%. The background becomes around 10% for $m_{\ell\ell}$ outside of the Z boson mass peak and up to 30% in some bins. The simulated samples are processed through a GEANT4 [74] based simulation of the CMS detector, with the same reconstruction algorithms as of data. They also include a pileup profile that is reweighed to match the profile of the data.

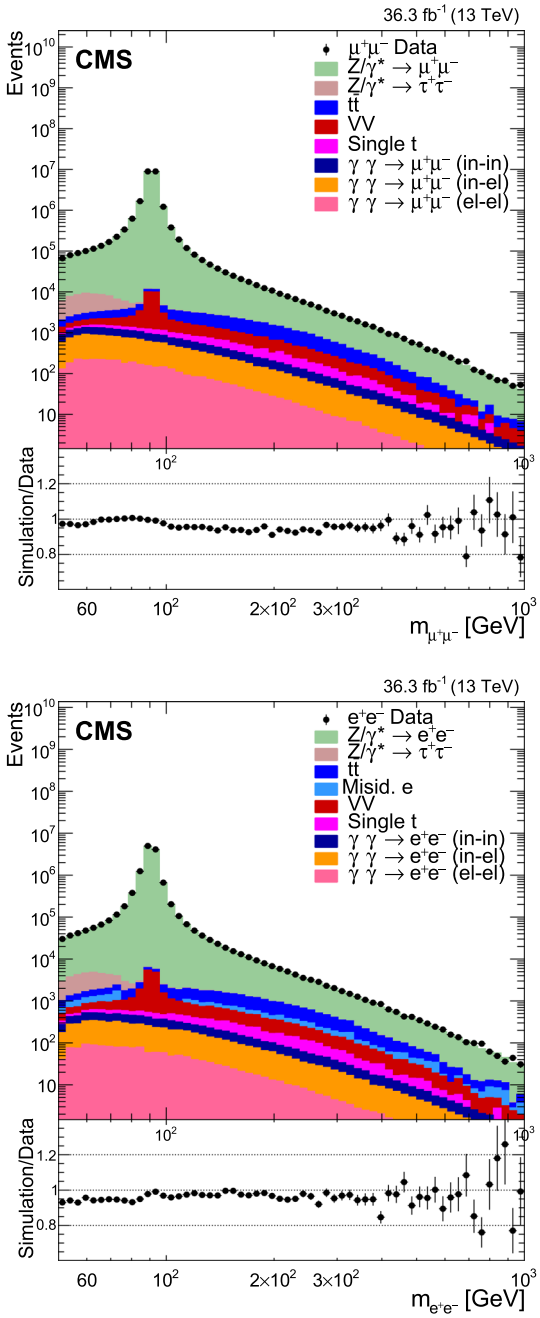

Fig. 1 Distributions of events passing the selection requirements in the muon (left) and electron channels (right). Each plot also presents in the lower part a ratio of simulation over data. Only statistical uncertainties are shown as error bars on the data points, whereas the ratio presents the statistical uncertainty in the simulation and the data. The plots show the number of events without normalization to the bin width. The different background contributions are discussed in the text

5 Measured observables and unfolding procedure

The measurement of the DY cross section is carried out with respect to the p_{T} and φ_{η}^{*} of the dilepton pairs produced inclusively, and with respect to p_{T} for pairs produced in association with at least one jet. For the inclusive case, the measurement is divided into five invariant mass bins: 50–76, 76–106, 106–170, 170–350, 350–1000 GeV; the last bin is not included when requiring at least one jet because of the small number of events available. The measurement of the ratio of cross section in mass bins 50–76, 106–170, 170–350, 350–1000 GeV to the cross section around the Z mass peak(76–106 GeV) is also performed. The bin widths are chosen to be as small as possible, based on the detector resolution and the number of events.

To correct for the detector resolution and the efficiency of the selection, an unfolding procedure is applied to the measured distributions one dimensionally in each mass bin. To

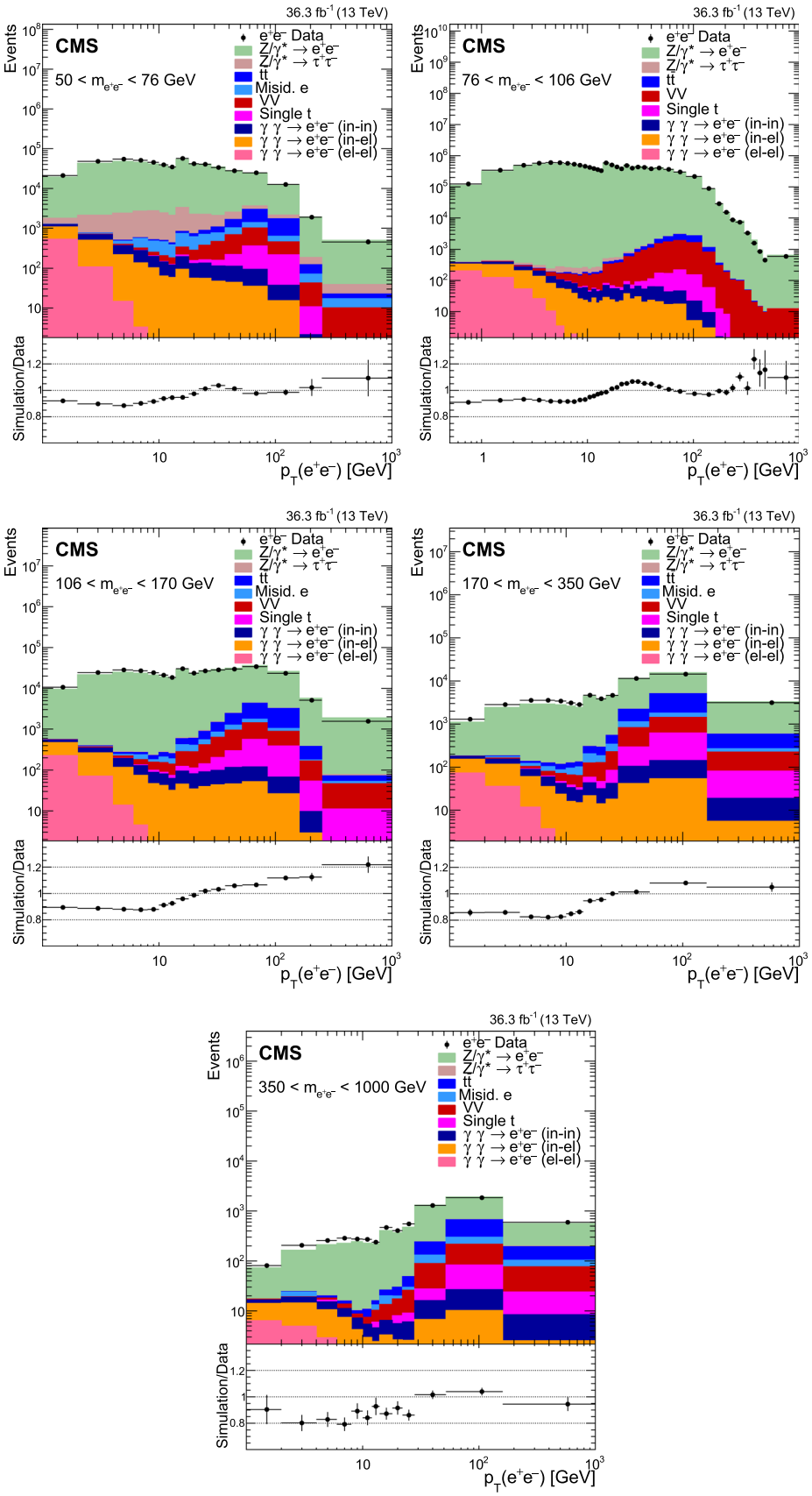

Fig. 2 Distributions of events passing the selection requirements in the electron channel as a function of the dilepton p_{T} in five ranges of invariant mass: 50–76 GeV (upper left), 76–106 GeV (upper right), 106–170 GeV (middle left), 170–350 GeV (middle right), and 350–1000 GeV (lower). More details are given in Fig. 1

obtain the particle-level distributions from the reconstructed distributions, the unfolding uses a response matrix based on the simulated signal sample. To unfold, the D'Agostini iterative method with early stopping is used as implemented in RooUnfold [75]. The result, converging towards the maximum likelihood estimate, is affected by fluctuations increasing with the number of iterations. The fluctuations are studied using pseudo-experiments for each number of iterations following the method used in Ref. [76]. The procedure is stopped just before the fluctuations become significant with respect to the statistical uncertainty. The number of iterations ranges between 4 and 25.

The particle level refers to stable particles ($c\tau > 1$ cm), other than neutrinos, in the final state. To correct for energy losses due to QED FSR, leptons are "dressed", i.e., all the prompt photons with a distance smaller than $\Delta R = 0.1$ to the lepton axis are added to the lepton momentum. The cross section is extracted in the following phase space: leading and subleading dressed leptons satisfying $p_{\mathrm{T}} > 25$ and 20 GeV and $|\eta| < 2.4$. When at least one additional jet is required, it must satisfy $p_{\mathrm{T}} > 30$ GeV, $|y| < 2.4$, and be spatially separated from the dressed leptons by $\Delta R > 0.4$.

The cross sections are first extracted separately for the electron and muon channels. They are compatible for all studied distributions and the two channels are combined to reduce the statistical uncertainties. The combined differential cross sections are calculated bin-by-bin as the weighted mean values of the differential cross sections of the two channels. The systematic and statistical uncertainties are obtained using the linear combination method described in Ref. [77], considering as fully correlated the uncertainties in the jet energy scale and resolution, the pileup, the background subtraction, b tagging, and the integrated luminosity. Other uncertainties are considered as uncorrelated.

6 Systematic uncertainties

Several sources of uncertainties in the measurement are considered. The integrated luminosity is measured with a precision of 1.2% [78], which results in a relative uncertainty of almost the same value in the measurement. Small variations are caused by the subtraction of the background contributions estimated from the simulation.

The uncertainties coming from the lepton trigger efficiencies are estimated by varying the applied scale factors up and down by one standard deviation. The uncertainties from identification and reconstruction efficiencies are estimated for various sources including QED FSR, resolution, background modeling, and the tag object selection in the tag-and-probe procedure, as well as the statistical component treated separately for each scale factor in p_{T} and η of the lepton [26]. The efficiency uncertainties include a one percent effect in the L1 trigger caused by a timing problem in ECAL endcaps. The lepton energy scale uncertainties are estimated by varying the lepton energy and p_{T} by ± 1 standard deviation (reach 0.75% (0.5%) for electrons (muons) depending on η and p_{T}). Uncertainties coming from the lepton energy resolution are estimated by spreading the lepton energy using the generator-level information.

The uncertainty in the jet energy scale is estimated by varying the jet momenta in data by 2.5–5%, depending on the energy and pseudorapidity of the jet. The uncertainty in the jet energy resolution is estimated by varying the smearing factor used to match the simulated jet energy resolution to data by ± 1 standard deviation around its central value.

A systematic uncertainty is attributed to the normalisation of the background samples estimated by Monte Carlo event generators. The theoretical uncertainty in the cross section of the dominant $\mathrm{t\bar{t}}$ background is ≈6%, using the Top++ 2.0 program and including scale and PDF variations. The uncertainties in the other background cross sections are smaller. In particular, it has been verified that 6% covers the differences of the $\gamma\gamma \to \ell^+\ell^-$ samples generated using Suri–Yennie and LuxQED [79,80] photon PDFs. In a conservative way, the uncertainties in all other Monte Carlo based background estimates are also estimated to be 6%. This uncertainty is applied to fully-elastic, semi- and fully-inelastic cases.

The uncertainty in the misidentified electron background estimation using same-sign events is obtained using an uncertainty in the charge misidentification estimation of about 10% per electron at $p_{\mathrm{T}}(\mathrm{e}) = 150$ GeV, rising with $p_{\mathrm{T}}(\mathrm{e})$. A 20% total uncertainty in the charge misidentification is used and propagated to the estimate of this background.

Alternative pileup profiles are generated by varying the amount of pileup events by 5%, and the difference to the nominal sample is propagated to the final results.

The unfolding model uncertainty is estimated by reweighting the simulated sample to match the data shape for each distribution, and using this as an alternate model for unfolding. The difference with respect to the results obtained with the simulated sample is assigned as the uncertainty. The statistical uncertainty coming from the limited sample size is also included, provided by the RooUnfold package.

The systematic uncertainties are propagated to the measurement through the unfolding procedure by computing new response matrices varying the quantities by one standard deviation up and down. All the experimental uncertainties are symmetrized by taking the average of the deviations from the central value. The uncertainty sources are independent and the resulting uncertainties are added in quadrature.

For the inclusive measurement the main sources of uncertainties are the integrated luminosity measurement, the identification and trigger efficiency corrections of the leptons, and the energy scale of the leptons. For the DY + ≥1 jet case, the major uncertainties come from the jet energy scale and

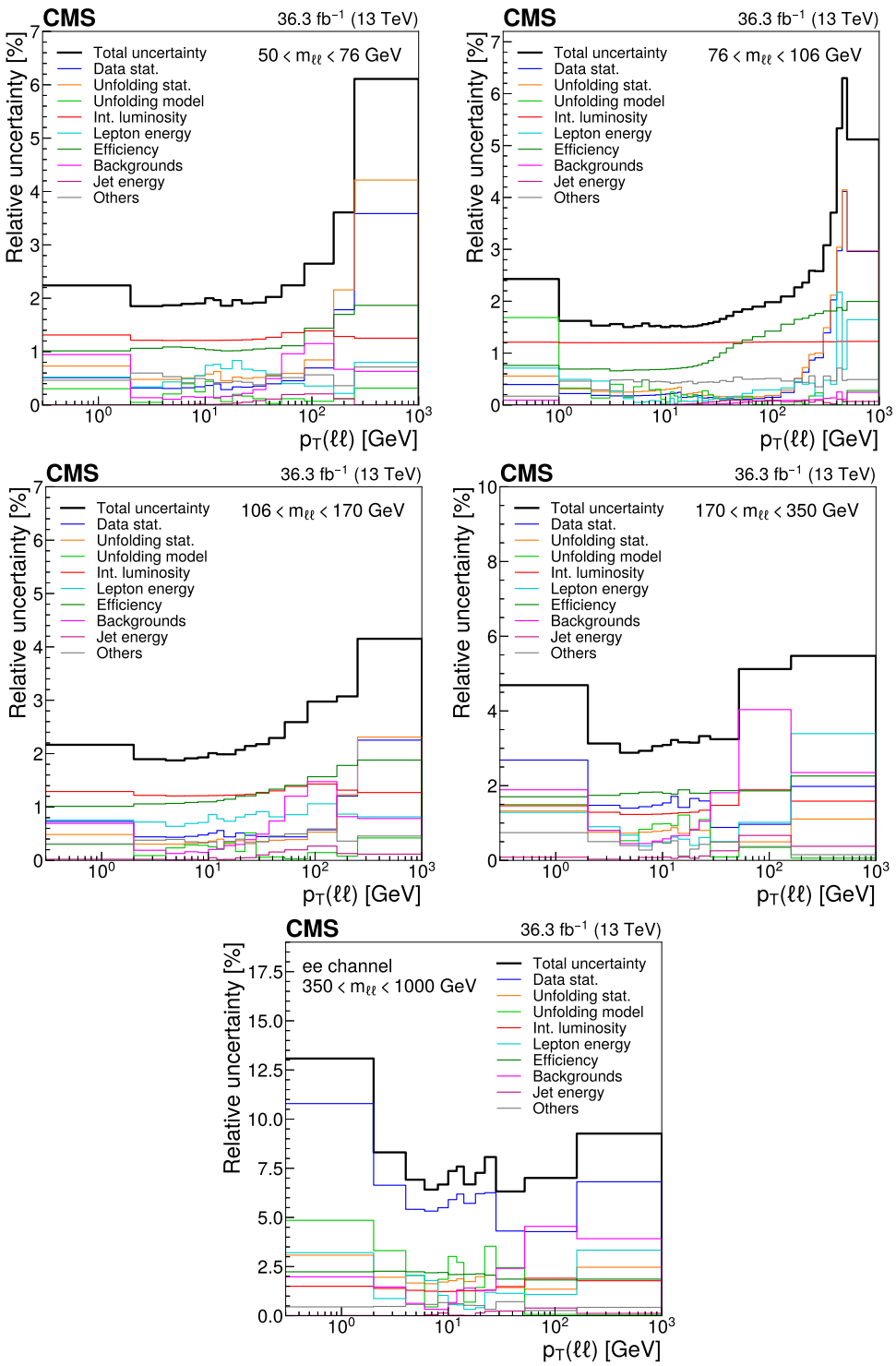

Fig. 3 Estimates of the uncertainties in inclusive differential cross sections in $p_{\mathrm{T}}(\ell\ell)$ in various invariant mass ranges: $50 < m_{\ell\ell} < 76$ GeV (upper left), $76 < m_{\ell\ell} < 106$ GeV (upper right), $106 < m_{\ell\ell} < 170$ GeV (middle left), $170 < m_{\ell\ell} < 350$ GeV (middle right), and $350 < m_{\ell\ell} < 1000$ GeV (lower). The black line is the quadratic sum of the colored lines

the unfolding model. The estimates of systematic uncertainties for the inclusive differential cross sections in $p_{\mathrm{T}}(\ell\ell)$ for various $m_{\ell\ell}$ ranges are shown in Fig. 3.

When calculating the cross section ratios, for each $p_{\mathrm{T}}(\ell\ell)$ or φ^*_η bin, all uncertainties are taken as fully correlated between the numerator and the denominator, except the data and Monte Carlo statistical uncertainties. The total uncertainty corresponds to the quadratic sum of the sources. The estimates of systematic uncertainties for the ratios of the inclusive $p_{\mathrm{T}}(\ell\ell)$ distributions are shown in Fig. 4.

7 Theory predictions

The measured data are compared with the MG5_aMC + PYTHIA 8 baseline sample described in Sect. 4. The QCD

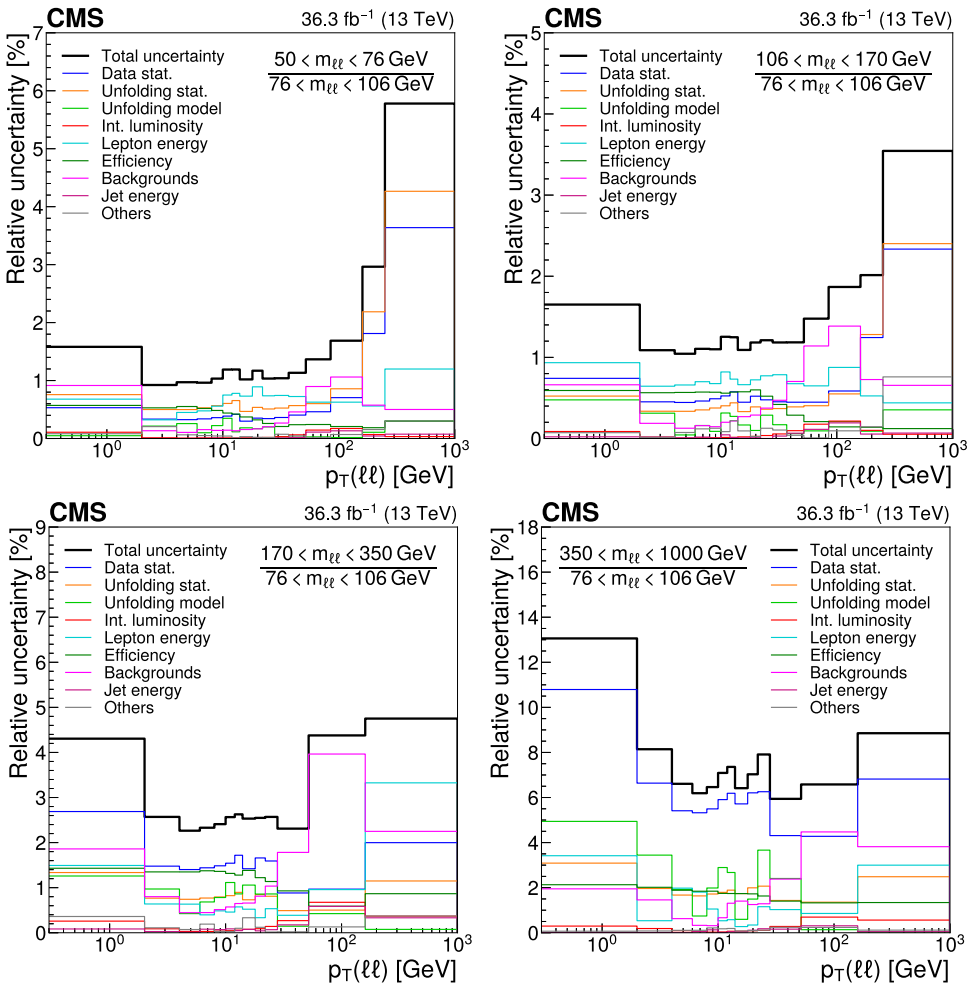

Fig. 4 Estimates of the uncertainties in inclusive differential cross section ratios in $p_T(\ell\ell)$ for invariant mass ranges with respect to the peak region $76 < m_{\ell\ell} < 106$ GeV: $50 < m_{\ell\ell} < 76$ GeV (upper left), $106 < m_{\ell\ell} < 170$ GeV (upper right), $170 < m_{\ell\ell} < 350$ GeV (lower left), and $350 < m_{\ell\ell} < 1000$ GeV (lower right). The black line is the quadratic sum of the colored lines

scale uncertainties are estimated by varying the renormalisation and factorisation scales simultaneously by factors of 2 and 1/2 (omitting the variations in opposite direction and taking the envelope). The strong coupling (α_S) and PDF uncertainties are estimated as the standard deviation of weights from the replicas provided in the NNPDF 3.0 PDF set [62].

An event sample at NNLO with a jet merging method is generated with MiNNLO$_{PS}$ [81,82]. The coupling α_S is evaluated independently at each vertex at a scale that depends on the kinematic configuration. Sudakov form factors are used to interpolate between the scales. The NNLO version of the NNPDF 3.1 PDF set [83] is used along with the PYTHIA version 8 [60] for the parton showers based on the CP5 tune [84] and multiparton interactions (MPI), but including a harder primordial k_T of 2.2 GeV obtained from tuning the k_T parameter to describe the observed φ^*_η distribution of Ref. [26].

The results are also compared with a third prediction from the parton branching (PB) TMD method [14,15] obtained from CASCADE 3 [85]. This prediction is of particular interest since the initial-state parton showers are fully determined by TMD and their backward PB evolution, and therefore are free of tuning parameters. The matrix element calculation is performed at NLO for Z + 0 jet using MG5_aMC for the inclusive distributions (labelled MG5_aMC (0 jet at NLO)+ PB (CASCADE)), and for Z + 1 jet for the distributions where one jet is required in the final state (labelled MG5_aMC (1 jet at NLO)+ PB (CASCADE)). Initial-state parton showers, provided by the PB TMD method are matched to the NLO matrix element [86], using the latest TMD PB set: PB-NLO-HERAI+II-2018-set2 [87]. The final parton shower, hadronization, and QED FSR steps are performed with PYTHIA 6 [88]. This approach is equivalent to the inclusion of the next-to-leading logarithmic soft-gluon resummation on top of the fixed-order NLO calculations. The theoretical uncertainties in the cross section are estimated by variation of scales and from TMD uncertainties. This approach is expected to describe the inclusive cross section at low $p_T(\ell\ell)$ (< 20 GeV) well, and to fail for larger $p_T(\ell\ell)$, since higher-order matrix element contributions are missing, as already observed for the Z boson mass peak range [26]. Recently, this approach has been developed to include multi-jet merging [89] at LO, which allows a larger $p_T(\ell\ell)$ region to be described as well.

A fourth prediction is based on an independent approach relying on TMDs obtained from fits to DY and Z boson measurements at different energies [90,91] using an NNLO evolution. The corresponding numerical evaluations are provided by the ARTEMIDE 2.02 code [92]. The resummation corresponds to an N^{3}LL approximation. The uncertainty is obtained from scale variations. Due to the approximation of ordering among the scales, the prediction has a limited range of validity for the calculation of: $p_{\mathrm{T}}(\ell\ell) < 0.2\, m_{\ell\ell}$. Predictions for the φ^*_η cross section dependence as well as the 1 jet case are not provided by ARTEMIDE. The ARTEMIDE sample does not include the QED FSR; a correction is derived from the PYTHIA 8 shower in the MG5_aMC sample. The uncertainty is derived by taking the difference with respect to corrections derived from the POWHEG sample described in Ref. [26]. This uncertainty is smaller than 1% for $p_{\mathrm{T}}(\ell\ell) < 0.2\, m_{\ell\ell}$

Two more predictions are obtained from the GENEVA 1.0-RC3 program [93–95] combining higher-order resummation with a DY calculation at NNLO. Originally, the resummation was carried out at NNLL including partially N^{3}LL on the 0-jettiness variable τ_0 [96]. More recently it includes the q_{T} resummation at N^{3}LL in the Radish formalism [97,98] for the 0 jet case, whereas it keeps the 1-jettiness resummation for the 1 jet case. Two samples are generated, one in the 0-jettiness approach and one in the q_{T} resummation approach. The calculation uses the PDF4LHC15 NNLO [99] PDF set with $\alpha_{\mathrm{S}}(m_{\mathrm{Z}}) = 0.118$, the world average. The events are showered using a specially modified version of PYTHIA 8, which is also used for nonperturbative effects and QED radiation in the initial and final states using a modified tune based on CUETP8M1. The theoretical uncertainties are estimated by variation of scales and from the resummation as described in Ref. [94]. No uncertainty is assigned to the jetiness resummation.

8 Results and discussion

8.1 $p_{\mathrm{T}}(\ell\ell)$ results

The differential cross sections in $p_{\mathrm{T}}(\ell\ell)$ are shown in Fig. 5 for invariant mass ranges between 50 GeV and 1 TeV. Because of the lack of precision of the muon transverse momentum measurement at high p_{T}, the cross section measurement in the highest mass range is based on the electron channel only. The ratio of the predictions to the data are presented in Figs. 6, 7 and 8. The comparison with different predictions is discussed later in the text. The ratios of the unfolded distributions for invariant masses outside the Z boson peak to the distribution within the Z boson peak ($76 < m_{\ell\ell} < 106$ GeV) are shown in Fig. 9, and the comparisons to predictions in Figs. 10, 11 and 12.

The measured cross sections are presented in Fig. 13 as a function of $p_{\mathrm{T}}(\ell\ell)$ for at least one jet, for the same mass ranges except the highest. Ratios of the predictions to the data are presented in Figs. 14 and 15. The ratio of these differential cross sections for various mass ranges with respect to the same distribution in the Z boson peak region are shown in Fig. 16, and the comparisons to predictions in Figs. 17 and 18.

The measurements show that the differential cross sections in $p_{\mathrm{T}}(\ell\ell)$ are rising from small $p_{\mathrm{T}}(\ell\ell)$ values up to a maximum between 4 and 6 GeV and then falling towards large $p_{\mathrm{T}}(\ell\ell)$ (Fig. 5). For these cross sections, the variation of the dilepton invariant mass does not have a visible effect on the peak position (around 5 GeV) or on the rising shape for the values below the peak. However, the increase of $m_{\ell\ell}$ results in a broader distribution for $p_{\mathrm{T}}(\ell\ell)$ values above the peak. These effects are highlighted by the cross section ratios presented in Fig. 9. It has to be noted that the rising ratio for the lowest $m_{\ell\ell}$ range (Fig. 9 top left) up to a $p_{\mathrm{T}}(\ell\ell)$ value of 20 GeV is due to QED radiative effects on the final-state leptons (photon radiations at $\Delta R(\ell, \gamma) > 0.1$) inducing migrations from the Z mass peak towards lower masses. When a jet with a large transverse momentum is required (Fig. 13), the peak is shifted towards larger $p_{\mathrm{T}}(\ell\ell)$ values corresponding to the jet selection threshold, here 30 GeV regardless of the $m_{\ell\ell}$. As in the inclusive case, the distributions become broader for $p_{\mathrm{T}}(\ell\ell)$ values larger than the peak for increasing $m_{\ell\ell}$.

A description of these measurements based on QCD requires both multi-gluon resummation and a fixed-order matrix element. The description of the distributions at small $p_{\mathrm{T}}(\ell\ell)$ values requires an approach taking into account initial-state nonperturbative and perturbative multi-gluon resummation. The falling behaviour at large $p_{\mathrm{T}}(\ell\ell)$ is sensitive to hard QCD radiation, which is expected to be well described by matrix element calculations including at least NLO corrections. The size of the QCD radiation is driven by the available kinematic phase space and the value of α_{S}. An increase of $m_{\ell\ell}$ extends the phase space for hard radiations, slightly compensated by the decrease of α_{S} with increasing $m_{\ell\ell}$. The tail at large $p_{\mathrm{T}}(\ell\ell)$ is dominated by jet multiplicities above one. For the inclusive cross sections, the resummation effects are concentrated at small $p_{\mathrm{T}}(\ell\ell)$. The value of the maximum of the distributions is expected to depend weakly on $m_{\ell\ell}$. In the presence of a hard jet, multiple gluon emissions also affect the perturbative region located in η between the jet and the vector boson. The corresponding cross section measurements therefore provide additional constraints on the resummation treatment in the predictions.

The MG5_aMC + PYTHIA 8 prediction describes the data well globally (Fig. 6), although it predicts a too-small cross section for $p_{\mathrm{T}}(\ell\ell)$ values below 30 GeV in the inclusive case. This disagreement is more pronounced at higher $m_{\ell\ell}$ and reaches about 20% for masses above 170 GeV. The

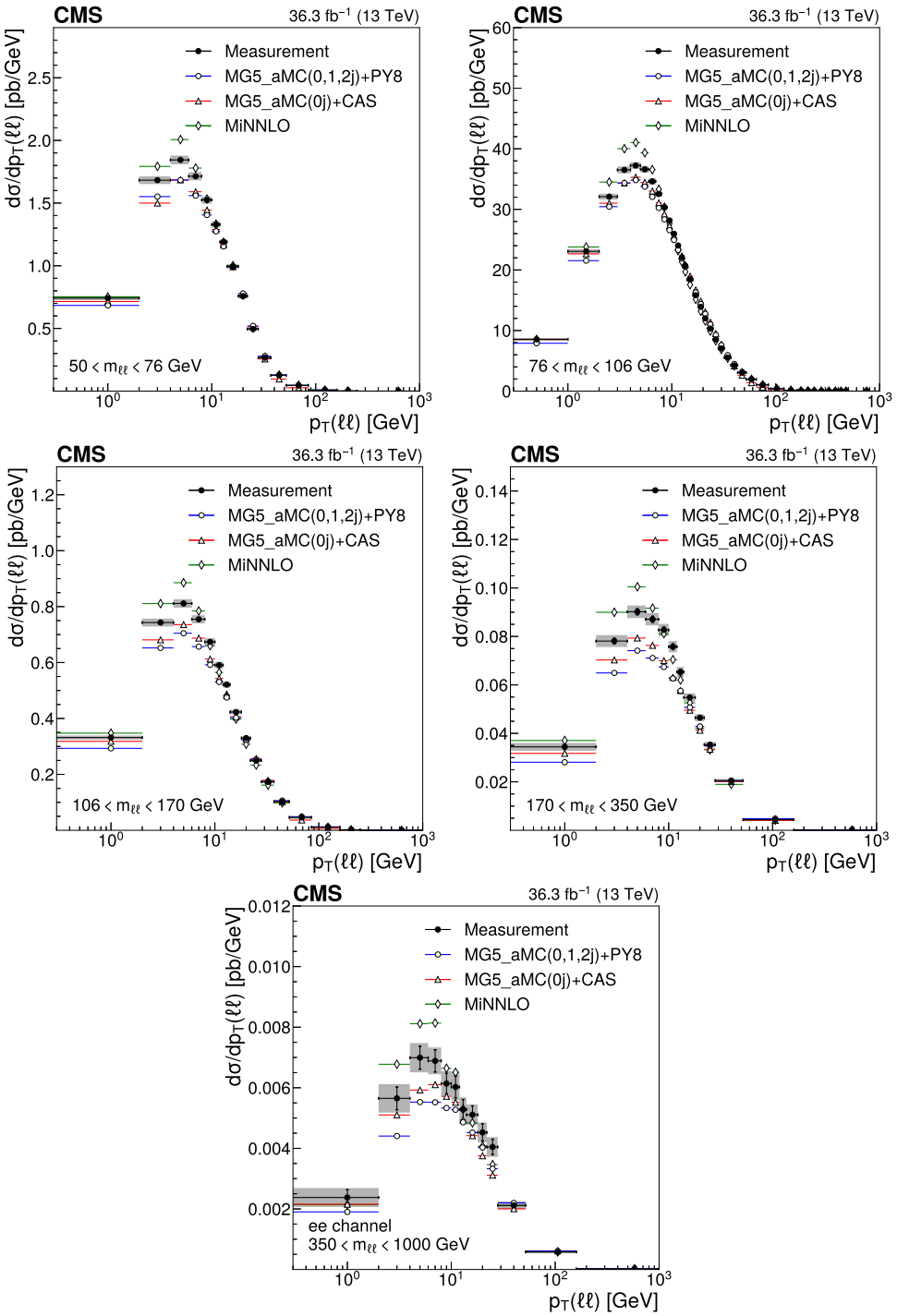

Fig. 5 Differential cross sections in $p_T(\ell\ell)$ in various invariant mass ranges: $50 < m_{\ell\ell} < 76$ GeV (upper left), $76 < m_{\ell\ell} < 106$ GeV (upper right), $106 < m_{\ell\ell} < 170$ GeV (middle left), $170 < m_{\ell\ell} < 350$ GeV (middle right), and $350 < m_{\ell\ell} < 1000$ GeV (lower). The error bars on data points (black dots) correspond to the statistical uncertainty of the measurement and the shaded bands around the data points correspond to the total experimental uncertainty. The measurement is compared with MG5_aMC (0, 1, and 2 jets at NLO) + PYTHIA 8 (blue dots), MiNNLO$_{PS}$ (green diamonds) and MG5_aMC (0 jet at NLO)+ PB (CASCADE) (red triangles)

low-$p_T(\ell\ell)$ region is sensitive to gluon resummation. In MG5_aMC, the resummation effects are simulated by the parton shower, modelled in PYTHIA 8 depending on parameters tuned on previously published measurements, including DY cross sections in the Z boson mass peak region. It has to be noted that the low $p_T(\ell\ell)$ spectrum is sensitive to the choice of the tuned parameters [84] and that no related systematic uncertainty is available. The large $p_T(\ell\ell)$ distributions are well described by MG5_aMC, which relies on NLO matrix elements for 0, 1 and 2 partons in the final state. Nevertheless, MG5_aMC predicts cross sections larger than those observed for the highest $p_T(\ell\ell)$ values measured in the mass ranges $106 < m_{\ell\ell} < 170$ GeV for both the inclusive and 1 jet cases. Since the theoretical uncertainty is dominant in that region, a better agreement might be found using higher-order (e.g., NNLO) multiparton predictions.

The MiNNLO$_{PS}$ prediction provides the best global description of the data among the predictions presented in

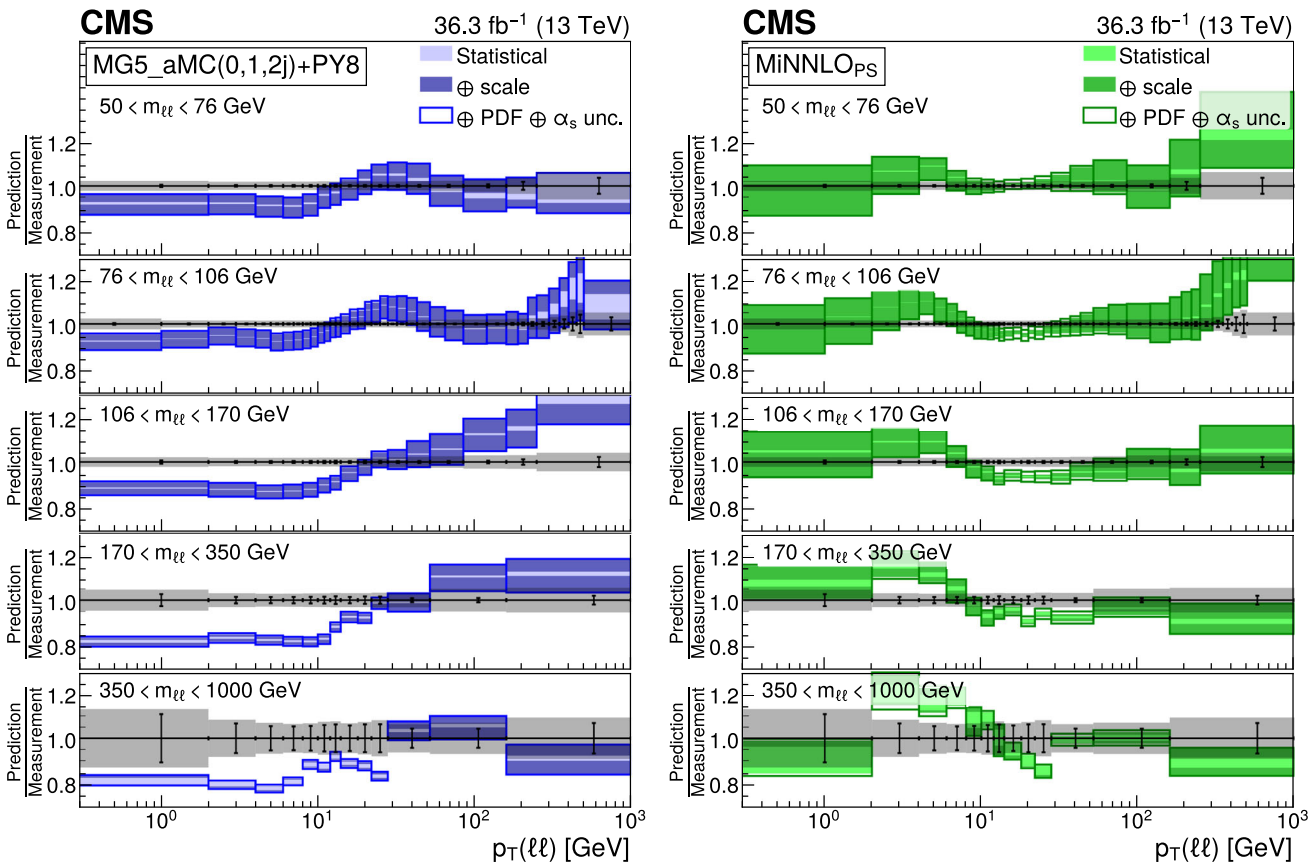

Fig. 6 Comparison to Monte Carlo predictions based on a matrix element with parton shower merging. The ratio of MG5_aMC (0, 1, and 2 jets at NLO) + PYTHIA 8 (left) and MiNNLO$_{PS}$ (right) predictions to the measured differential cross sections in $p_T(\ell\ell)$ are presented for various $m_{\ell\ell}$ ranges. The error bars correspond to the statistical uncertainty of the measurement and the shaded bands to the total experimental uncertainty. The light color band corresponds to the statistical uncertainty of the simulation and the dark color band includes the scale uncertainty. The largest bands include PDF and α_S uncertainties, added in quadrature

this paper. This approach, based on NNLO matrix element and PYTHIA 8 parton shower and MPI, describes well the large $p_T(\ell\ell)$ cross sections (Fig. 6) and ratios (Fig. 17), except above 400 GeV, for $m_{\ell\ell}$ around the Z boson peak. The medium and low $p_T(\ell\ell)$ cross sections are also well described by MiNNLO$_{PS}$ which relies on parton showers, a harder primordial k_T and Sudakov form factors. The same observation can be made in the one jet case. The inclusion of an NNLO matrix element reduces significantly the scale uncertainties, in particular for the inclusive cross section in for the medium $p_T(\ell\ell)$ values where the PDF uncertainty becomes significant with respect to other model uncertainties. It has to be noted that no parton shower tune uncertainty is assigned in the case of MiNNLO$_{PS}$ as well as in the case of MG5_aMC.

We see that the CASCADE predictions (MG5_aMC + PB(CASCADE)) involving TMDs produce a better description in the low-$p_T(\ell\ell)$ part than MG5_aMC + PYTHIA 8, which is valid for all $m_{\ell\ell}$ bins. The predicted cross section for medium $p_T(\ell\ell)$ values is 5 to 10% too low (Fig. 7). What is remarkable is that this prediction is based on TMDs obtained from totally independent data, from a fit to electron-proton deep inelastic scattering measurements performed at HERA. The high $p_T(\ell\ell)$ part is not described by the Z +0,1 jet matrix element calculations from MG5_aMC with CASCADE due to missing higher fixed-order calculations. The range of $p_T(\ell\ell)$ values well described extends with increasing $m_{\ell\ell}$. For the one jet case (Fig. 14), the low-$p_T(\ell\ell)$ part is mainly dominated by Z+2 jet events, and the CASCADE predictions are missing the contributions from the double parton scattering. It thus fails to describe the low $p_T(\ell\ell)$ region. In the low-$p_T(\ell\ell)$ region of the 1 jet case double parton scattering contributions play a significant role and thus CASCADE without it cannot describe this region. The CASCADE predictions give an overall good description of the ratio measurements (Fig. 17). Recently the predictions have been extended by including multi-jet merging [89] for an improved description of the full $p_T(\ell\ell)$ spectrum, shown in the Appendix A.

Within its range of validity, $p_T(\ell\ell) < 0.2\ m_{\ell\ell}$, the ARTEMIDE prediction describes the measurements very

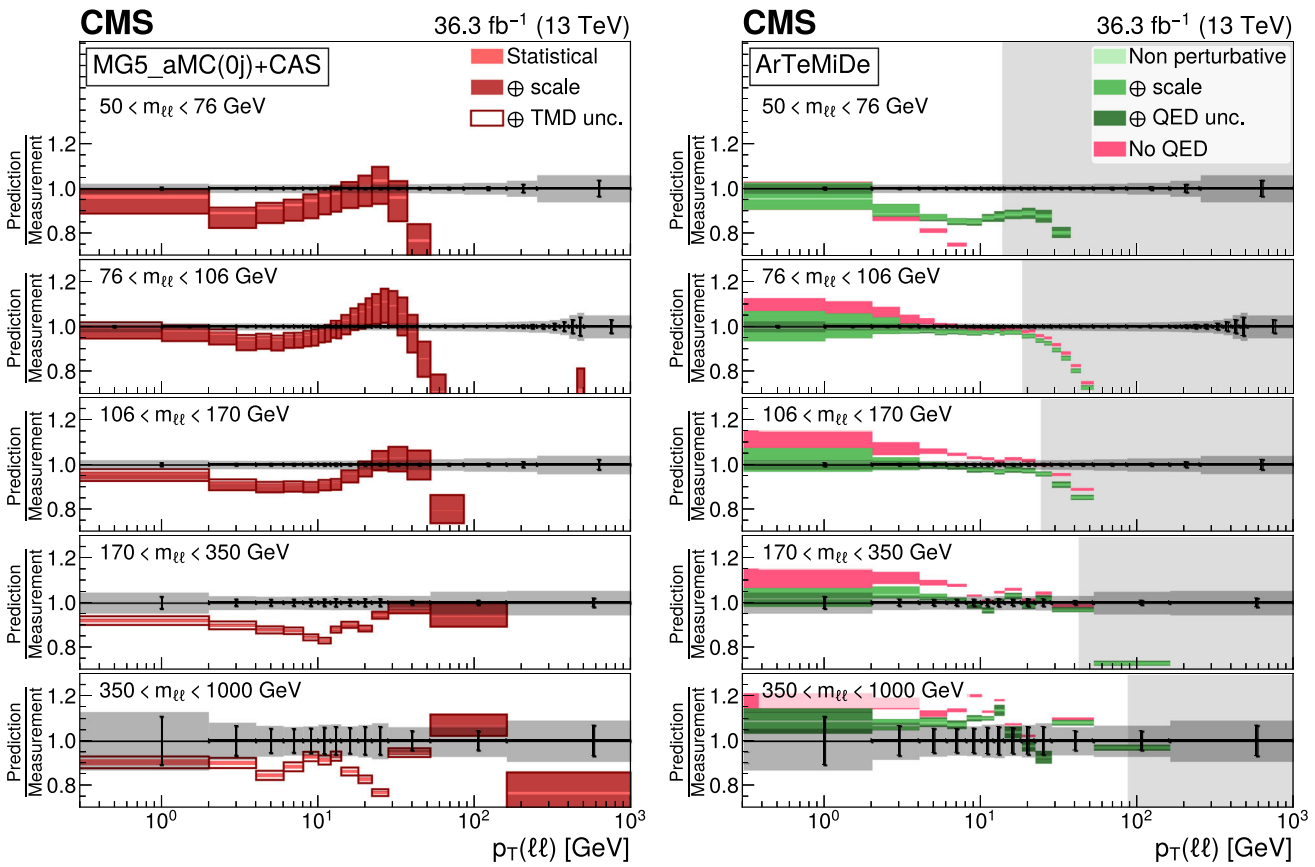

Fig. 7 Comparison to TMD based predictions. The ratio of MG5_aMC (0 jet at NLO) + PB (CASCADE) (left) and ARTEMIDE (right) predictions to the measured differential cross sections in $p_T(\ell\ell)$ are presented for various $m_{\ell\ell}$ ranges. The error bars correspond to the statistical uncertainty of the measurement and the shaded bands to the total experimental uncertainty. The light (dark) green band around ARTEMIDE predictions represent the nonperturbative (QCD scale) uncertainties, the darker green representing the QED FSR correction uncertainties. The range of invalidity is shaded with a gray band. The light color band around CASCADE prediction corresponds to the statistical uncertainty of the simulation and the dark color band includes the scale uncertainty. The largest bands include TMD uncertainty, added in quadrature

well. For all $m_{\ell\ell}$, the low-$p_T(\ell\ell)$ distributions predicted by ARTEMIDE, based on TMDs corresponding to an N^{3}LL approximation, are in very good agreement with the data, except for the highest masses. Figure 7 shows the prediction with and without QED FSR corrections. This underlines the importance of migrations from the Z boson peak towards lower masses, inducing the peak structure in the $p_T(\ell\ell)$ ratio distribution of Fig. 9. The remarkable agreement of the ARTEMIDE prediction with the measurement at the Z boson peak is expected since the prediction relies on TMDs fitted on previous DY measurements at the Z boson peak though at lower centre of mass energies. The excellent agreement for higher $m_{\ell\ell}$ confirms the validity of the approach and in particular of the TMD factorization when the mass scale largely dominates over the transverse momentum. No prediction is provided by ARTEMIDE for the 1 jet case nor for the φ^*_η cross section dependence.

Comparisons of the inclusive cross section as a function of $p_T(\ell\ell)$ with two predictions of GENEVA are presented in Fig. 8 for the inclusive cross sections and in Fig. 15 for the one jet cross sections. The original prediction combining NNLL resummation on the 0-jettiness variable τ_0 (GENEVA-τ) and NNLO corrections does not describe the data well for $p_T(\ell\ell)$ values below 40 GeV. This too hard $p_T(\ell\ell)$ spectrum might be related to the choice of α_S, as discussed in Ref. [94]. For the high $p_T(\ell\ell)$ region, which is dominated by the fixed-order effects, the inclusion of NNLO corrections provides a good description of the measured cross section. The more recent GENEVA prediction (GENEVA-q_T), using a q_T resummation at N^{3}LL, provides a much better description of the measured inclusive cross sections, describing very well the data in the full $p_T(\ell\ell)$ range except for middle $p_T(\ell\ell)$ values in the lowest mass bin. Here, as in MINNLO$_{PS}$ case, the inclusion of NNLO corrections provides a significant reduction of the scale uncertainties, leading to very small theory uncertainties in the middle $p_T(\ell\ell)$ range. The two GENEVA predictions compared with the measured one jet cross sections are similar because both use 1- jettiness in this part of the phase space.

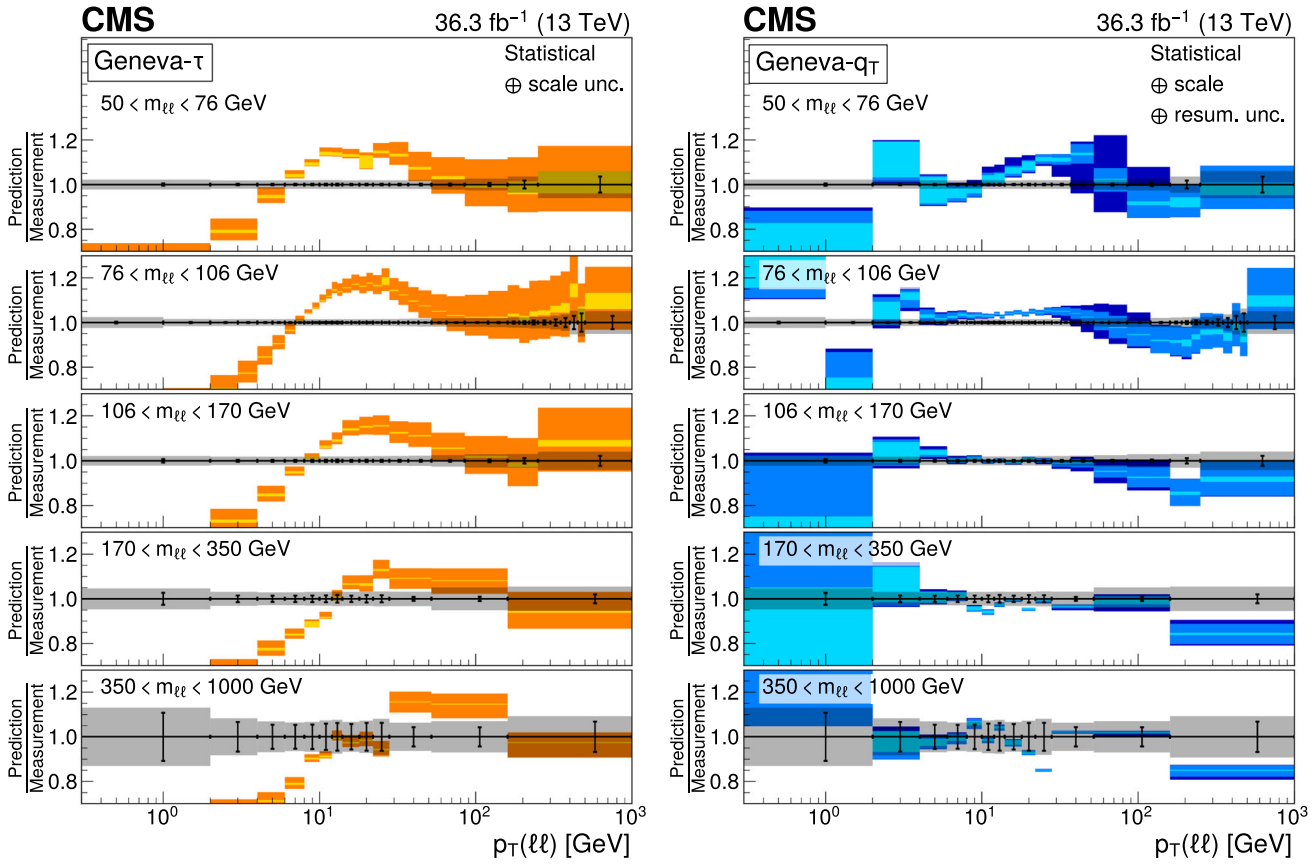

Fig. 8 Comparison to resummation based predictions. The ratio of GENEVA-τ (left) and GENEVA-q_T (right) predictions to the measured differential cross sections in $p_T(\ell\ell)$ are presented for various $m_{\ell\ell}$ ranges. The error bars correspond to the statistical uncertainty of the measurement and the shaded bands to the total experimental uncertainty. The light color bands around the predictions represents the statistical uncertainties and the middle color bands represents the scale uncertainties. The dark outer bands of GENEVA-q_T prediction represent the resummation uncertainties

This could explain that GENEVA predicts a too hard $p_T(\ell\ell)$ spectrum, similarly to the 0-jettiness inclusive case.

8.2 φ_η^* results

The φ_η^* variable is highly correlated with $p_T(\ell\ell)$ and it offers a complementary access to the underlying QCD dynamics. Being based only on angle measurements of the final-state charged leptons, the φ_η^* variable can be measured with greater accuracy which allows us to include the muon channel for all $m_{\ell\ell}$ ranges. Figure 19 presents the inclusive differential cross sections in φ_η^* for the same invariant mass ranges as above and comparisons to models. More complete comparisons to model predictions are presented as ratios of the prediction divided by the measurement in Figs. 20 and 21. The results are discussed below. The ratio of these differential cross sections for various $m_{\ell\ell}$ ranges are computed with respect to the same distribution in the Z peak region. They are shown in Fig. 22 and further compared with models in Figs. 23 and 24.

The φ_η^* distributions are monotonic functions, in particular they do not present a peak structure as measured in the $p_T(\ell\ell)$ distributions. At small values, the φ_η^* distributions contain a plateau whose length decreases with increasing $m_{\ell\ell}$, and more generally the φ_η^* distributions fall more rapidly with increasing $m_{\ell\ell}$ as clearly shown in Fig. 19. Because the lepton direction is much less affected by QED FSR than the energy, the effect of migrations from the Z boson mass bin towards lower masses is relatively invisible in the φ_η^* shape as highlighted by the ratio distribution in Fig. 22 (upper left).

Since φ_η^* is highly correlated with $p_T(\ell\ell)$, the comparison of the φ_η^* distributions to theoretical predictions leads to the same basic observations and remarks as related above. The MG5_aMC + PYTHIA 8 prediction describes the measured φ_η^* distributions well globally and predicts a too small cross section in the region sensitive to gluon resummation, i.e., $\varphi_\eta^* \lesssim 0.1$ on the Z boson mass peak, as shown in Fig. 20. The increase of this disagreement for higher $m_{\ell\ell}$ is also observed, clearly visible in the ratio distributions of Fig. 23.

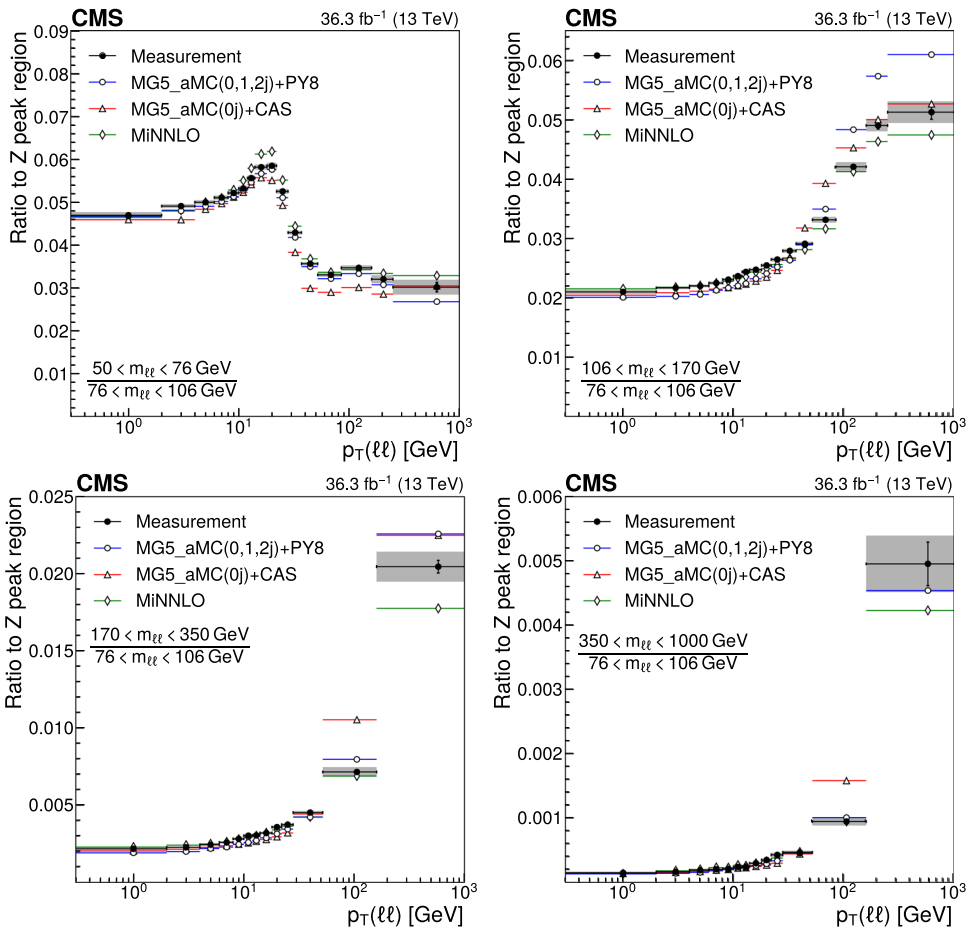

Fig. 9 Ratios of differential cross sections in $p_T(\ell\ell)$ for invariant mass ranges with respect to the peak region $76 < m_{\ell\ell} < 106$ GeV: $50 < m_{\ell\ell} < 76$ GeV (upper left), $106 < m_{\ell\ell} < 170$ GeV (upper right), $170 < m_{\ell\ell} < 350$ GeV (lower left), and $350 < m_{\ell\ell} < 1000$ GeV (lower right). Details on the presentation of the results are given in Fig. 5 caption

As for the $p_T(\ell\ell)$ distributions, the MiNNLO$_{PS}$ prediction provides the best global description of the data (Fig. 20). In contrast to the disagreement for $p_T(\ell\ell)$ above 400 GeV for $m_{\ell\ell}$ around the Z peak that appeared both in the inclusive case (Fig. 6) and in the one jet case (Fig. 17) the large φ^*_η values are well described by MiNNLO$_{PS}$. The inclusion of NNLO corrections reduces scale uncertainties making the PDF uncertainty dominant for medium φ^*_η values in the central $m_{\ell\ell}$ bins. The PDF uncertainty is significantly reduced in the ratio distributions (Fig. 23) leading to remarkable prediction precision of the level of 1.5% in several bins.

The MG5_aMC + PB(CASCADE) prediction describes well the measured shapes for $\varphi^*_\eta \lesssim 0.1$ in all $m_{\ell\ell}$ bins (Fig. 20). This contrasts with the description of the $p_T(\ell\ell)$ dependence by the same prediction (Fig. 7), owing to the washing out of the details of the $p_T(\ell\ell)$ distribution in the φ^*_η distribution. The normalisation of the prediction is good for the Z boson mass peak region but underestimates more and more the cross section with increasing $m_{\ell\ell}$, in a way relatively close to MG5_aMC predictions. The ratio distributions (Fig. 23) also illustrate this, but a compensation effect leads to predictions in agreement over the full φ^*_η range.

The measured cross sections as a function of φ^*_η are compared with GENEVA predictions in Fig. 21. Similar to previous discussions of the $p_T(\ell\ell)$ distributions, GENEVA-q_T improves significantly the description of the data with respect to GENEVA-τ. The discrepancy of GENEVA-q_T for low $p_T(\ell\ell)$ values in the two lowest $m_{\ell\ell}$ bins is smoothed here leading to a global agreement everywhere. The cross section ratio distributions of the different $m_{\ell\ell}$ bins over the Z boson mass peak bin, as a function of φ^*_η are shown in Fig. 24. Here both GENEVA predictions provide a good description of the measurements. This indicates that, although the precise shape in φ^*_η is not well reproduced by GENEVA-τ, the scale dependence is well described over the large range covered by the present measurement.

The differential cross section measurements are presented in the HEPData entry [100].

9 Summary

Measurements of differential Drell–Yan cross sections in proton–proton collisions at $\sqrt{s} = 13$ TeV in the dielectron and dimuon final states are presented, using data collected with the CMS detector, corresponding to an integrated luminosity of 36.3 fb^{-1}. The measurements are corrected for detector effects and the two leptonic channels are combined.

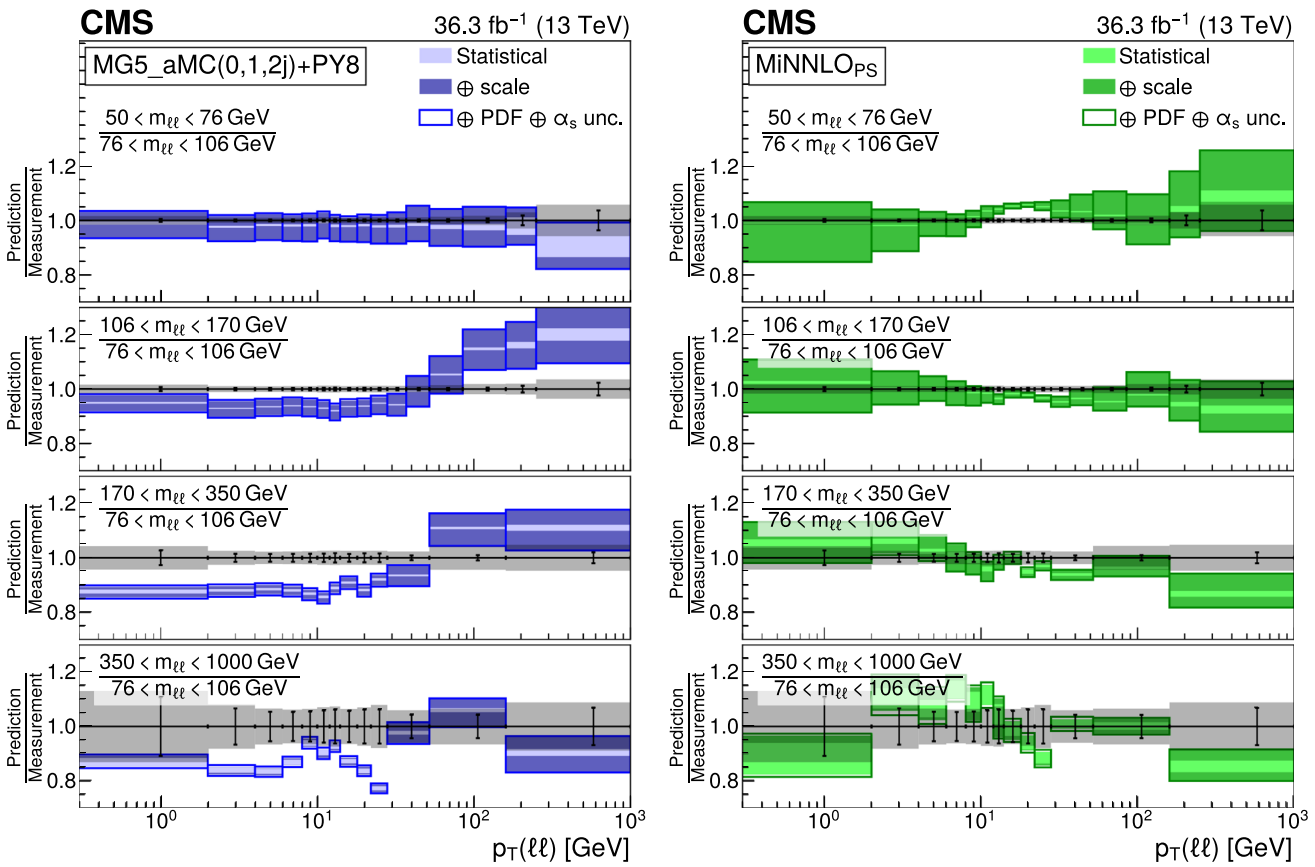

Fig. 10 Comparison to Monte Carlo predictions based on a matrix element with parton shower merging. The distributions show the ratio of differential cross sections as a function of $p_T(\ell\ell)$ for a given $m_{\ell\ell}$ range to the cross section at the peak region $76 < m_{\ell\ell} < 106$ GeV. The predictions are MG5_aMC (0, 1, and 2 jets at NLO) + PYTHIA 8 (left) and MiNNLO$_{PS}$ (right). Details on the presentation of the results are given in Fig. 6 caption

Differential cross sections in the dilepton transverse momentum, $p_T(\ell\ell)$, and in the lepton angular variable φ^*_η are measured for different values of the dilepton mass, $m_{\ell\ell}$, between 50 GeV and 1 TeV. To highlight the evolution with the dilepton mass scale, ratios of these distributions for various masses are presented. In addition, dilepton transverse momentum distributions are shown in the presence of at least one jet within the detector acceptance.

The rising behaviour of the Drell–Yan inclusive cross section at small $p_T(\ell\ell)$ is attributed to soft QCD radiations, whereas the tail at large $p_T(\ell\ell)$ is only expected to be well described by models relying on higher-order matrix element calculations. Therefore, this variable provides a good sensitivity to initial-state QCD radiations and can be compared with different predictions relying on matrix element calculations at different orders and using different methods to resum the initial-state soft QCD radiations. The measurements show that the peak in the $p_T(\ell\ell)$ distribution, located around 5 GeV, is not significantly modified by changing the $m_{\ell\ell}$ value in the covered range. However, for higher values of $m_{\ell\ell}$ above the peak, the $p_T(\ell\ell)$ distributions fall less steeply.

The φ^*_η variable, highly correlated with $p_T(\ell\ell)$, offers a complementary access to the underlying QCD dynamics. Since it is based only on angle measurements of the final-state charged leptons, it offers, a priori, measurements with greater accuracy. However, these measurements demonstrate that the φ^*_η distributions discriminate between the models less than the $p_T(\ell\ell)$ distributions, since they wash out the peak structure of the $p_T(\ell\ell)$ distributions, which reflect the initial-state QCD radiation effects in a more detailed way.

This publication presents comparisons of the measurements to six predictions using different treatments of soft initial-state QCD radiations. Two of them, MG5_aMC + PYTHIA 8 and MiNNLO$_{PS}$, are based on a matrix element calculation merged with parton showers. Two others, ARTEMIDE and CASCADE use transverse momentum dependent parton distributions (TMD). Finally, GENEVA combines a higher-order resummation with a Drell–Yan calculation at next-to-next-to-leading order (NNLO), in two different ways.

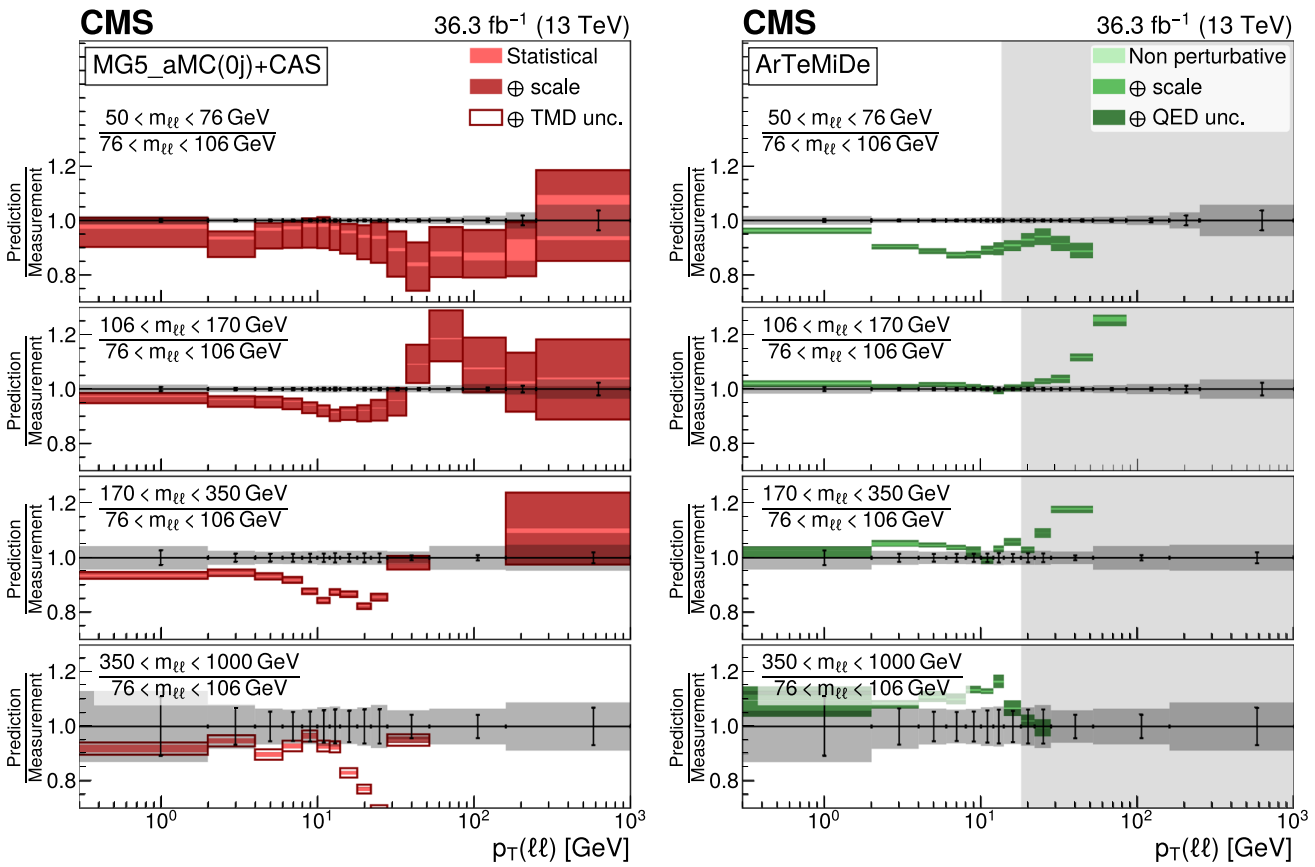

Fig. 11 Comparison to TMD based predictions. The distributions show the ratio of differential cross sections as a function of $p_T(\ell\ell)$ for a given $m_{\ell\ell}$ range to the cross section at the peak region 76 < $m_{\ell\ell}$ < 106 GeV. The predictions are MG5_aMC (0 jet at NLO) + PB (CASCADE) (left) and ARTEMIDE (right). Details on the presentation of the results are given in Fig. 7 caption

One carries out the resummation at next-to-next-to-leading logarithm in the 0-jettiness variable τ_0, the other at N^{3}LL in the q_T variable.

The comparison of the measurement with the MG5_aMC + PYTHIA 8 Monte Carlo predictions using matrix element calculations including Z + 0, 1, 2 partons at next-to-leading order (NLO) merged with a parton shower, shows generally good agreement, except at $p_T(\ell\ell)$ values below 10 GeV both for the inclusive and one jet cross sections. This disagreement is enhanced for masses away from the Z mass peak and is more pronounced for the higher dilepton masses, reaching 20% for the highest mass bin.

The MiNNLO$_{PS}$ prediction provides the best global description of the data among the predictions presented in this paper, both for the inclusive and the one jet cross sections. This approach, based on NNLO matrix element and PYTHIA 8 parton shower and MPI, describes well the large $p_T(\ell\ell)$ cross sections and ratios, except for $p_T(\ell\ell)$ values above 400 GeV for dilepton masses around the Z mass peak. A good description of the medium and low $p_T(\ell\ell)$ cross sections is obtained using a modified primordial k_T parameter of the CP5 parton shower tune.

MG5_aMC + PB(CASCADE) predictions are based on Parton Branching TMDs obtained only from a fit to electron-proton deep inelastic scattering measurements performed at HERA. These TMDs are merged with NLO matrix element calculations. Low $p_T(\ell\ell)$ values are globally well described but with too low cross sections at medium $p_T(\ell\ell)$ values. This discrepancy increases with increasing $m_{\ell\ell}$ in a way similar to the MG5_aMC + PYTHIA 8 predictions. The high part of the $p_T(\ell\ell)$ distribution is not described by CASCADE due to missing higher fixed-order terms. The model can not describe the low $p_T(\ell\ell)$ region of the cross section in the presence of one jet due to the missing double parton scattering contributions. The recent inclusion of multi-jet merging allows a larger $p_T(\ell\ell)$ region to be described as well.

ARTEMIDE provides predictions based on TMDs extracted from previous measurements including the Drell-Yan transverse momentum cross section at the LHC at the Z mass peak. By construction, the validity of ARTEMIDE predictions are limited to the range $p_T(\ell\ell) < 0.2\ m_{\ell\ell}$. In that range, they

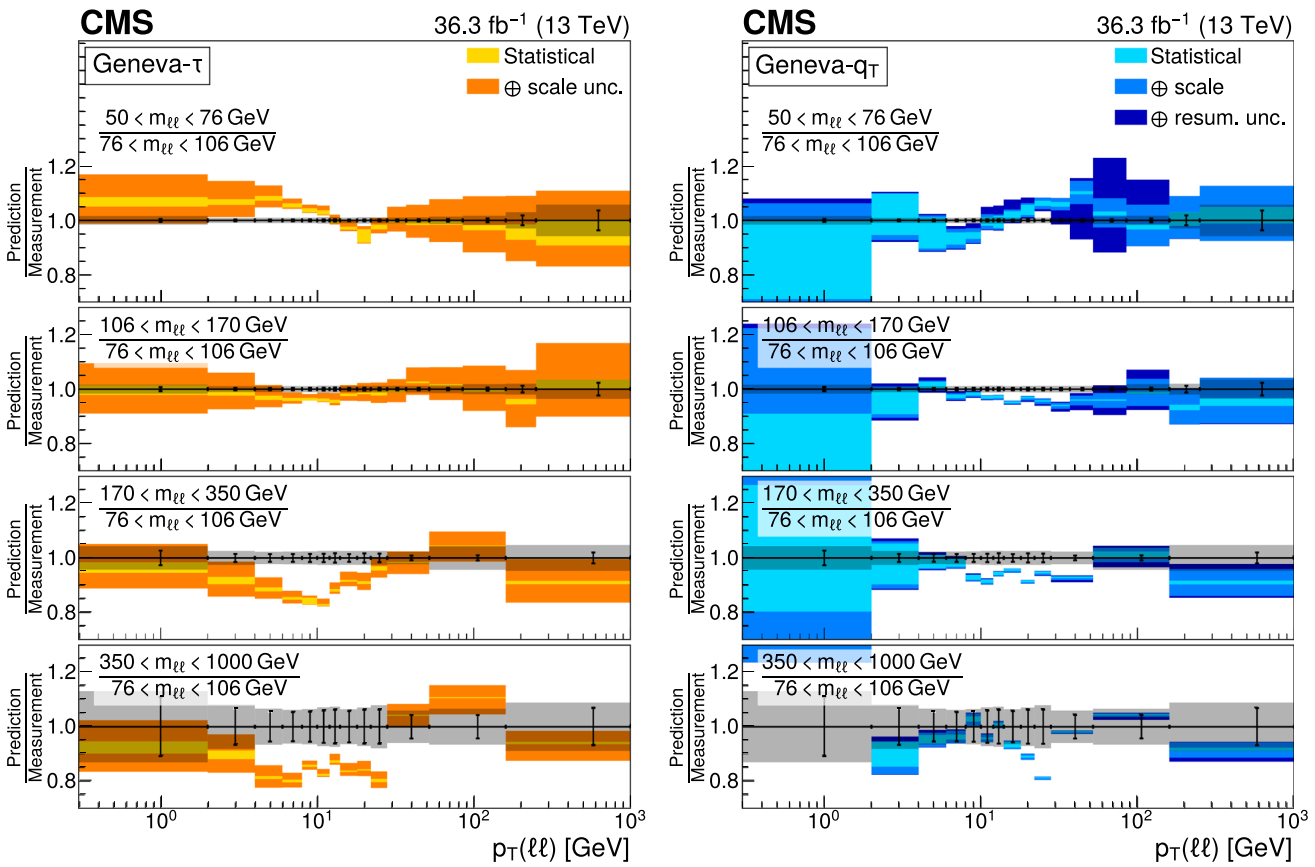

Fig. 12 Comparison to resummation based predictions. The distributions show the ratio of differential cross sections as a function of $p_T(\ell\ell)$ for a given $m_{\ell\ell}$ range to the cross section at the peak region $76 < m_{\ell\ell} < 106$ GeV. The predictions are GENEVA-τ (left) and GENEVA-q_T (right). Details on the presentation of the results are given in Fig. 8 caption

describe well the present measurements up to the highest dilepton masses.

The GENEVA prediction, combining resummation in the 0-jettiness variable τ_0 (GENEVA-τ) and NNLO matrix element does not describe the measurement well for $p_T(\ell\ell)$ values below 40 GeV. For the high $p_T(\ell\ell)$ region the inclusion of NNLO in the matrix element provides a good description of the measured cross section. The recent GENEVA prediction (GENEVA-q_T), using a q_T resummation, provides a much better description of the measured inclusive cross sections, describing very well the data in the full $p_T(\ell\ell)$ range except for middle $p_T(\ell\ell)$ values in the lowest mass bin. Both GENEVA approaches predict too hard $p_T(\ell\ell)$ spectra for the one jet cross sections.

The ratio distributions presented in this paper confirm most of the observations based on the comparison between the measurement and the predictions at the cross section level. The observed scale dependence is well described by the different models. Furthermore the partial cancellation of the uncertainties in the cross section ratios allows a higher level of precision to be reached for both the measurement and the predictions.

The present analysis shows the relevance of measuring the Drell–Yan cross section in a wide range in dilepton masses to probe the interplay between the transverse momentum and the mass scales of the process. Important theoretical efforts have been made during the last decade to improve the detailed description of high energy processes involving multiple scales and partonic final states. The understanding of the Drell–Yan process directly benefited from these developments. The present paper shows that they individually describe the measurements well in the regions they were designed for. Nevertheless, no model is able to reproduce all dependencies over the complete covered range. Further progress might come from combining these approaches.

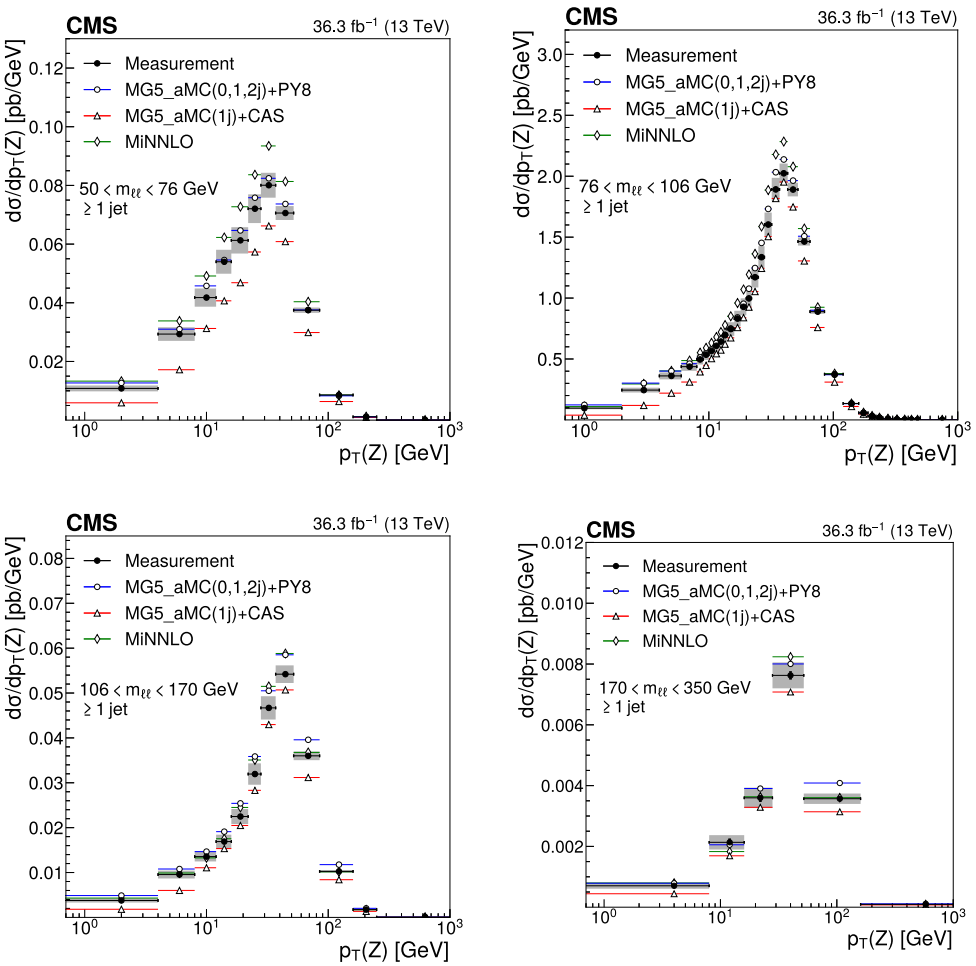

Fig. 13 Differential cross sections in $p_{\mathrm{T}}(\ell\ell)$ for one or more jets in various invariant mass ranges: $50 < m_{\ell\ell} < 76$ GeV (upper left), $76 < m_{\ell\ell} < 106$ GeV (upper right), $106 < m_{\ell\ell} < 170$ GeV (lower left), and $170 < m_{\ell\ell} < 350$ GeV (lower right). The measurement is compared with MG5_aMC (0, 1, and 2 jets at NLO) + PYTHIA 8 (blue dots), MiNNLO$_{\mathrm{PS}}$ (green diamonds) and MG5_aMC (1 jet at NLO)+ PB (CASCADE) (red triangles). Details on the presentation of the results are given in Fig. 5 caption

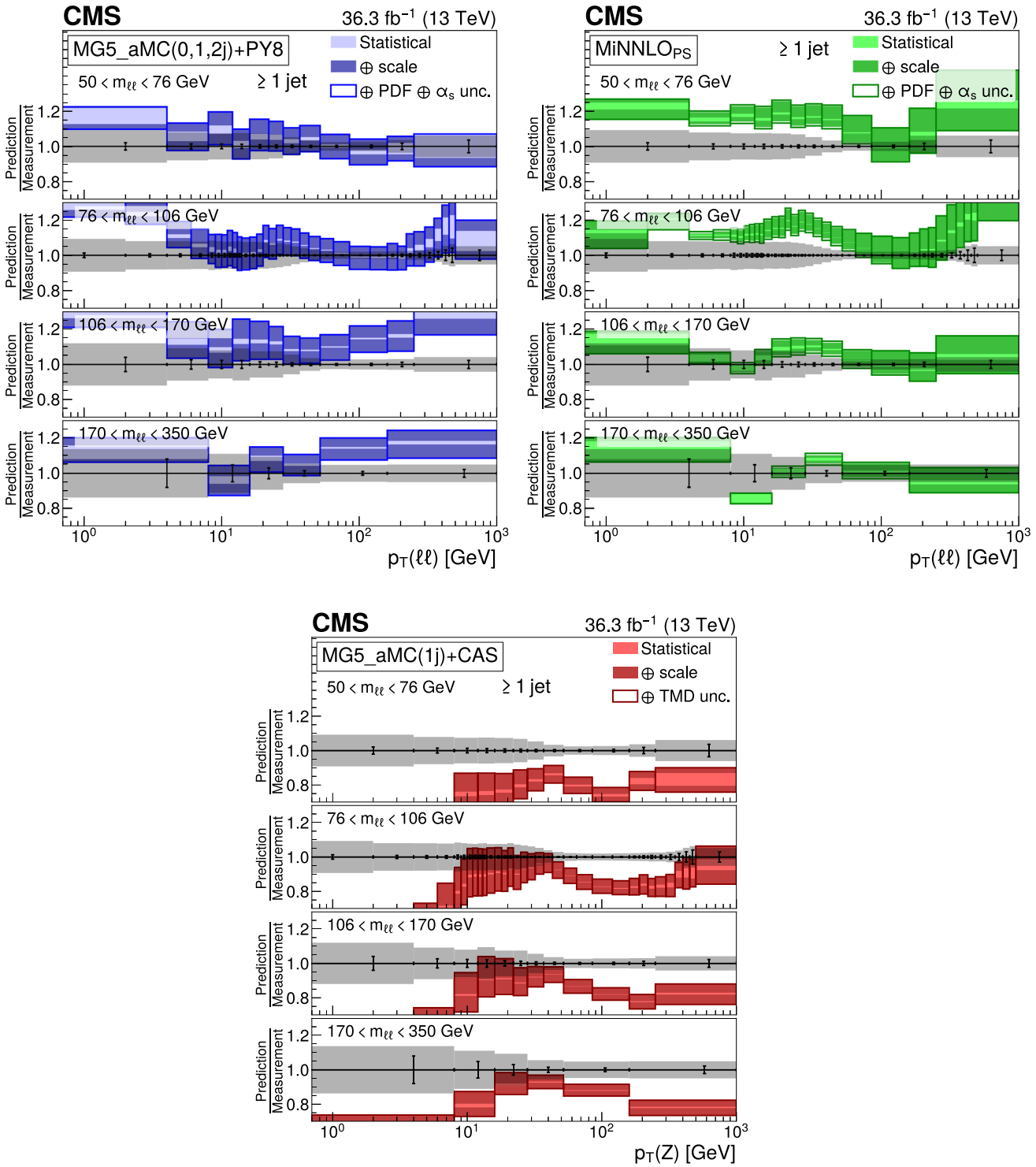

Fig. 14 Comparison of the differential cross sections in $p_T(\ell\ell)$ to predictions in various invariant mass ranges for the one or more jets case. The measurement is compared with MG5_aMC (0, 1, and 2 jets at NLO) + PYTHIA 8 (upper left), MiNNLO$_{PS}$ (upper right) and MG5_aMC (1 jet at NLO) + PB (CASCADE) (lower). Details on the presentation of the results are given in Fig. 6 caption

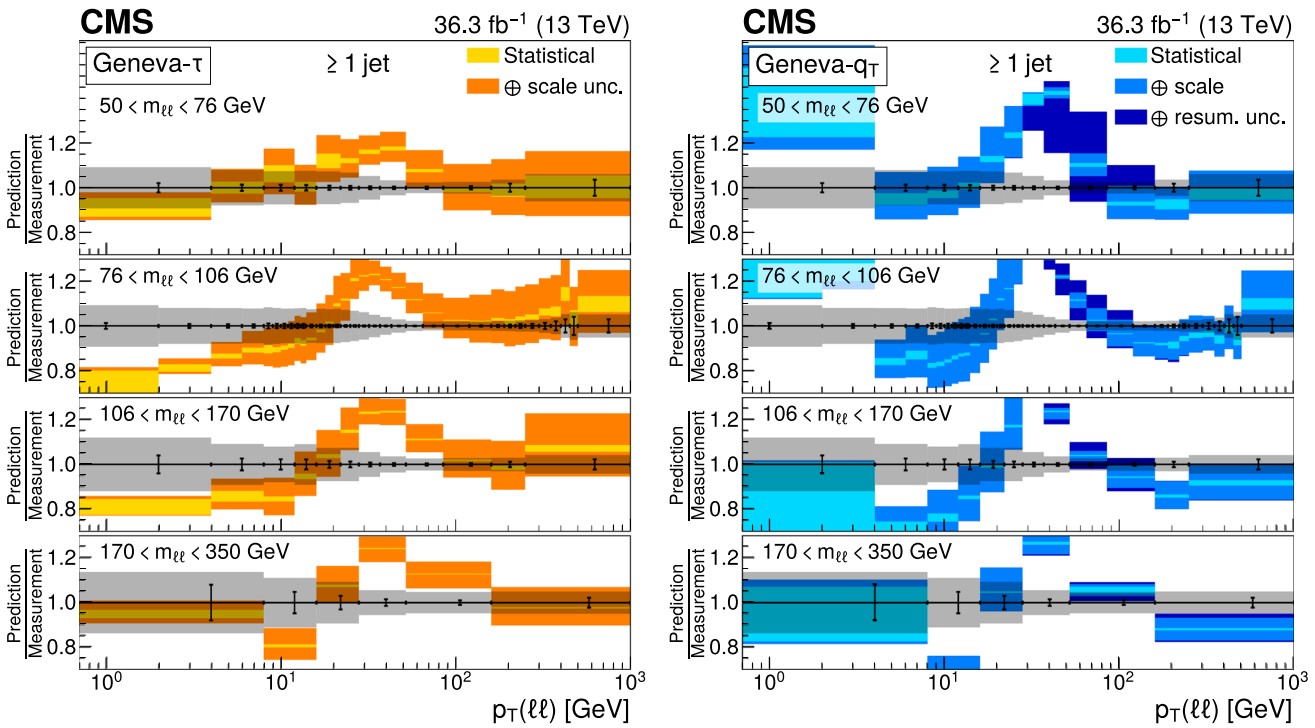

Fig. 15 Comparison of the differential cross sections in $p_T(\ell\ell)$ to predictions in various invariant mass ranges for the one or more jets case. The measurement is compared with GENEVA-τ (left) and GENEVA-q_T (right) predictions. Details on the presentation of the results are given in Fig. 8 caption

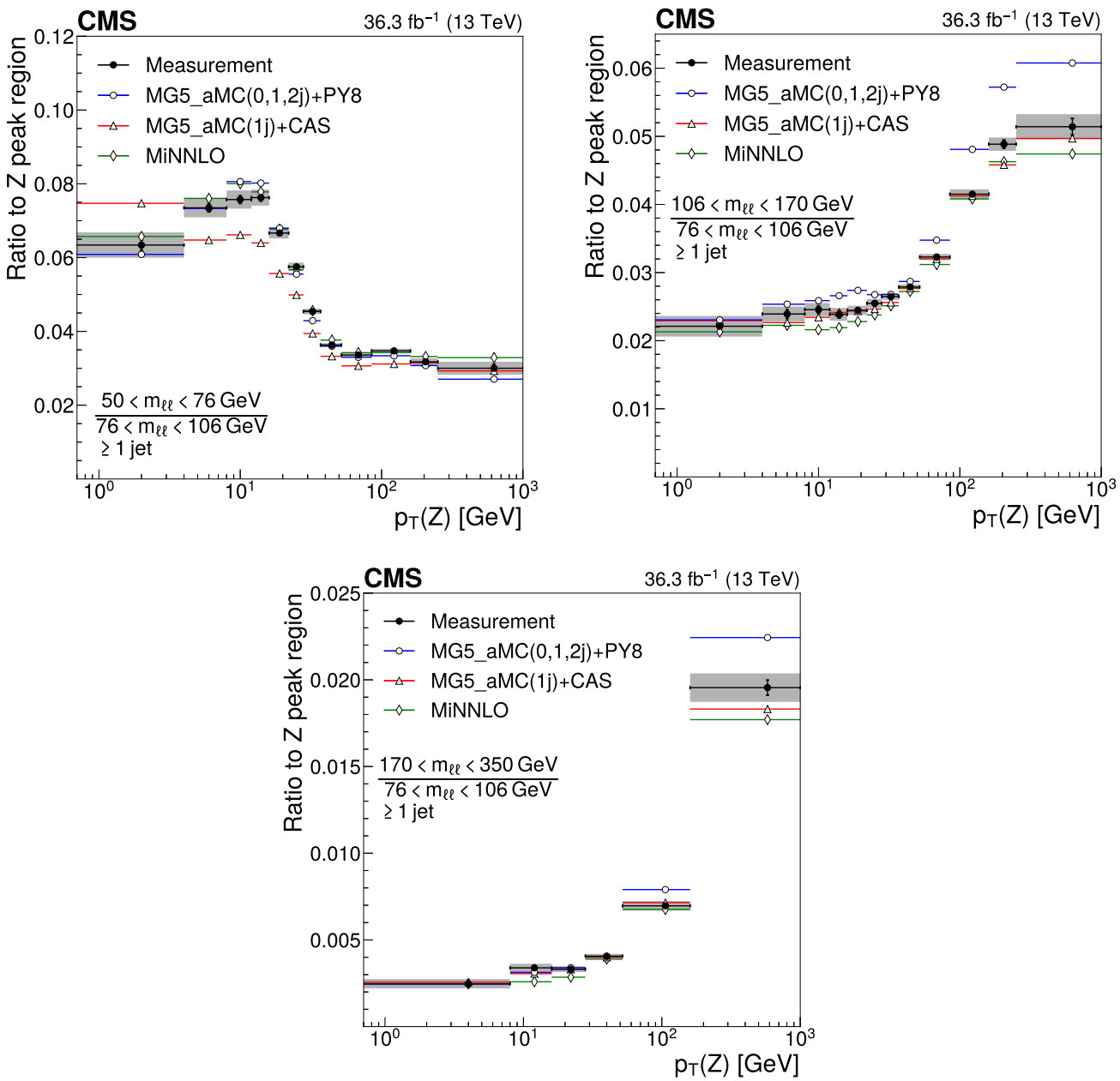

Fig. 16 Ratios of differential cross sections in $p_T(\ell\ell)$ for one or more jets in various invariant mass ranges with respect to the peak region $76 < m_{\ell\ell} < 106$ GeV: $50 < m_{\ell\ell} < 76$ GeV (upper left), $106 < m_{\ell\ell} < 170$ GeV (upper right), and $170 < m_{\ell\ell} < 350$ GeV (lower). The measurement is compared with MG5_aMC (0, 1, and 2 jets at NLO) + PYTHIA 8 (blue dots), MiNNLO$_{PS}$ (green diamonds) and MG5_aMC (1 jet at NLO)+ PB (CASCADE) (red triangles). Details on the presentation of the results are given in Fig. 5 caption

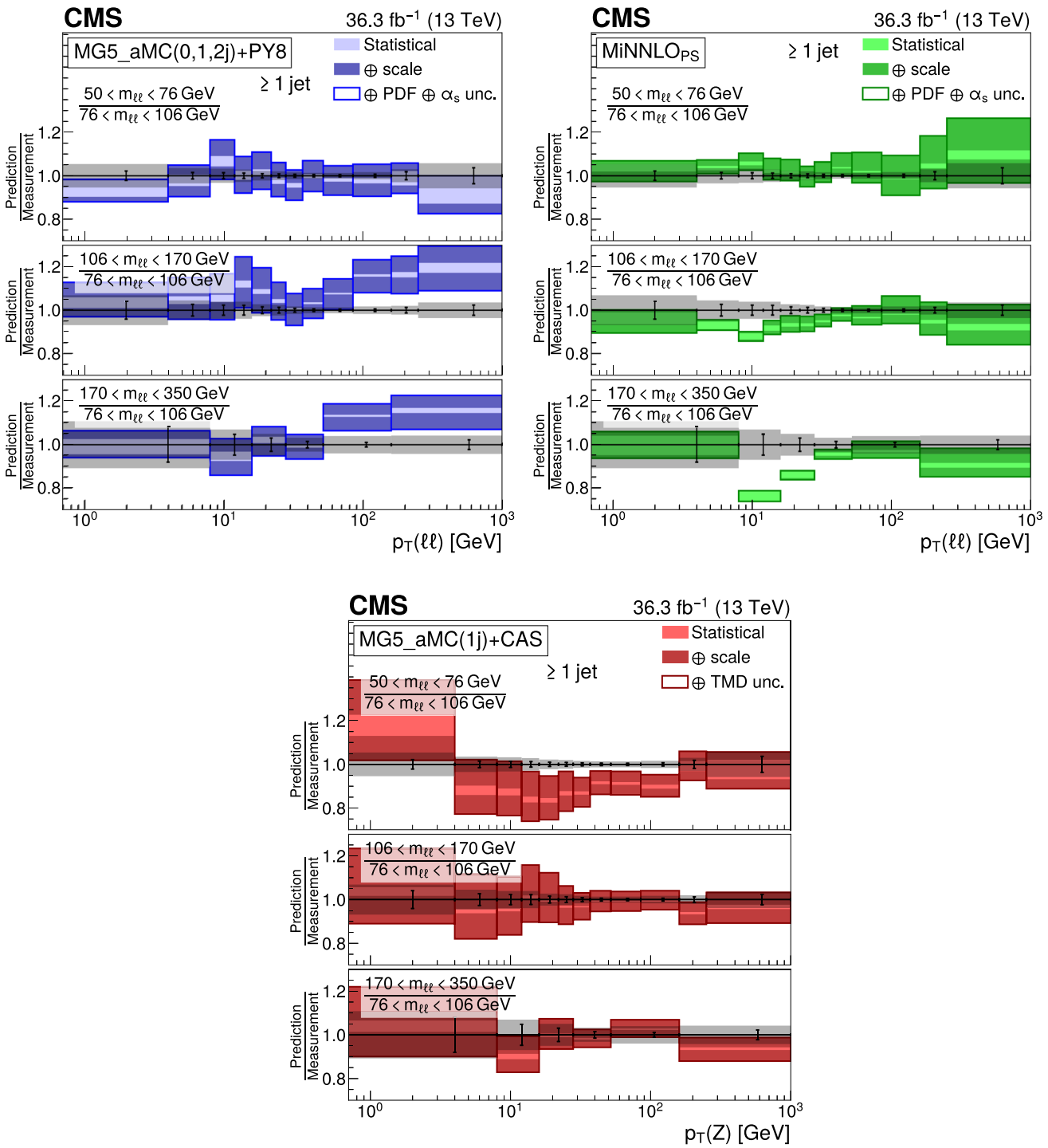

Fig. 17 Comparison of the ratios of differential cross sections in $p_T(\ell\ell)$ for one or more jets in various invariant mass ranges with respect to the peak region $76 < m_{\ell\ell} < 106$ GeV. The measured ratio is compared with MG5_aMC (0, 1, and 2 jets at NLO) + PYTHIA 8 (upper left), MiNNLO$_{PS}$ (upper right) and MG5_aMC (1 jet at NLO) + PB (CASCADE) (lower). Details on the presentation of the results are given in Fig. 6 caption

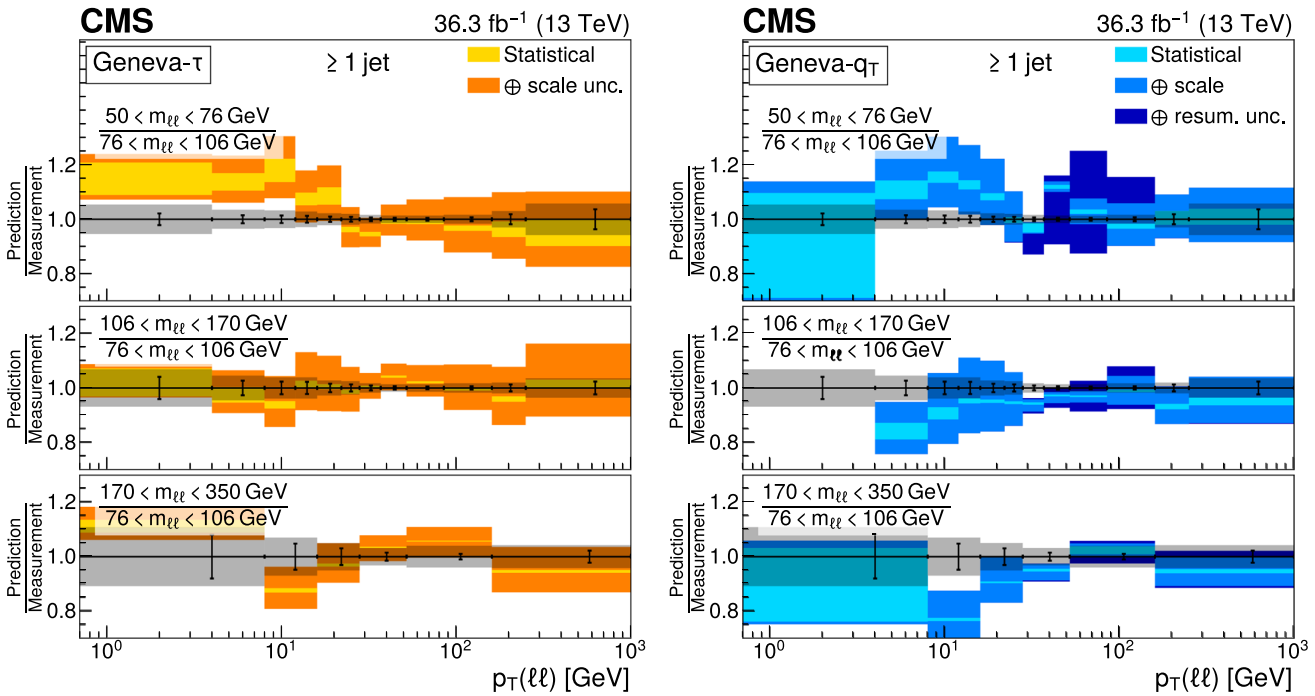

Fig. 18 Comparison of the ratios of differential cross sections in $p_T(\ell\ell)$ for one or more jets in various invariant mass ranges with respect to the peak region $76 < m_{\ell\ell} < 106$ GeV. The measured ratio is compared with GENEVA-τ (left) and GENEVA-q_T (right) predictions. Details on the presentation of the results are given in Fig. 8 caption

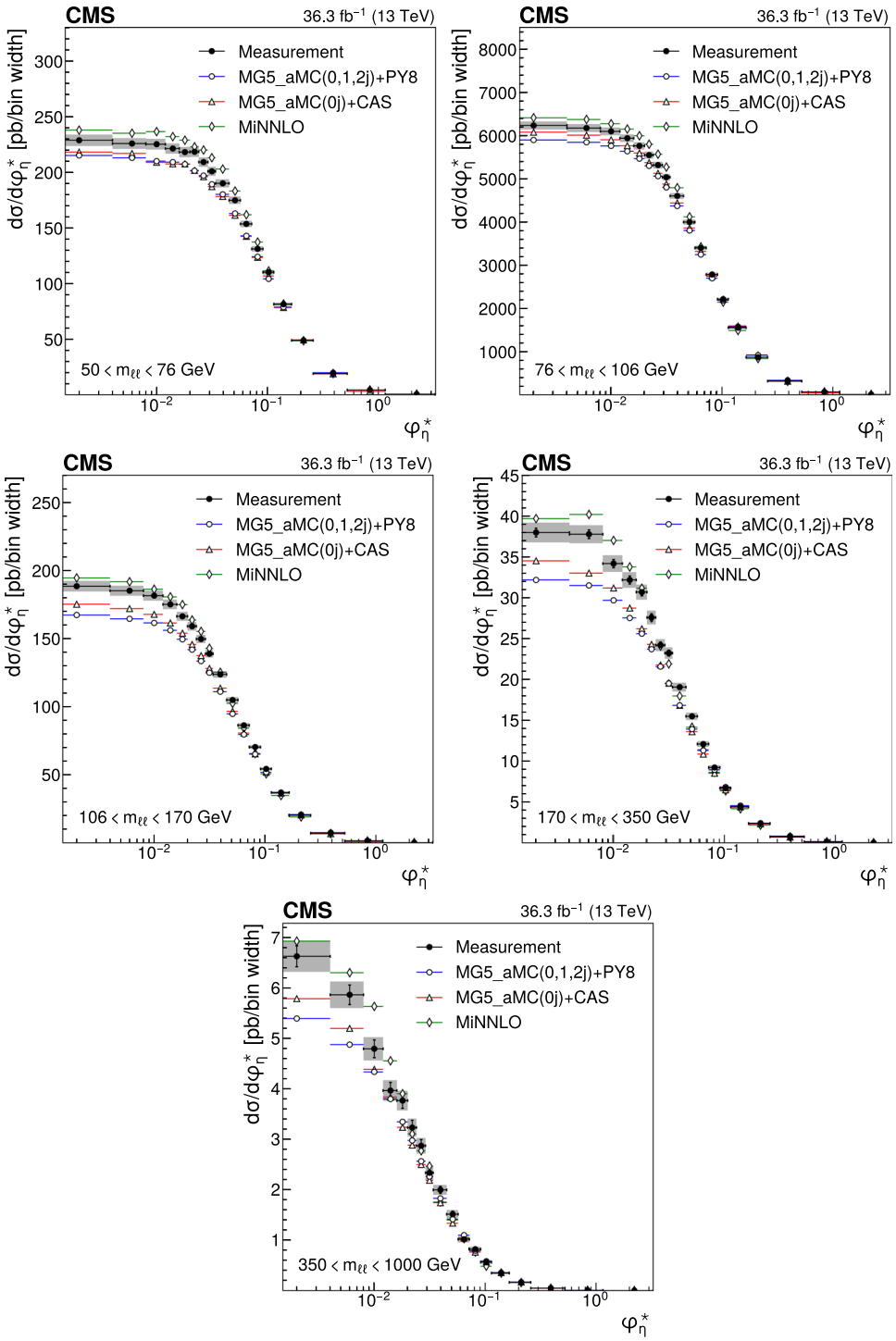

Fig. 19 Differential cross sections in $\varphi^*_\eta(\ell\ell)$ in various invariant mass ranges: $50 < m_{\ell\ell} < 76$ GeV (upper left), $76 < m_{\ell\ell} < 106$ GeV (upper right), $106 < m_{\ell\ell} < 170$ GeV (middle left), $170 < m_{\ell\ell} < 350$ GeV (middle right), and $350 < m_{\ell\ell} < 1000$ GeV (lower). The measurement is compared with MG5_aMC (0, 1, and 2 jets at NLO) + PYTHIA 8 (blue dots), MiNNLO$_{PS}$ (green diamonds) and MG5_aMC (0 jet at NLO)+ PB (CASCADE) (red triangles). Details on the presentation of the results are given in Fig. 5 caption

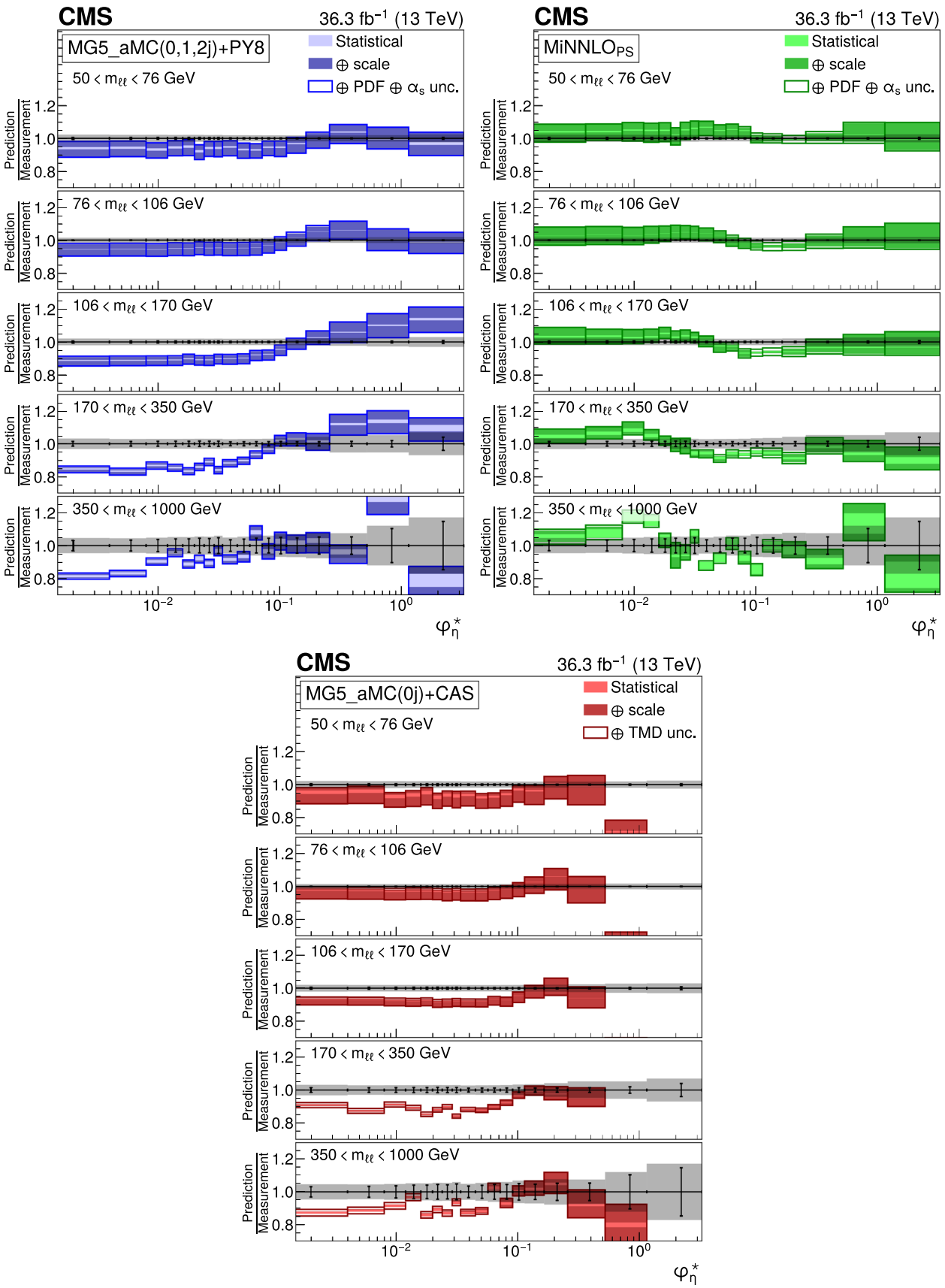

Fig. 20 Comparison of the differential cross sections in $\varphi^*_\eta(\ell\ell)$ to predictions in various $m_{\ell\ell}$ ranges. The measurement is compared with MG5_aMC (0, 1, and 2 jets at NLO) + PYTHIA 8 (upper left), MiNNLO$_{PS}$ (upper right) and MG5_aMC + PB (CASCADE) (lower). Details on the presentation of the results are given in Fig. 6 caption

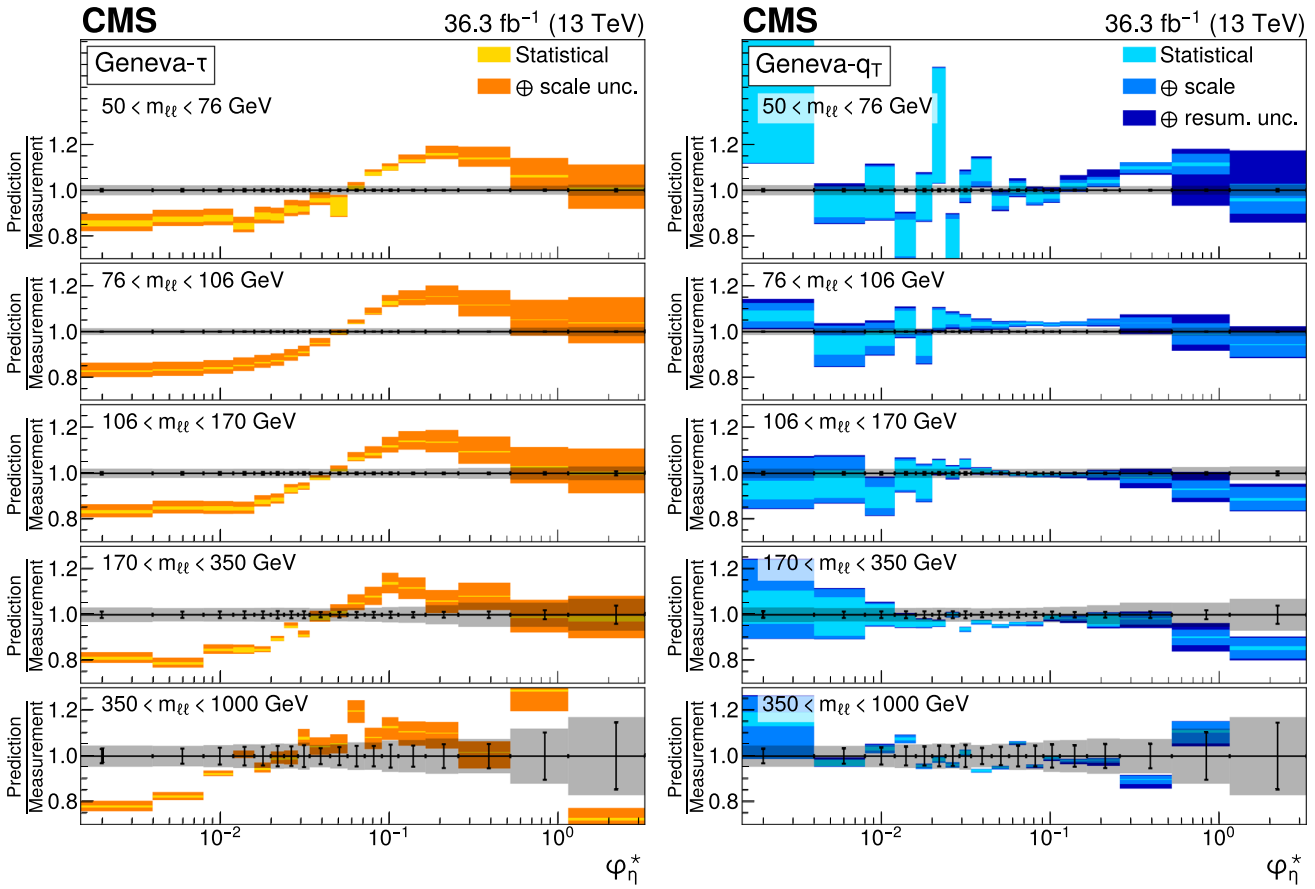

Fig. 21 Comparison of the differential cross sections in $\varphi^{*}_{\eta}(\ell\ell)$ to predictions in various $m_{\ell\ell}$ ranges. The measurement is compared with GENEVA-τ (left) and GENEVA-q_{T} (right) predictions. Details on the presentation of the results are given in Fig. 8 caption

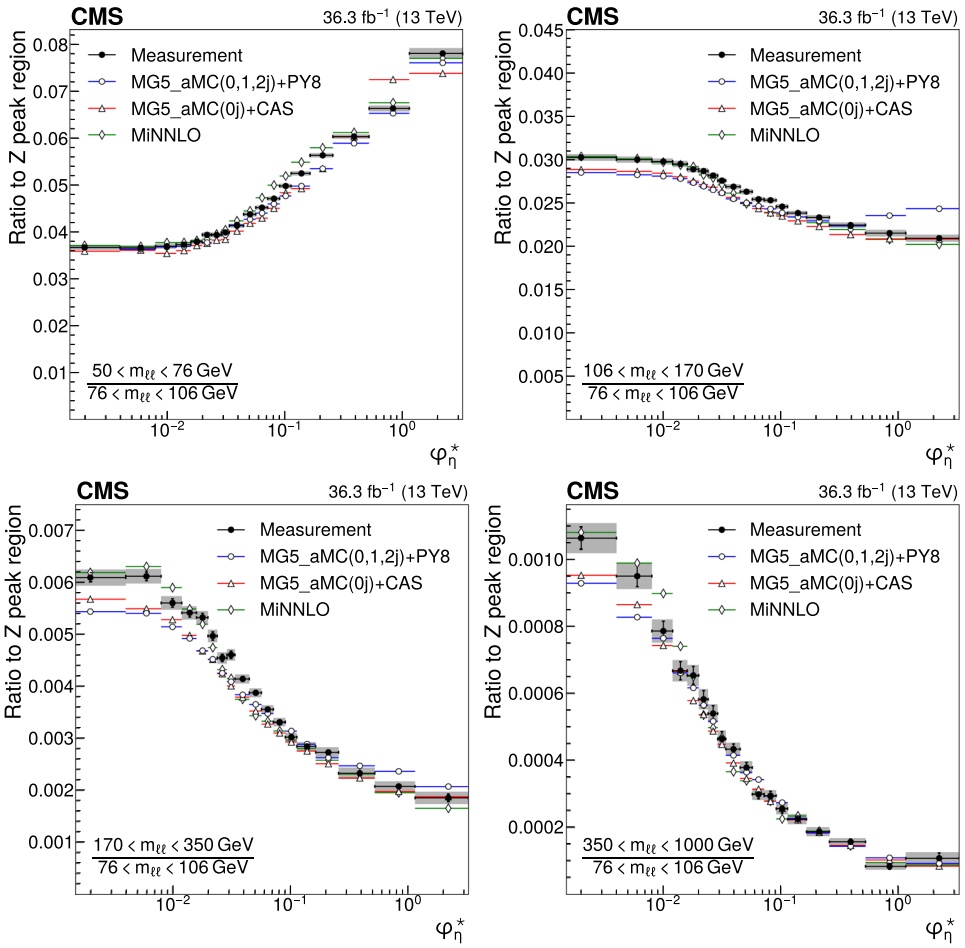

Fig. 22 Ratios of differential cross sections in $\varphi_\eta^*(\ell\ell)$ for invariant mass ranges with respect to the peak region $76 < m_{\ell\ell} < 106$ GeV: $50 < m_{\ell\ell} < 76$ GeV (upper left), $106 < m_{\ell\ell} < 170$ GeV (upper right), $170 < m_{\ell\ell} < 350$ GeV (lower left), and $350 < m_{\ell\ell} < 1000$ GeV (lower right). The measurement is compared with MG5_aMC (0, 1, and 2 jets at NLO) + PYTHIA 8 (blue dots), MiNNLO$_{\mathrm{PS}}$ (green diamonds) and MG5_aMC (0 jet at NLO)+ PB (CASCADE) (red triangles). Details on the presentation of the results are given in Fig. 5 caption

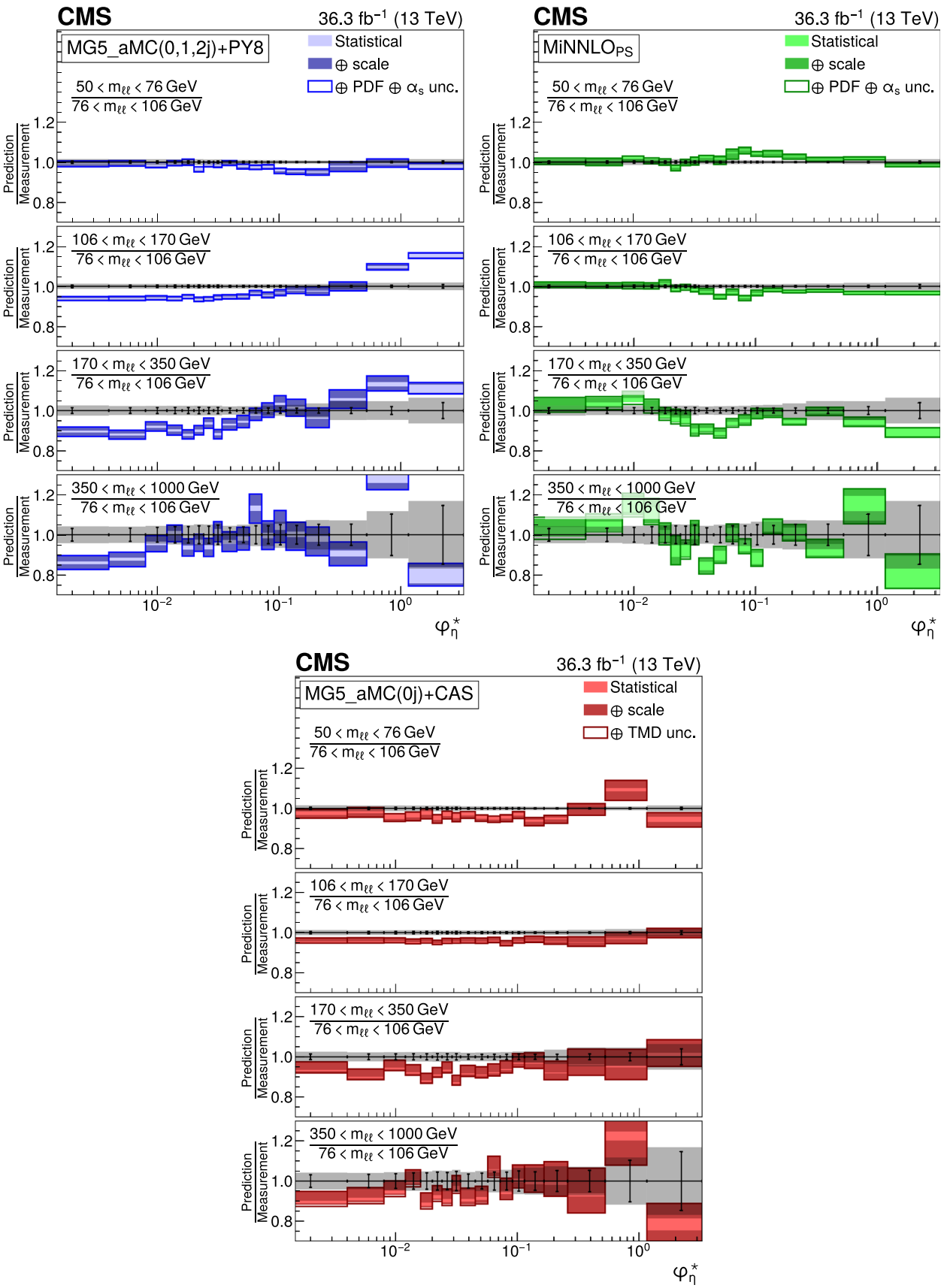

Fig. 23 Ratios of differential cross sections in $\varphi_\eta^*(\ell\ell)$ for invariant $m_{\ell\ell}$ with respect to the peak region $76 < m_{\ell\ell} < 106$ GeV. Compared to model predictions from MG5_aMC (0, 1, and 2 jets at NLO) + PYTHIA 8 (upper left), MiNNLO$_{PS}$ (upper right) and MG5_aMC (0 jet at NLO) + PB (CASCADE) (lower). Details on the presentation of the results are given in Fig. 6 caption

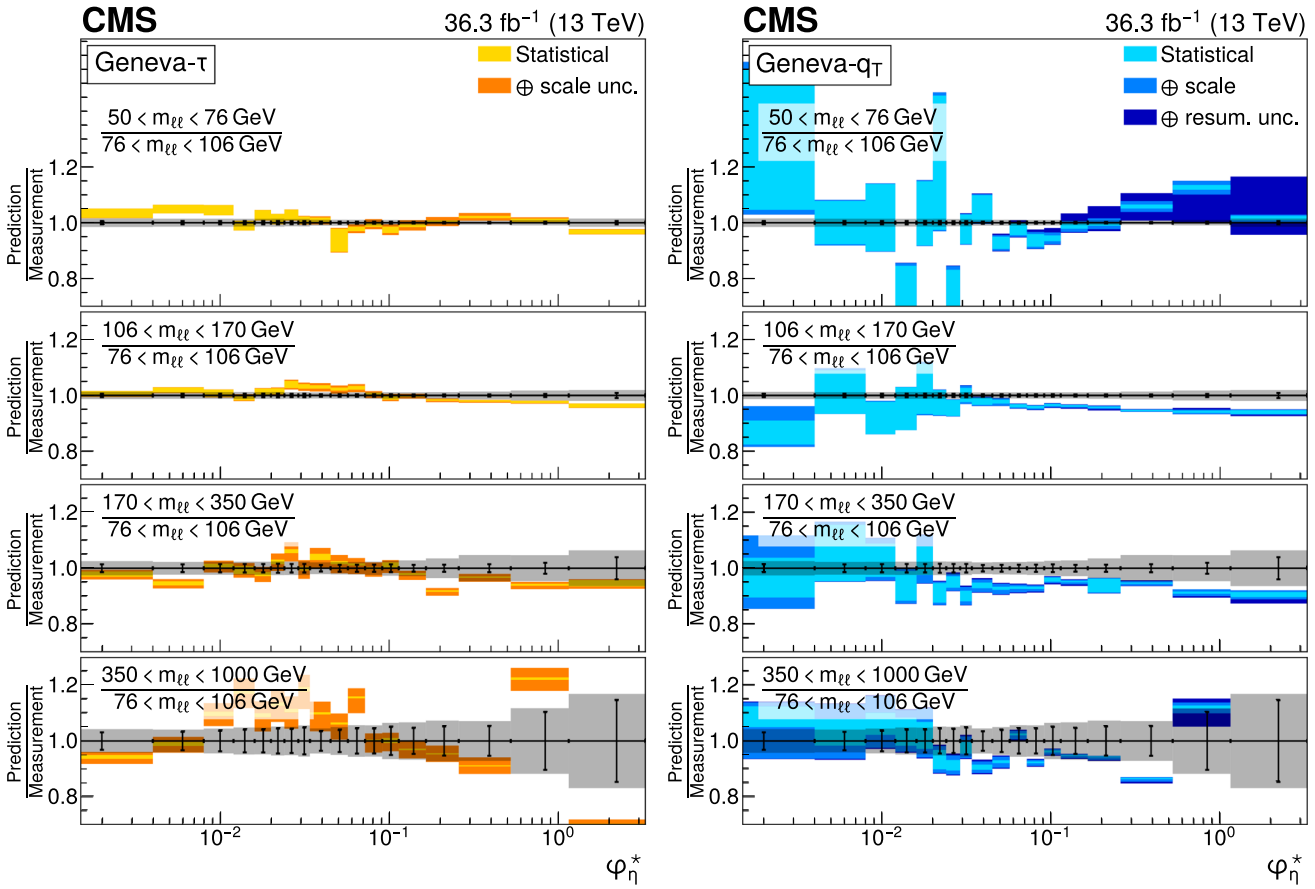

Fig. 24 Ratios of differential cross sections in $\varphi_\eta^*(\ell\ell)$ for invariant $m_{\ell\ell}$ with respect to the peak region $76 < m_{\ell\ell} < 106$ GeV. Compared to model predictions from GENEVA-τ (left) and GENEVA-q_T (right). Details on the presentation of the results are given in Fig. 8 caption

Data Availability Statement This manuscript has no associated data or the data will not be deposited. [Authors' comment: Release and preservation of data used by the CMS Collaboration as the basis for publications is guided by the CMS policy as stated in https://cms-docdb.cern.ch/cgi-bin/PublicDocDB/RetrieveFile?docid=6032&filename=CMSDataPolicyV1.2.pdf&version=2 CMS data preservation, re-use and open access policy.]

Declarations

Conflict of interest The authors declare that they have no conflict of interest.

Funded by SCOAP^3. SCOAP^3 supports the goals of the International Year of Basic Sciences for Sustainable Development.

Appendix A: Comparisons to other models

In this section, comparisons of the obtained measurement results with predictions from a more recent parton branching (PB) TMD method from CASCADE are presented. The predictions are based on MG5_aMC ME up to three partons at LO in QCD with multi-jet merging [89]. The ratio of the predictions over the data are presented in Fig. 25. The comparisons to predictions for the ratio of the cross sections for invariant masses outside the Z boson peak to the distribution within the Z boson peak ($76 < m_{\ell\ell} < 106$ GeV) are shown in Fig. 26.

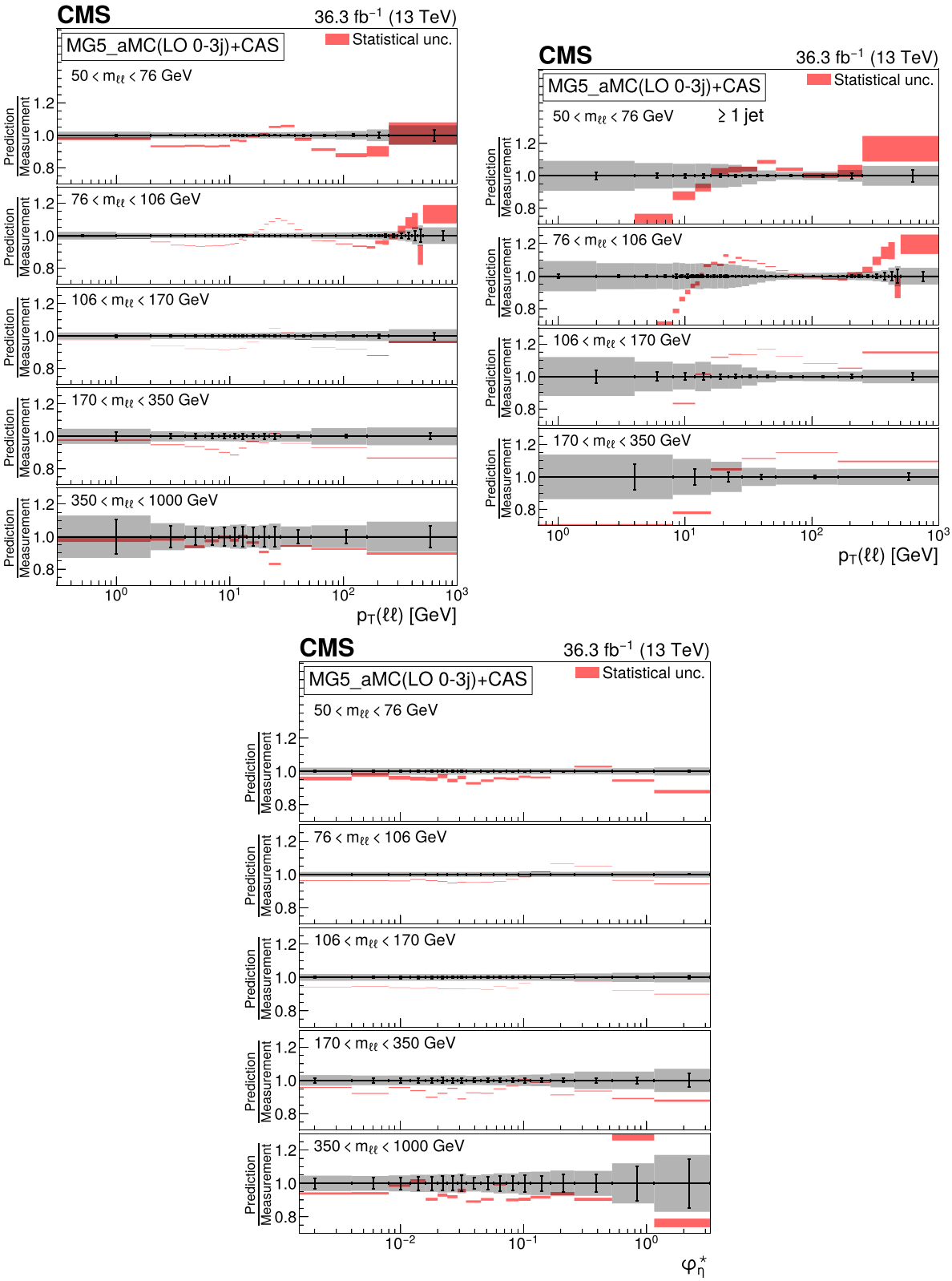

Fig. 25 The ratio of MG5_aMC (0, 1, 2 and 3 jets at LO) + PB (CASCADE) predictions to the measured differential cross sections in $p_T(\ell\ell)$ (upper left), in $p_T(\ell\ell)$ for the one or more jets case (upper right), and in φ^*_η (bottom) are presented for various $m_{\ell\ell}$ ranges. The error bars correspond to the statistical uncertainty of the measurement and the shaded bands to the total experimental uncertainty. The light color band around CASCADE prediction corresponds to the statistical uncertainty of the simulation

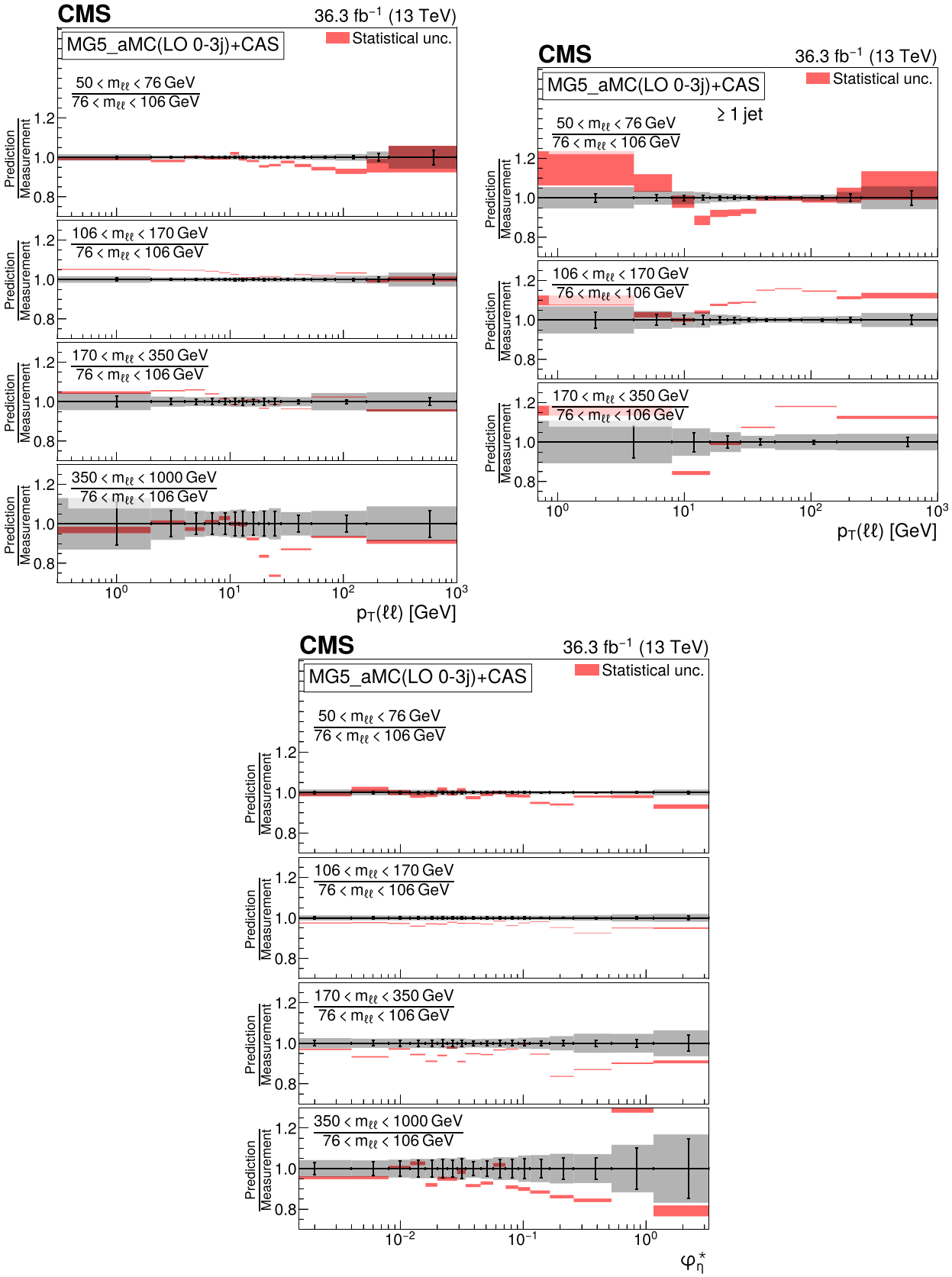

Fig. 26 The ratio of MG5_aMC (0, 1, 2 and 3 jets at LO) + PB (CASCADE) predictions to the ratios of differential cross sections for $m_{\ell\ell}$ ranges with respect to the peak region in $p_T(\ell\ell)$ (upper left), in $p_T(\ell\ell)$ for the one or more jets case (upper right), and in φ^*_η (bottom). The error bars correspond to the statistical uncertainty of the measurement and the shaded bands to the total experimental uncertainty. The light color band around CASCADE prediction corresponds to the statistical uncertainty of the simulation

References

1. S.D. Drell, T.-M. Yan, Massive lepton pair production in hadron–hadron collisions at high energies. Phys. Rev. Lett. **25**, 316 (1970). https://doi.org/10.1103/PhysRevLett.25.316 (**Erratum: 10.1103/PhysRevLett.25.902.2**)
2. Y.L. Dokshitzer, D. Diakonov, S.I. Troyan, On the transverse momentum distribution of massive lepton pairs. Phys. Lett. B **79**, 269 (1978). https://doi.org/10.1016/0370-2693(78)90240-X
3. J.C. Collins, D.E. Soper, G.F. Sterman, Transverse momentum distribution in Drell–Yan pair and W and Z boson production. Nucl. Phys. B **250**, 199 (1985). https://doi.org/10.1016/0550-3213(85)90479-1
4. R. Hamberg, W.L. van Neerven, T. Matsuura, A complete calculation of the order α_s^2 correction to the Drell–Yan K-factor. Nucl. Phys. B **359**, 343 (1991). https://doi.org/10.1016/S0550-3213(02)00814-3 (**Erratum: 10.1016/0550-3213(91)90064-5**)
5. S. Catani et al., Vector boson production at hadron colliders: a fully exclusive QCD calculation at NNLO. Phys. Rev. Lett. **103**, 082001 (2009). https://doi.org/10.1103/PhysRevLett.103.082001. arXiv:0903.2120
6. S. Catani, M. Grazzini, An NNLO subtraction formalism in hadron collisions and its application to Higgs boson production at the LHC. Phys. Rev. Lett. **98**, 222002 (2007). https://doi.org/10.1103/PhysRevLett.98.222002. arXiv:hep-ph/0703012
7. K. Melnikov, F. Petriello, Electroweak gauge boson production at hadron colliders through $\mathcal{O}(\alpha_s^2)$. Phys. Rev. D **74**, 114017 (2006). https://doi.org/10.1103/PhysRevD.74.114017. arXiv:hep-ph/0609070
8. A. Bacchetta et al., Extraction of partonic transverse momentum distributions from semi-inclusive deep-inelastic scattering, Drell–Yan and Z-boson production. JHEP **06**, 081 (2017). https://doi.org/10.1007/JHEP06(2017)081 (**Erratum: JHEP 06, 051 (2019)**). arXiv:1703.10157
9. A. Bacchetta et al., Transverse-momentum-dependent parton distributions up to N^{3}LL from Drell–Yan data. JHEP **07**, 117 (2020). https://doi.org/10.1007/JHEP07(2020)117. arXiv:1912.07550
10. S. Camarda et al., DYTurbo: fast predictions for Drell–Yan processes. Eur. Phys. J. C **80**, 251 (2020). https://doi.org/10.1140/epjc/s10052-020-7757-5 (**Erratum: Eur. Phys. J. C 80, 440 (2020)**). arXiv:1910.07049
11. W. Bizoń et al., Fiducial distributions in Higgs and Drell–Yan production at N^{3}LL+NNLO. JHEP **12**, 132 (2018). https://doi.org/10.1007/JHEP12(2018)132. arXiv:1805.05916
12. M.A. Ebert, J.K.L. Michel, I.W. Stewart, F.J. Tackmann, Drell–Yan q_T resummation of fiducial power corrections at N^{3}LL. JHEP **04**, 102 (2021). https://doi.org/10.1007/JHEP04(2021)102. arXiv:2006.11382
13. T. Becher, T. Neumann, Fiducial q_T resummation of color-singlet processes at N^{3}LL+NNLO. JHEP **03**, 199 (2021). https://doi.org/10.1007/JHEP03(2021)199. arXiv:2009.11437
14. F. Hautmann et al., Soft-gluon resolution scale in QCD evolution equations. Phys. Lett. B **772**, 446 (2017). https://doi.org/10.1016/j.physletb.2017.07.005. arXiv:1704.01757
15. F. Hautmann et al., Collinear and TMD quark and gluon densities from parton branching solution of QCD evolution equations. JHEP **01**, 070 (2018). https://doi.org/10.1007/JHEP01(2018)070. arXiv:1708.03279
16. A. Banfi et al., Optimisation of variables for studying dilepton transverse momentum distributions at hadron colliders. Eur. Phys. J. C **71**, 1600 (2011). https://doi.org/10.1140/epjc/s10052-011-1600-y. arXiv:1009.1580
17. A. Banfi, M. Dasgupta, S. Marzani, L. Tomlinson, Predictions for Drell–Yan ϕ^* and Q_T observables at the LHC. Phys. Lett. B **715**, 152 (2012). https://doi.org/10.1016/j.physletb.2012.07.035. arXiv:1205.4760
18. S. Marzani, Q_T and ϕ^* observables in Drell–Yan processes. Eur. Phys. J. Web Conf. **49**, 14007 (2013). https://doi.org/10.1051/epjconf/20134914007
19. L. Moureaux, Measurement of the transverse momentum of Drell–Yan lepton pairs over a wide mass range in proton–proton collisions at $\sqrt{s} = 13$ TeV in CMS. Ph.D. thesis, Université libre de Bruxelles, 2021. Presented 24 Sep 2021
20. CMS Collaboration, Measurement of the inclusive W and Z production cross sections in pp collisions at $\sqrt{s} = 7$ TeV. JHEP **10**, 132 (2011). https://doi.org/10.1007/JHEP10(2011)132. arXiv:1107.4789
21. CMS Collaboration, Measurement of the Drell–Yan cross section in pp collisions at $\sqrt{s} = 7$ TeV. JHEP **10**, 007 (2011). https://doi.org/10.1007/JHEP10(2011)007. arXiv:1108.0566
22. CMS Collaboration, Measurement of the differential and double-differential Drell–Yan cross sections in proton–proton collisions at $\sqrt{s} = 7$ TeV. JHEP **12**, 030 (2013). https://doi.org/10.1007/JHEP12(2013)030. arXiv:1310.7291
23. CMS Collaboration, Measurements of differential and double-differential Drell–Yan cross sections in proton–proton collisions at 8 TeV. Eur. Phys. J. C **75**, 147 (2015). https://doi.org/10.1140/epjc/s10052-015-3364-2. arXiv:1412.1115
24. CMS Collaboration, Measurement of the Z boson differential cross section in transverse momentum and rapidity in proton–proton collisions at 8 TeV. Phys. Lett. B **749**, 187 (2015). https://doi.org/10.1016/j.physletb.2015.07.065. arXiv:1504.03511
25. CMS Collaboration, Measurement of the differential Drell–Yan cross section in proton–proton collisions at $\sqrt{s} = 13$ TeV. JHEP **12**, 059 (2019). https://doi.org/10.1007/JHEP12(2019)059. arXiv:1812.10529
26. CMS Collaboration, Measurements of differential Z boson production cross sections in proton–proton collisions at $\sqrt{s} = 13$ TeV. JHEP **12**, 061 (2019). https://doi.org/10.1007/JHEP12(2019)061. arXiv:1909.04133
27. ATLAS Collaboration, Measurement of the inclusive $W^{\pm}$ and Z/γ^* cross sections in the electron and muon decay channels in pp collisions at $\sqrt{s} = 7$ TeV with the ATLAS detector. Phys. Rev. D **85**, 072004 (2012). https://doi.org/10.1103/PhysRevD.85.072004. arXiv:1109.5141
28. ATLAS Collaboration, Measurement of the high-mass Drell–Yan differential cross-section in pp collisions at $\sqrt{s} = 7$ TeV with the ATLAS detector. Phys. Lett. B **725**, 223 (2013). https://doi.org/10.1016/j.physletb.2013.07.049. arXiv:1305.4192
29. ATLAS Collaboration, Measurement of the Z/γ^* boson transverse momentum distribution in pp collisions at $\sqrt{s} = 7$ TeV with the ATLAS detector. JHEP **09**, 145 (2014). https://doi.org/10.1007/JHEP09(2014)145. arXiv:1406.3660
30. ATLAS Collaboration, Measurement of the low-mass Drell–Yan differential cross section at $\sqrt{s} = 7$ TeV using the ATLAS detector. JHEP **06**, 112 (2014). https://doi.org/10.1007/JHEP06(2014)112. arXiv:1404.1212
31. ATLAS Collaboration, Measurement of the transverse momentum and ϕ_η^* distributions of Drell–Yan lepton pairs in proton–proton collisions at $\sqrt{s} = 8$ TeV with the ATLAS detector. Eur. Phys. J. C **76**, 291 (2016). https://doi.org/10.1140/epjc/s10052-016-4070-4. arXiv:1512.02192
32. ATLAS Collaboration, Precision measurement and interpretation of inclusive W^+, W^- and Z/γ^* production cross sections with the ATLAS detector. Eur. Phys. J. C **77**, 367 (2017). https://doi.org/10.1140/epjc/s10052-017-4911-9. arXiv:1612.03016
33. ATLAS Collaboration, Measurement of the transverse momentum distribution of Drell–Yan lepton pairs in proton–proton collisions at $\sqrt{s} = 13$ TeV with the ATLAS detector.

Eur. Phys. J. C **80**, 616 (2020). https://doi.org/10.1140/epjc/s10052-020-8001-z. arXiv:1912.02844
34. LHCb Collaboration, Inclusive W and Z production in the forward region at $\sqrt{s} = 7$ TeV. JHEP **06**, 058 (2012). https://doi.org/10.1007/JHEP06(2012)058. arXiv:1204.1620
35. LHCb Collaboration, Measurement of the cross-section for $Z \to e^+e^-$ production in pp collisions at $\sqrt{s} = 7$ TeV. JHEP **02**, 106 (2013). https://doi.org/10.1007/JHEP02(2013)106. arXiv:1212.4620
36. LHCb Collaboration, Measurement of the forward Z boson production cross-section in pp collisions at $\sqrt{s} = 7$ TeV. JHEP **08**, 039 (2015). https://doi.org/10.1007/JHEP08(2015)039. arXiv:1505.07024
37. LHCb Collaboration, Measurement of forward W and Z boson production in pp collisions at $\sqrt{s} = 8$ TeV. JHEP **01**, 155 (2016). https://doi.org/10.1007/JHEP01(2016)155. arXiv:1511.08039
38. LHCb Collaboration, Measurement of the forward Z boson production cross-section in pp collisions at $\sqrt{s} = 13$ TeV. JHEP **09**, 136 (2016). https://doi.org/10.1007/JHEP09(2016)136. arXiv:1607.06495
39. CDF Collaboration, The transverse momentum and total cross section of e^+e^- pairs in the Z boson region from $p\bar{p}$ collisions at $\sqrt{s} = 1.8$ TeV. Phys. Rev. Lett. **84**, 845 (2000). https://doi.org/10.1103/PhysRevLett.84.845. arXiv:hep-ex/0001021
40. D0 Collaboration, Differential production cross section of Z bosons as a function of transverse momentum at $\sqrt{s} = 1.8$ TeV. Phys. Rev. Lett. **84**, 2792 (2000). https://doi.org/10.1103/PhysRevLett.84.2792. arXiv:hep-ex/9909020
41. D0 Collaboration, Measurement of the shape of the boson transverse momentum distribution in $p\bar{p} \to Z/\gamma^* \to e^+e^- + X$ events produced at $\sqrt{s} = 1.96$ TeV. Phys. Rev. Lett. **100**, 102002 (2008). https://doi.org/10.1103/PhysRevLett.100.102002. arXiv:0712.0803
42. D0 Collaboration, Measurement of the normalized $Z/\gamma^* \to \mu^+\mu^-$ transverse momentum distribution in $p\bar{p}$ collisions at $\sqrt{s} = 1.96$ TeV'. Phys. Lett. B **693**, 522 (2010). https://doi.org/10.1016/j.physletb.2010.09.012. arXiv:1006.0618
43. D0 Collaboration, Precise study of the Z/γ^* boson transverse momentum distribution in $p\bar{p}$ collisions using a novel technique. Phys. Rev. Lett. **106**, 122001 (2011). https://doi.org/10.1103/PhysRevLett.106.122001. arXiv:1010.0262
44. CDF Collaboration, Transverse momentum cross section of e^+e^- pairs in the Z-boson region from $p\bar{p}$ collisions at $\sqrt{s} = 1.96$ TeV. Phys. Rev. D **86**, 052010 (2012). https://doi.org/10.1103/PhysRevD.86.052010. arXiv:1207.7138
45. D0 Collaboration, Measurement of the ϕ^*_η distribution of muon pairs with masses between 30 and 500 GeV in 10.4fb^{-1} of $p\bar{p}$ collisions. Phys. Rev. D **91**, 072002 (2015). https://doi.org/10.1103/PhysRevD.91.072002. arXiv:1410.8052
46. CMS Collaboration, Particle-flow reconstruction and global event description with the CMS detector. JINST **12**, P10003 (2017). https://doi.org/10.1088/1748-0221/12/10/P10003. arXiv:1706.04965
47. CMS Collaboration, Electron and photon reconstruction and identification with the CMS experiment at the CERN LHC. JINST **16**, P05014 (2021). https://doi.org/10.1088/1748-0221/16/05/P05014. arXiv:2012.06888
48. CMS Collaboration, Performance of the CMS muon detector and muon reconstruction with proton-proton collisions at $\sqrt{s} = 13$ TeV. JINST **13**, P06015 (2018). https://doi.org/10.1088/1748-0221/13/06/P06015. arXiv:1804.04528
49. A. Bodek et al., Extracting muon momentum scale corrections for hadron collider experiments. Eur. Phys. J. C **72**, 2194 (2012). https://doi.org/10.1140/epjc/s10052-012-2194-8. arXiv:1208.3710
50. M. Cacciari, G.P. Salam, G. Soyez, The anti-k_T jet clustering algorithm. JHEP **04**, 063 (2008). https://doi.org/10.1088/1126-6708/2008/04/063. arXiv:0802.1189
51. M. Cacciari, G.P. Salam, G. Soyez, FastJet user manual. Eur. Phys. J. C **72**, 1896 (2012). https://doi.org/10.1140/epjc/s10052-012-1896-2. arXiv:1111.6097
52. CMS Collaboration, "Technical proposal for the Phase-II upgrade of the Compact Muon Solenoid", CMS Technical Proposal CERN-LHCC-2015-010, CMS-TDR-15-02 (2015)
53. CMS Collaboration, Performance of the CMS Level-1 trigger in proton–proton collisions at $\sqrt{s} = 13$ TeV. JINST **15**, P10017 (2020). https://doi.org/10.1088/1748-0221/15/10/P10017. arXiv:2006.10165
54. CMS Collaboration, The CMS trigger system. JINST **12**, P01020 (2017). https://doi.org/10.1088/1748-0221/12/01/P01020. arXiv:1609.02366
55. CMS Collaboration, The CMS experiment at the CERN LHC. JINST **3**, S08004 (2008). https://doi.org/10.1088/1748-0221/3/08/S08004
56. CMS Collaboration, Pileup mitigation at CMS in 13 TeV data. JINST **15**, P09018 (2020). https://doi.org/10.1088/1748-0221/15/09/P09018. arXiv:2003.00503
57. CMS Collaboration, Identification of heavy-flavour jets with the CMS detector in pp collisions at 13 TeV. JINST **13**, P05011 (2018). https://doi.org/10.1088/1748-0221/13/05/P05011. arXiv:1712.07158
58. J. Alwall et al., The automated computation of tree-level and next-to-leading order differential cross sections, and their matching to parton shower simulations. JHEP **07**, 079 (2014). https://doi.org/10.1007/JHEP07(2014)079. arXiv:1405.0301
59. R. Frederix, S. Frixione, Merging meets matching in MC@NLO. JHEP **12**, 061 (2012). https://doi.org/10.1007/JHEP12(2012)061. arXiv:1209.6215
60. T. Sjöstrand et al., An introduction to PYTHIA 8.2. Comput. Phys. Commun. **191**, 159 (2015). https://doi.org/10.1016/j.cpc.2015.01.024. arXiv:1410.3012
61. CMS Collaboration, Event generator tunes obtained from underlying event and multiparton scattering measurements. Eur. Phys. J. C **76**, 155 (2016). https://doi.org/10.1140/epjc/s10052-016-3988-x. arXiv:1512.00815
62. NNPDF Collaboration, Parton distributions for the LHC Run II. JHEP **04**, 040 (2015). https://doi.org/10.1007/JHEP04(2015)040. arXiv:1410.8849
63. P. Nason, A new method for combining NLO QCD with shower Monte Carlo algorithms. JHEP **11**, 040 (2004). https://doi.org/10.1088/1126-6708/2004/11/040. arXiv:hep-ph/0409146
64. S. Frixione, P. Nason, C. Oleari, Matching NLO QCD computations with parton shower simulations: the POWHEG method. JHEP **11**, 070 (2007). https://doi.org/10.1088/1126-6708/2007/11/070. arXiv:0709.2092
65. S. Alioli, P. Nason, C. Oleari, E. Re, A general framework for implementing NLO calculations in shower Monte Carlo programs: the POWHEG BOX. JHEP **06**, 043 (2010). https://doi.org/10.1007/JHEP06(2010)043. arXiv:1002.2581
66. S. Frixione, P. Nason, G. Ridolfi, A positive-weight next-to-leading-order Monte Carlo for heavy flavour hadroproduction. JHEP **09**, 126 (2007). https://doi.org/10.1088/1126-6708/2007/09/126. arXiv:0707.3088
67. P. Nason, G. Zanderighi, W^+W^-, WZ and ZZ production in the powheg-box-v2. Eur. Phys. J. C **74**, 2702 (2014). https://doi.org/10.1140/epjc/s10052-013-2702-5. arXiv:1311.1365
68. J.A.M. Vermaseren, Two photon processes at very high-energies. Nucl. Phys. B **229**, 347 (1983). https://doi.org/10.1016/0550-3213(83)90336-X

69. S.P. Baranov, O. Duenger, H. Shooshtari, J.A.M. Vermaseren, LPAIR: a generator for lepton pair production, In Workshop on Physics at HERA (1991), p. 1478
70. A. Suri, D.R. Yennie, The space-time phenomenology of photon absorption and inelastic electron scattering. Ann. Phys. **72**, 243 (1972). https://doi.org/10.1016/0003-4916(72)90242-4
71. J.M. Campbell, R.K. Ellis, W.T. Giele, A multi-threaded version of MCFM. Eur. Phys. J. C **75**, 246 (2015). https://doi.org/10.1140/epjc/s10052-015-3461-2. arXiv:1503.06182
72. T. Gehrmann et al., W^+W^- production at hadron colliders in next to next to leading order QCD. Phys. Rev. Lett. **113**, 212001 (2014). https://doi.org/10.1103/PhysRevLett.113.212001. arXiv:1408.5243
73. M. Czakon, A. Mitov, Top++: a program for the calculation of the top-pair cross-section at hadron colliders. Comput. Phys. Commun. **185**, 2930 (2014). https://doi.org/10.1016/j.cpc.2014.06.021. arXiv:1112.5675
74. Geant4 Collaboration, Geant4—a simulation toolkit. Nucl. Instrum. Methods A **506**, 250 (2003). https://doi.org/10.1016/S0168-9002(03)01368-8
75. G. D'Agostini, A multidimensional unfolding method based on Bayes' theorem. Nucl. Instrum. Methods A **362**, 487 (1995). https://doi.org/10.1016/0168-9002(95)00274-X
76. CMS Collaboration, Measurement of differential cross sections for Z boson production in association with jets in proton–proton collisions at $\sqrt{s} = 13$ TeV. Eur. Phys. J. C **78**, 965 (2018). https://doi.org/10.1140/epjc/s10052-018-6373-0. arXiv:1804.05252
77. CMS Collaboration, Measurements of differential production cross sections for a Z boson in association with jets in pp collisions at $\sqrt{s} = 8$ TeV. JHEP **04**, 022 (2017). https://doi.org/10.1007/JHEP04(2017)022. arXiv:1611.03844
78. CMS Collaboration, Precision luminosity measurement in proton–proton collisions at $\sqrt{s} = 13$ TeV in 2015 and 2016 at CMS. Eur. Phys. J. C **81**, 800 (2021). https://doi.org/10.1140/epjc/s10052-021-09538-2. arXiv:2104.01927
79. A. Manohar, P. Nason, G.P. Salam, G. Zanderighi, How bright is the proton? A precise determination of the photon parton distribution function. Phys. Rev. Lett. **117**, 242002 (2016). https://doi.org/10.1103/PhysRevLett.117.242002. arXiv:1607.04266
80. A.V. Manohar, P. Nason, G.P. Salam, G. Zanderighi, The photon content of the proton. JHEP **12**, 046 (2017). https://doi.org/10.1007/JHEP12(2017)046. arXiv:1708.01256
81. P.F. Monni et al., MiNNLO$_{\rm PS}$: a new method to match NNLO QCD to parton showers. JHEP **05**, 143 (2020). https://doi.org/10.1007/JHEP05(2020)143. arXiv:1908.06987
82. P.F. Monni, E. Re, M. Wiesemann, MiNNLO$_{\rm PS}$: optimizing $2 \to 1$ hadronic processes. Eur. Phys. J. C **80**, 1075 (2020). https://doi.org/10.1140/epjc/s10052-020-08658-5. arXiv:2006.04133
83. NNPDF Collaboration, Parton distributions from high-precision collider data. Eur. Phys. J. C **77**, 663 (2017). https://doi.org/10.1140/epjc/s10052-017-5199-5. arXiv:1706.00428
84. CMS Collaboration, Extraction and validation of a new set of CMS PYTHIA8 tunes from underlying-event measurements. Eur. Phys. J. C **80**, 4 (2020). https://doi.org/10.1140/epjc/s10052-019-7499-4. arXiv:1903.12179
85. S. Baranov et al., CASCADE3 A Monte Carlo event generator based on TMDs. Eur. Phys. J. C **81**, 425 (2021). https://doi.org/10.1140/epjc/s10052-021-09203-8. arXiv:2101.10221
86. A. Bermudez Martinez et al., Production of Z-bosons in the parton branching method. Phys. Rev. D **100**, 074027 (2019). https://doi.org/10.1103/PhysRevD.100.074027. arXiv:1906.00919
87. A. Bermudez Martinez et al., Collinear and TMD parton densities from fits to precision DIS measurements in the parton branching method. Phys. Rev. D **99**, 074008 (2019). https://doi.org/10.1103/PhysRevD.99.074008. arXiv:1804.11152
88. T. Sjöstrand, S. Mrenna, P.Z. Skands, PYTHIA 6.4 physics and manual. JHEP **05**, 026 (2006). https://doi.org/10.1088/1126-6708/2006/05/026. arXiv:hep-ph/0603175
89. A. Bermudez Martinez, F. Hautmann, M.L. Mangano, TMD evolution and multi-jet merging. Phys. Lett. B **822**, 136700 (2021). https://doi.org/10.1016/j.physletb.2021.136700. arXiv:2107.01224
90. I. Scimemi, A. Vladimirov, Analysis of vector boson production within TMD factorization. Eur. Phys. J. C **78**, 89 (2018). https://doi.org/10.1140/epjc/s10052-018-5557-y. arXiv:1706.01473
91. I. Scimemi, A. Vladimirov, Non-perturbative structure of semi-inclusive deep-inelastic and Drell–Yan scattering at small transverse momentum. JHEP **06**, 137 (2020). https://doi.org/10.1007/JHEP06(2020)137. arXiv:1912.06532
92. "arTeMiDe public repository". https://github.com/VladimirovAlexey/artemide-public (2020)
93. S. Alioli et al., Combining higher-order resummation with multiple NLO calculations and parton showers in GENEVA. JHEP **09**, 120 (2013). https://doi.org/10.1007/jhep09(2013)120. arXiv:1211.7049
94. S. Alioli et al., Drell–Yan production at NNLL'+NNLO matched to parton showers. Phys. Rev. D **92**, 094020 (2015). https://doi.org/10.1103/PhysRevD.92.094020. arXiv:1508.01475
95. S. Alioli et al., Matching NNLO predictions to parton showers using N^{3}LL color-singlet transverse momentum resummation in GENEVA. Phys. Rev. D **104**, 094020 (2021). https://doi.org/10.1103/PhysRevD.104.094020. arXiv:2102.08390
96. I.W. Stewart, F.J. Tackmann, W.J. Waalewijn, N-jettiness: an inclusive event shape to veto jets. Phys. Rev. Lett. **105**, 092002 (2010). https://doi.org/10.1103/PhysRevLett.105.092002. arXiv:1004.2489
97. P.F. Monni, E. Re, P. Torrielli, Higgs transverse-momentum resummation in direct space. Phys. Rev. Lett. **116**, 242001 (2016). https://doi.org/10.1103/PhysRevLett.116.242001. arXiv:1604.02191
98. W. Bizon et al., Momentum-space resummation for transverse observables and the Higgs $p_\perp$ at N^{3}LL+NNLO. JHEP **02**, 108 (2018). https://doi.org/10.1007/JHEP02(2018)108. arXiv:1705.09127
99. J. Butterworth et al., PDF4LHC recommendations for LHC Run II. J. Phys. G **43**, 023001 (2016). https://doi.org/10.1088/0954-3899/43/2/023001. arXiv:1510.03865
100. "HEPData record for this analysis" (2022). https://doi.org/10.17182/hepdata.115656

CMS Collaboration

Yerevan Physics Institute, Yerevan, Armenia
A. Tumasyan

Institut für Hochenergiephysik, Vienna, Austria
W. Adam, J. W. Andrejkovic, T. Bergauer, S. Chatterjee, M. Dragicevic, A. Escalante Del Valle, R. Frühwirth[1], M. Jeitler[1], N. Krammer, L. Lechner, D. Liko, I. Mikulec, P. Paulitsch, F. M. Pitters, J. Schieck[1], R. Schöfbeck, M. Spanring, S. Templ, W. Waltenberger, C. -E. Wulz[1]

Universiteit Antwerpen, Antwerpen, Belgium
M. R. Darwish[2], E. A. De Wolf, T. Janssen, T. Kello[3], A. Lelek, H. Rejeb Sfar, P. Van Mechelen, S. Van Putte, N. Van Remortel

Vrije Universiteit Brussel, Brussels, Belgium
F. Blekman, E. S. Bols, J. D'Hondt, M. Delcourt, H. El Faham, S. Lowette, S. Moortgat, A. Morton, D. Müller, A. R. Sahasransu, S. Tavernier, W. Van Doninck, P. Van Mulders

Université Libre de Bruxelles, Brussels, Belgium
D. Beghin, B. Bilin, B. Clerbaux, G. De Lentdecker, L. Favart, A. Grebenyuk, A. K. Kalsi, K. Lee, M. Mahdavikhorrami, I. Makarenko, L. Moureaux, L. Pétré, A. Popov, N. Postiau, E. Starling, L. Thomas, M. Vanden Bemden, C. Vander Velde, P. Vanlaer, D. Vannerom, L. Wezenbeek

Ghent University, Ghent, Belgium
T. Cornelis, D. Dobur, J. Knolle, L. Lambrecht, G. Mestdach, M. Niedziela, C. Roskas, A. Samalan, K. Skovpen, M. Tytgat, B. Vermassen, M. Vit

Université Catholique de Louvain, Louvain-la-Neuve, Belgium
A. Bethani, G. Bruno, F. Bury, C. Caputo, P. David, C. Delaere, I. S. Donertas, A. Giammanco, K. Jaffel, Sa. Jain, V. Lemaitre, K. Mondal, J. Prisciandaro, A. Taliercio, M. Teklishyn, T. T. Tran, P. Vischia, S. Wertz

Centro Brasileiro de Pesquisas Fisicas, Rio de Janeiro, Brazil
G. A. Alves, C. Hensel, A. Moraes

Universidade do Estado do Rio de Janeiro, Rio de Janeiro, Brazil
W. L. Aldá Júnior, M. Alves Gallo Pereira, M. Barroso Ferreira Filho, H. Brandao Malbouisson, W. Carvalho, J. Chinellato[4], E. M. Da Costa, G. G. Da Silveira[5], D. De Jesus Damiao, S. Fonseca De Souza, D. Matos Figueiredo, C. Mora Herrera, K. Mota Amarilo, L. Mundim, H. Nogima, P. Rebello Teles, A. Santoro, S. M. Silva Do Amaral, A. Sznajder, M. Thiel, F. Torres Da Silva De Araujo, A. Vilela Pereira

Universidade Estadual Paulista, Universidade Federal do ABC, São Paulo, Brazil
C. A. Bernardes[5], L. Calligaris, T. R. Fernandez Perez Tomei, E. M. Gregores, D. S. Lemos, P. G. Mercadante, S. F. Novaes, Sandra S. Padula

Institute for Nuclear Research and Nuclear Energy, Bulgarian Academy of Sciences, Sofia, Bulgaria
A. Aleksandrov, G. Antchev, R. Hadjiiska, P. Iaydjiev, M. Misheva, M. Rodozov, M. Shopova, G. Sultanov

University of Sofia, Sofia, Bulgaria
A. Dimitrov, T. Ivanov, L. Litov, B. Pavlov, P. Petkov, A. Petrov

Beihang University, Beijing, China
T. Cheng, Q. Guo, T. Javaid[6], M. Mittal, H. Wang, L. Yuan

Department of Physics, Tsinghua University, Beijing, China
M. Ahmad, G. Bauer, C. Dozen, Z. Hu, J. Martins[7], Y. Wang, K. Yi[8,9]

Institute of High Energy Physics, Beijing, China
E. Chapon, G. M. Chen[6], H. S. Chen[6], M. Chen, F. Iemmi, A. Kapoor, D. Leggat, H. Liao, Z.-A. Liu[10], V. Milosevic, F. Monti, R. Sharma, J. Tao, J. Thomas-Wilsker, J. Wang, H. Zhang, S. Zhang[6], J. Zhao

State Key Laboratory of Nuclear Physics and Technology, Peking University, Beijing, China
A. Agapitos, Y. An, Y. Ban, C. Chen, A. Levin, Q. Li, X. Lyu, Y. Mao, S. J. Qian, D. Wang, Q. Wang, J. Xiao

Sun Yat-Sen University, Guangzhou, China
M. Lu, Z. You

Institute of Modern Physics and Key Laboratory of Nuclear Physics and Ion-beam Application (MOE), Fudan University, Shanghai, China
X. Gao[3], H. Okawa

Zhejiang University, Hangzhou, Zhejiang, China
Z. Lin, M. Xiao

Universidad de Los Andes, Bogotá, Colombia
C. Avila, A. Cabrera, C. Florez, J. Fraga

Universidad de Antioquia, Medellín, Colombia
J. Mejia Guisao, F. Ramirez, J. D. Ruiz Alvarez, C. A. Salazar González

Faculty of Electrical Engineering, Mechanical Engineering and Naval Architecture, University of Split, Split, Croatia
D. Giljanovic, N. Godinovic, D. Lelas, I. Puljak

Faculty of Science, University of Split, Split, Croatia
Z. Antunovic, M. Kovac, T. Sculac

Institute Rudjer Boskovic, Zagreb, Croatia
V. Brigljevic, D. Ferencek, D. Majumder, M. Roguljic, A. Starodumov[11], T. Susa

University of Cyprus, Nicosia, Cyprus
A. Attikis, K. Christoforou, E. Erodotou, A. Ioannou, G. Kole, M. Kolosova, S. Konstantinou, J. Mousa, C. Nicolaou, F. Ptochos, P. A. Razis, H. Rykaczewski, H. Saka

Charles University, Prague, Czech Republic
M. Finger[11], M. Finger Jr.[11], A. Kveton

Escuela Politecnica Nacional, Quito, Ecuador
E. Ayala

Universidad San Francisco de Quito, Quito, Ecuador
E. Carrera Jarrin

Academy of Scientific Research and Technology of the Arab Republic of Egypt, Egyptian Network of High Energy Physics, Cairo, Egypt
A. A. Abdelalim[12,13], S. Elgammal[14]

Center for High Energy Physics (CHEP-FU), Fayoum University, El-Fayoum, Egypt
A. Lotfy, M. A. Mahmoud

National Institute of Chemical Physics and Biophysics, Tallinn, Estonia
S. Bhowmik, R. K. Dewanjee, K. Ehataht, M. Kadastik, S. Nandan, C. Nielsen, J. Pata, M. Raidal, L. Tani, C. Veelken

Department of Physics, University of Helsinki, Helsinki, Finland
P. Eerola, L. Forthomme, H. Kirschenmann, K. Osterberg, M. Voutilainen

Helsinki Institute of Physics, Helsinki, Finland
S. Bharthuar, E. Brücken, F. Garcia, J. Havukainen, M. S. Kim, R. Kinnunen, T. Lampén,

K. Lassila-Perini, S. Lehti, T. Lindén, M. Lotti, L. Martikainen, M. Myllymäki, J. Ott, H. Siikonen, E. Tuominen, J. Tuominiemi

Lappeenranta-Lahti University of Technology, Lappeenranta, Finland
P. Luukka, H. Petrow, T. Tuuva

IRFU, CEA, Université Paris-Saclay, Gif-sur-Yvette, France
C. Amendola, M. Besancon, F. Couderc, M. Dejardin, D. Denegri, J. L. Faure, F. Ferri, S. Ganjour, A. Givernaud, P. Gras, G. Hamel de Monchenault, P. Jarry, B. Lenzi, E. Locci, J. Malcles, J. Rander, A. Rosowsky, M. Ö. Sahin, A. Savoy-Navarro[15], M. Titov, G. B. Yu

Laboratoire Leprince-Ringuet, CNRS/IN2P3, Ecole Polytechnique, Institut Polytechnique de Paris, Palaiseau, France
S. Ahuja, F. Beaudette, M. Bonanomi, A. Buchot Perraguin, P. Busson, A. Cappati, C. Charlot, O. Davignon, B. Diab, G. Falmagne, S. Ghosh, R. Granier de Cassagnac, A. Hakimi, I. Kucher, J. Motta, M. Nguyen, C. Ochando, P. Paganini, J. Rembser, R. Salerno, J. B. Sauvan, Y. Sirois, A. Tarabini, A. Zabi, A. Zghiche

Université de Strasbourg, CNRS, IPHC UMR 7178, Strasbourg, France
J.-L. Agram[16], J. Andrea, D. Apparu, D. Bloch, G. Bourgatte, J.-M. Brom, E. C. Chabert, C. Collard, D. Darej, J. -C. Fontaine[16], U. Goerlach, C. Grimault, A.-C. Le Bihan, E. Nibigira, P. Van Hove

Institut de Physique des 2 Infinis de Lyon (IP2I), Villeurbanne, France
E. Asilar, S. Beauceron, C. Bernet, G. Boudoul, C. Camen, A. Carle, N. Chanon, D. Contardo, P. Depasse, H. El Mamouni, J. Fay, S. Gascon, M. Gouzevitch, B. Ille, I. B. Laktineh, H. Lattaud, A. Lesauvage, M. Lethuillier, L. Mirabito, S. Perries, K. Shchablo, V. Sordini, L. Torterotot, G. Touquet, M. Vander Donckt, S. Viret

Georgian Technical University, Tbilisi, Georgia
I. Lomidze, T. Toriashvili[17], Z. Tsamalaidze[11]

I. Physikalisches Institut, RWTH Aachen University, Aachen, Germany
V. Botta, L. Feld, K. Klein, M. Lipinski, D. Meuser, A. Pauls, M. P. Rauch, N. Röwert, J. Schulz, M. Teroerde

III. Physikalisches Institut A, RWTH Aachen University, Aachen, Germany
A. Dodonova, D. Eliseev, M. Erdmann, P. Fackeldey, B. Fischer, S. Ghosh, T. Hebbeker, K. Hoepfner, F. Ivone, H. Keller, L. Mastrolorenzo, M. Merschmeyer, A. Meyer, G. Mocellin, S. Mondal, S. Mukherjee, D. Noll, A. Novak, T. Pook, A. Pozdnyakov, Y. Rath, H. Reithler, J. Roemer, A. Schmidt, S. C. Schuler, A. Sharma, L. Vigilante, S. Wiedenbeck, S. Zaleski

III. Physikalisches Institut B, RWTH Aachen University, Aachen, Germany
C. Dziwok, G. Flügge, W. Haj Ahmad[18], O. Hlushchenko, T. Kress, A. Nowack, C. Pistone, O. Pooth, D. Roy, H. Sert, A. Stahl[19], T. Ziemons

Deutsches Elektronen-Synchrotron, Hamburg, Germany
H. Aarup Petersen, M. Aldaya Martin, P. Asmuss, I. Babounikau, S. Baxter, O. Behnke, A. Bermúdez Martínez, S. Bhattacharya, A. A. Bin Anuar, K. Borras[20], D. Brunner, A. Campbell, A. Cardini, C. Cheng, F. Colombina, S. Consuegra Rodríguez, G. Correia Silva, V. Danilov, M. De Silva, L. Didukh, G. Eckerlin, D. Eckstein, L. I. Estevez Banos, O. Filatov, E. Gallo[21], A. Geiser, A. Giraldi, A. Grohsjean, M. Guthoff, A. Jafari[22], N. Z. Jomhari, A. Kasem[20], M. Kasemann, H. Kaveh, C. Kleinwort, D. Krücker, W. Lange, J. Lidrych, K. Lipka, W. Lohmann[23], R. Mankel, I. -A. Melzer-Pellmann, M. Mendizabal Morentin, J. Metwally, A. B. Meyer, M. Meyer, J. Mnich, A. Mussgiller, Y. Otarid, D. Pérez Adán, D. Pitzl, A. Raspereza, B. Ribeiro Lopes, J. Rübenach, A. Saggio, A. Saibel, M. Savitskyi, M. Scham, V. Scheurer, P. Schütze, C. Schwanenberger[21], A. Singh, R. E. Sosa Ricardo, D. Stafford, N. Tonon, O. Turkot, M. Van De Klundert, R. Walsh, D. Walter, Y. Wen, K. Wichmann, L. Wiens, C. Wissing, S. Wuchterl

University of Hamburg, Hamburg, Germany
R. Aggleton, S. Albrecht, S. Bein, L. Benato, A. Benecke, P. Connor, K. De Leo, M. Eich, F. Feindt, A. Fröhlich, C. Garbers, E. Garutti, P. Gunnellini, J. Haller, A. Hinzmann, G. Kasieczka, R. Klanner, R. Kogler, T. Kramer, V. Kutzner, J. Lange, T. Lange, A. Lobanov, A. Malara, A. Nigamova, K. J. Pena Rodriguez, O. Rieger, P. Schleper, M. Schröder, J. Schwandt, D. Schwarz, J. Sonneveld, H. Stadie, G. Steinbrück, A. Tews, B. Vormwald, I. Zoi

Karlsruher Institut fuer Technologie, Karlsruhe, Germany
J. Bechtel, T. Berger, E. Butz, R. Caspart, T. Chwalek, W. De Boer†, A. Dierlamm, A. Droll, K. El Morabit, N. Faltermann, M. Giffels, J.o. Gosewisch, A. Gottmann, F. Hartmann[19], C. Heidecker, U. Husemann, P. Keicher, R. Koppenhöfer, S. Maier, M. Metzler, S. Mitra, Th. Müller, M. Neukum, A. Nürnberg, G. Quast, K. Rabbertz, J. Rauser, D. Savoiu, M. Schnepf, D. Seith, I. Shvetsov, H. J. Simonis, R. Ulrich, J. Van Der Linden, R. F. Von Cube, M. Wassmer, M. Weber, S. Wieland, R. Wolf, S. Wozniewski, S. Wunsch

Institute of Nuclear and Particle Physics (INPP), NCSR Demokritos, Aghia Paraskevi, Greece
G. Anagnostou, G. Daskalakis, T. Geralis, A. Kyriakis, A. Stakia

National and Kapodistrian University of Athens, Athens, Greece
M. Diamantopoulou, D. Karasavvas, G. Karathanasis, P. Kontaxakis, C. K. Koraka, A. Manousakis-Katsikakis, A. Panagiotou, I. Papavergou, N. Saoulidou, K. Theofilatos, E. Tziaferi, K. Vellidis, E. Vourliotis

National Technical University of Athens, Athens, Greece
G. Bakas, K. Kousouris, I. Papakrivopoulos, G. Tsipolitis, A. Zacharopoulou

University of Ioánnina, Ioannina, Greece
K. Adamidis, I. Bestintzanos, I. Evangelou, C. Foudas, P. Gianneios, P. Katsoulis, P. Kokkas, N. Manthos, I. Papadopoulos, J. Strologas

MTA-ELTE Lendület CMS Particle and Nuclear Physics Group, Eötvös Loránd University, Budapest, Hungary
M. Csanád, K. Farkas, M. M. A. Gadallah[24], S. Lökös[25], P. Major, K. Mandal, A. Mehta, G. Pásztor, A. J. Rádl, O. Surányi, G. I. Veres

Wigner Research Centre for Physics, Budapest, Hungary
M. Bartók[26], G. Bencze, C. Hajdu, D. Horvath[27], F. Sikler, V. Veszpremi, G. Vesztergombi†,[28]

Institute of Nuclear Research ATOMKI, Debrecen, Hungary
S. Czellar, J. Karancsi[26], J. Molnar, Z. Szillasi, D. Teyssier

Institute of Physics, University of Debrecen, Debrecen, Hungary
P. Raics, Z. L. Trocsanyi[28], B. Ujvari

Karoly Robert Campus, MATE Institute of Technology, Gyongyos, Hungary
T. Csorgo[29], F. Nemes[29], T. Novak

Indian Institute of Science (IISc), Bangalore, India
J. R. Komaragiri, D. Kumar, L. Panwar, P. C. Tiwari

Panjab University, Chandigarh, India
S. Bansal, S. B. Beri, V. Bhatnagar, G. Chaudhary, S. Chauhan, N. Dhingra[30], R. Gupta, A. Kaur, M. Kaur, S. Kaur, P. Kumari, M. Meena, K. Sandeep, J. B. Singh, A. K. Virdi

University of Delhi, Delhi, India
A. Ahmed, A. Bhardwaj, B. C. Choudhary, M. Gola, S. Keshri, A. Kumar, M. Naimuddin, P. Priyanka, K. Ranjan, A. Shah

Saha Institute of Nuclear Physics, HBNI, Kolkata, India
M. Bharti[31], R. Bhattacharya, S. Bhattacharya, D. Bhowmik, S. Dutta, S. Dutta, B. Gomber[32], M. Maity[33], P. Palit, P. K. Rout, G. Saha, B. Sahu, S. Sarkar, M. Sharan, B. Singh[31], S. Thakur[31]

Indian Institute of Technology Madras, Madras, India
P. K. Behera, S. C. Behera, P. Kalbhor, A. Muhammad, R. Pradhan, P. R. Pujahari, A. Sharma, A. K. Sikdar

Bhabha Atomic Research Centre, Mumbai, India
D. Dutta, V. Jha, V. Kumar, D. K. Mishra, K. Naskar[34], P. K. Netrakanti, L. M. Pant, P. Shukla

Tata Institute of Fundamental Research-A, Mumbai, India
T. Aziz, S. Dugad, M. Kumar, G. B. Mohanty, U. Sarkar

Tata Institute of Fundamental Research-B, Mumbai, India
S. Banerjee, R. Chudasama, M. Guchait, S. Karmakar, S. Kumar, G. Majumder, K. Mazumdar, S. Mukherjee

National Institute of Science Education and Research, An OCC of Homi Bhabha National Institute, Bhubaneswar, Odisha, India
S. Bahinipati[35], C. Kar, P. Mal, T. Mishra, V. K. Muraleedharan Nair Bindhu[36], A. Nayak[36], P. Saha, N. Sur, S. K. Swain, D. Vats[36]

Indian Institute of Science Education and Research (IISER), Pune, India
K. Alpana, S. Dube, B. Kansal, A. Laha, S. Pandey, A. Rane, A. Rastogi, S. Sharma

Isfahan University of Technology, Isfahan, Iran
H. Bakhshiansohi[37], E. Khazaie, M. Zeinali[38]

Institute for Research in Fundamental Sciences (IPM), Tehran, Iran
S. Chenarani[39], S. M. Etesami, M. Khakzad, M. Mohammadi Najafabadi

University College Dublin, Dublin, Ireland
M. Grunewald

INFN Sezione di Bari[a], Università di Bari[b], Politecnico di Bari[c], Bari, Italy
M. Abbrescia[a,b], R. Aly[a,c,12], C. Aruta[a,b], A. Colaleo[a], D. Creanza[a,c], N. De Filippis[a,c], M. De Palma[a,b], A. Di Florio[a,b], A. Di Pilato[a,b], W. Elmetenawee[a,b], L. Fiore[a], A. Gelmi[a,b], M. Gul[a], G. Iaselli[a,c], M. Ince[a,b], S. Lezki[a,b], G. Maggi[a,c], M. Maggi[a], I. Margjeka[a,b], V. Mastrapasqua[a,b], J. A. Merlin[a], S. My[a,b], S. Nuzzo[a,b], A. Pellecchia[a,b], A. Pompili[a,b], G. Pugliese[a,c], A. Ranieri[a], G. Selvaggi[a,b], L. Silvestris[a], F. M. Simone[a,b], R. Venditti[a], P. Verwilligen[a]

INFN Sezione di Bologna[a], Università di Bologna[b], Bologna, Italy
G. Abbiendi[a], C. Battilana[a,b], D. Bonacorsi[a,b], L. Borgonovi[a], L. Brigliadori[a], R. Campanini[a,b], P. Capiluppi[a,b], A. Castro[a,b], F. R. Cavallo[a], M. Cuffiani[a,b], G. M. Dallavalle[a], T. Diotalevi[a,b], F. Fabbri[a], A. Fanfani[a,b], P. Giacomelli[a], L. Giommi[a,b], C. Grandi[a], L. Guiducci[a,b], S. Lo Meo[a,40], L. Lunerti[a,b], S. Marcellini[a], G. Masetti[a], F. L. Navarria[a,b], A. Perrotta[a], F. Primavera[a,b], A. M. Rossi[a,b], T. Rovelli[a,b], G. P. Siroli[a,b]

INFN Sezione di Catania[a], Università di Catania[b], Catania, Italy
S. Albergo[a,b,41], S. Costa[a,b,41], A. Di Mattia[a], R. Potenza[a,b], A. Tricomi[a,b,41], C. Tuve[a,b]

INFN Sezione di Firenze[a], Università di Firenze[b], Firenze, Italy
G. Barbagli[a], A. Cassese[a], R. Ceccarelli[a,b], V. Ciulli[a,b], C. Civinini[a], R. D'Alessandro[a,b], E. Focardi[a,b], G. Latino[a,b], P. Lenzi[a,b], M. Lizzo[a,b], M. Meschini[a], S. Paoletti[a], R. Seidita[a,b], G. Sguazzoni[a], L. Viliani[a]

INFN Laboratori Nazionali di Frascati, Frascati, Italy
L. Benussi, S. Bianco, D. Piccolo

INFN Sezione di Genova[a], Università di Genova[b], Genoa, Italy
M. Bozzo[a,b], F. Ferro[a], R. Mulargia[a,b], E. Robutti[a], S. Tosi[a,b]

INFN Sezione di Milano-Bicocca[a], Università di Milano-Bicocca[b], Milan, Italy
A. Benaglia[a], G. Boldrini[a], F. Brivio[a,b], F. Cetorelli[a,b], V. Ciriolo[a,b,19], F. De Guio[a,b], M. E. Dinardo[a,b], P. Dini[a], S. Gennai[a], A. Ghezzi[a,b], P. Govoni[a,b], L. Guzzi[a,b], M. Malberti[a], S. Malvezzi[a], A. Massironi[a], D. Menasce[a], L. Moroni[a], M. Paganoni[a,b], D. Pedrini[a], B. S. Pinolini[a], S. Ragazzi[a,b], N. Redaelli[a], T. Tabarelli de Fatis[a,b], D. Valsecchi[a,b,19], D. Zuolo[a,b]

INFN Sezione di Napoli[a], Università di Napoli 'Federico II'[b], Napoli, Italy; Università della Basilicata[c], Potenza, Italy; Università G. Marconi[d], Rome, Italy
S. Buontempo[a], F. Carnevali[a,b], N. Cavallo[a,c], A. De Iorio[a,b], F. Fabozzi[a,c], A. O. M. Iorio[a,b], L. Lista[a,b], S. Meola[a,d,19], P. Paolucci[a,19], B. Rossi[a], C. Sciacca[a,b]

INFN Sezione di Padova[a], Università di Padova[b], Padova, Italy; Università di Trento[c], Trento, Italy
P. Azzi[a], N. Bacchetta[a], D. Bisello[a,b], P. Bortignon[a], A. Bragagnolo[a,b], R. Carlin[a,b], P. Checchia[a], T. Dorigo[a], U. Dosselli[a], F. Gasparini[a,b], U. Gasparini[a,b], G. Grosso[a], S. Y. Hoh[a,b], L. Layer[a,42], E. Lusian i[a], M. Margoni[a,b], A. T. Meneguzzo[a,b], J. Pazzini[a,b], M. Presilla[a,b], P. Ronchese[a,b], R. Rossin[a,b], F. Simonetto[a,b], G. Strong[a], M. Tosi[a,b], H. Yarar[a,b], M. Zanetti[a,b], P. Zotto[a,b], A. Zucchetta[a,b], G. Zumerle[a,b]

INFN Sezione di Pavia[a], Università di Pavia[b], Pavia, Italy
C. Aime'[a,b], A. Braghieri[a], S. Calzaferri[a,b], D. Fiorina[a,b], P. Montagna[a,b], S. P. Ratti[a,b], V. Re[a], C. Riccardi[a,b], P. Salvini[a], I. Vai[a], P. Vitulo[a,b]

INFN Sezione di Perugia[a], Università di Perugia[b], Perugia, Italy
P. Asenov[a,43], G. M. Bilei[a], D. Ciangottini[a,b], L. Fanò[a,b], P. Lariccia[a,b], M. Magherini[a,b], G. Mantovani[a,b], V. Mariani[a,b], M. Menichelli[a], F. Moscatelli[a,43], A. Piccinelli[a,b], A. Rossi[a,b], A. Santocchia[a,b], D. Spiga[a], T. Tedeschi[a,b]

INFN Sezione di Pisa[a], Università di Pisa[b], Scuola Normale Superiore di Pisa[c], Pisa, Italy; Università di Siena[d], Siena, Italy
P. Azzurri[a], G. Bagliesi[a], V. Bertacchi[a,c], L. Bianchini[a], T. Boccali[a], E. Bossini[a,b], R. Castaldi[a], M. A. Ciocci[a,b], V. D'Amante[a,d], R. Dell'Orso[a], M. R. Di Domenico[a,d], S. Donato[a], A. Giassi[a], F. Ligabue[a,c], E. Manca[a,c], G. Mandorli[a,c], A. Messineo[a,b], F. Palla[a], S. Parolia[a,b], G. Ramirez-Sanchez[a,c], A. Rizzi[a,b], G. Rolandi[a,c], S. Roy Chowdhury[a,c], A. Scribano[a], N. Shafiei[a,b], P. Spagnolo[a], R. Tenchini[a], G. Tonelli[a,b], N. Turini[a,d], A. Venturi[a], P. G. Verdini[a]

INFN Sezione di Roma[a], Sapienza Università di Roma[b], Rome, Italy
M. Campana[a,b], F. Cavallari[a], D. Del Re[a,b], E. Di Marco[a], M. Diemoz[a], E. Longo[a,b], P. Meridiani[a], G. Organtini[a,b], F. Pandolfi[a], R. Paramatti[a,b], C. Quaranta[a,b], S. Rahatlou[a,b], C. Rovelli[a], F. Santanastasio[a,b], L. Soffi[a], R. Tramontano[a,b]

INFN Sezione di Torino[a], Università di Torino[b], Torino, Italy; Università del Piemonte Orientale[c], Novara, Italy
N. Amapane[a,b], R. Arcidiacono[a,c], S. Argiro[a,b], M. Arneodo[a,c], N. Bartosik[a], R. Bellan[a,b], A. Bellora[a,b], J. Berenguer Antequera[a,b], C. Biino[a], N. Cartiglia[a], S. Cometti[a], M. Costa[a,b], R. Covarelli[a,b], N. Demaria[a], B. Kiani[a,b], F. Legger[a], C. Mariotti[a], S. Maselli[a], E. Migliore[a,b], E. Monteil[a,b], M. Monteno[a], M. M. Obertino[a,b], G. Ortona[a], L. Pacher[a,b], N. Pastrone[a], M. Pelliccioni[a], G. L. Pinna Angioni[a,b], M. Ruspa[a,c], K. Shchelina[a,b], F. Siviero[a,b], V. Sola[a], A. Solano[a,b], D. Soldi[a,b], A. Staiano[a], M. Tornago[a,b], D. Trocino[a,b], A. Vagnerini[a]

INFN Sezione di Trieste[a], Università di Trieste[b], Trieste, Italy
S. Belforte[a], V. Candelise[a,b], M. Casarsa[a], F. Cossutti[a], A. Da Rold[a,b], G. Della Ricca[a,b], G. Sorrentino[a,b], F. Vazzoler[a,b]

Kyungpook National University, Daegu, Korea
S. Dogra, C. Huh, B. Kim, D. H. Kim, G. N. Kim, J. Kim, J. Lee, S. W. Lee, C. S. Moon, Y. D. Oh, S. I. Pak, B. C. Radburn-Smith, S. Sekmen, Y. C. Yang

Chonnam National University, Institute for Universe and Elementary Particles, Kwangju, Korea
H. Kim, D. H. Moon

Hanyang University, Seoul, Korea
B. Francois, T. J. Kim, J. Park

Korea University, Seoul, Korea
S. Cho, S. Choi, Y. Go, B. Hong, K. Lee, K. S. Lee, J. Lim, J. Park, S. K. Park, J. Yoo

Department of Physics, Kyung Hee University, Seoul, Korea
J. Goh, A. Gurtu

Sejong University, Seoul, Korea
H. S. Kim, Y. Kim

Seoul National University, Seoul, Korea
J. Almond, J. H. Bhyun, J. Choi, S. Jeon, J. Kim, J. S. Kim, S. Ko, H. Kwon, H. Lee, S. Lee, B. H. Oh, M. Oh, S. B. Oh, H. Seo, U. K. Yang, I. Yoon

University of Seoul, Seoul, Korea
W. Jang, D. Y. Kang, Y. Kang, S. Kim, B. Ko, J. S. H. Lee, Y. Lee, I. C. Park, Y. Roh, M. S. Ryu, D. Song, Watson I.J., S. Yang

Department of Physics, Yonsei University, Seoul, Korea
S. Ha, H. D. Yoo

Sungkyunkwan University, Suwon, Korea
M. Choi, Y. Jeong, H. Lee, Y. Lee, I. Yu

College of Engineering and Technology, American University of the Middle East (AUM), Dasman, Kuwait
T. Beyrouthy, Y. Maghrbi

Riga Technical University, Riga, Latvia
T. Torims, V. Veckalns

Vilnius University, Vilnius, Lithuania
M. Ambrozas, A. Carvalho Antunes De Oliveira, A. Juodagalvis, A. Rinkevicius, G. Tamulaitis

National Centre for Particle Physics, Universiti Malaya, Kuala Lumpur, Malaysia
N. Bin Norjoharuddeen, W. A. T. Wan Abdullah, M. N. Yusli, Z. Zolkapli

Universidad de Sonora (UNISON), Hermosillo, Mexico
J. F. Benitez, A. Castaneda Hernandez, M. León Coello, J. A. Murillo Quijada, A. Sehrawat, L. Valencia Palomo

Centro de Investigacion y de Estudios Avanzados del IPN, Mexico City, Mexico
G. Ayala, H. Castilla-Valdez, E. De La Cruz-Burelo, I. Heredia-De La Cruz[44], R. Lopez-Fernandez, C. A. Mondragon Herrera, D. A. Perez Navarro, A. Sánchez Hernández

Universidad Iberoamericana, Mexico City, Mexico
S. Carrillo Moreno, C. Oropeza Barrera, F. Vazquez Valencia

Benemerita Universidad Autonoma de Puebla, Puebla, Mexico
I. Pedraza, H. A. Salazar Ibarguen, C. Uribe Estrada

University of Montenegro, Podgorica, Montenegro
I. Bubanja, J. Mijuskovic[45], N. Raicevic

University of Auckland, Auckland, New Zealand
D. Krofcheck

University of Canterbury, Christchurch, New Zealand
S. Bheesette, P. H. Butler

National Centre for Physics, Quaid-I-Azam University, Islamabad, Pakistan
A. Ahmad, M. I. Asghar, A. Awais, M. I. M. Awan, H. R. Hoorani, W. A. Khan, M. A. Shah, M. Shoaib, M. Waqas

AGH University of Science and Technology Faculty of Computer Science, Electronics and Telecommunications, Kraków, Poland
V. Avati, L. Grzanka, M. Malawski

National Centre for Nuclear Research, Swierk, Poland
H. Bialkowska, M. Bluj, B. Boimska, M. Górski, M. Kazana, M. Szleper, P. Zalewski

Institute of Experimental Physics, Faculty of Physics, University of Warsaw, Warsaw, Poland
K. Bunkowski, K. Doroba, A. Kalinowski, M. Konecki, J. Krolikowski, M. Walczak

Laboratório de Instrumentação e Física Experimental de Partículas, Lisbon, Portugal
M. Araujo, P. Bargassa, D. Bastos, A. Boletti, P. Faccioli, M. Gallinaro, J. Hollar, N. Leonardo, T. Niknejad, M. Pisano, J. Seixas, O. Toldaiev, J. Varela

VINCA Institute of Nuclear Sciences, University of Belgrade, Belgrade, Serbia
P. Adzic[46], M. Dordevic, P. Milenovic, J. Milosevic

Centro de Investigaciones Energéticas Medioambientales y Tecnológicas (CIEMAT), Madrid, Spain
M. Aguilar-Benitez, J. Alcaraz Maestre, A. Álvarez Fernández, I. Bachiller, M. Barrio Luna, Cristina F. Bedoya, C. A. Carrillo Montoya, M. Cepeda, M. Cerrada, N. Colino, B. De La Cruz, A. Delgado Peris, J. P. Fernández Ramos, J. Flix, M. C. Fouz, O. Gonzalez Lopez, S. Goy Lopez, J. M. Hernandez, M. I. Josa, J. León Holgado, D. Moran, Á. Navarro Tobar, C. Perez Dengra, A. Pérez-Calero Yzquierdo, J. Puerta Pelayo, I. Redondo, L. Romero, S. Sánchez Navas, L. Urda Gómez, C. Willmott

Universidad Autónoma de Madrid, Madrid, Spain
J. F. de Trocóniz, R. Reyes-Almanza

Universidad de Oviedo, Instituto Universitario de Ciencias y Tecnologías Espaciales de Asturias (ICTEA), Oviedo, Spain
B. Alvarez Gonzalez, J. Cuevas, C. Erice, J. Fernandez Menendez, S. Folgueras, I. Gonzalez Caballero, J. R. González Fernández, E. Palencia Cortezon, C. Ramón Álvarez, V. Rodríguez Bouza, A. Trapote, N. Trevisani

Instituto de Física de Cantabria (IFCA), CSIC-Universidad de Cantabria, Santander, Spain
J. A. Brochero Cifuentes, I. J. Cabrillo, A. Calderon, J. Duarte Campderros, M. Fernandez, C. Fernandez Madrazo, P. J. Fernández Manteca, A. García Alonso, G. Gomez, C. Martinez Rivero, P. Martinez Ruiz del Arbol, F. Matorras, P. Matorras Cuevas, J. Piedra Gomez, C. Prieels, T. Rodrigo, A. Ruiz-Jimeno, L. Scodellaro, I. Vila, J. M. Vizan Garcia

University of Colombo, Colombo, Sri Lanka
M. K. Jayananda, B. Kailasapathy[47], D. U. J. Sonnadara, D. D. C. Wickramarathna

Department of Physics, University of Ruhuna, Matara, Sri Lanka
W. G. D. Dharmaratna, K. Liyanage, N. Perera, N. Wickramage

CERN, European Organization for Nuclear Research, Geneva, Switzerland
T. K. Aarrestad, D. Abbaneo, J. Alimena, E. Auffray, G. Auzinger, J. Baechler, P. Baillon†, D. Barney, J. Bendavid, M. Bianco, A. Bocci, T. Camporesi, M. Capeans Garrido, G. Cerminara, S. S. Chhibra, M. Cipriani, L. Cristella, D. d'Enterria, A. Dabrowski, A. David, A. De Roeck, M. M. Defranchis, M. Deile, M. Dobson, M. Dünser, N. Dupont, A. Elliott-Peisert, N. Emriskova, F. Fallavollita[48], D. Fasanella, A. Florent, G. Franzoni, W. Funk, S. Giani, D. Gigi, K. Gill, F. Glege, L. Gouskos, M. Haranko, J. Hegeman, Y. Iiyama, V. Innocente, T. James, P. Janot, J. Kaspar, J. Kieseler, M. Komm, N. Kratochwil, C. Lange, S. Laurila, P. Lecoq, K. Long, C. Lourenço, L. Malgeri, S. Mallios, M. Mannelli, A. C. Marini, F. Meijers, S. Mersi, E. Meschi, F. Moortgat, M. Mulders, S. Orfanelli, L. Orsini, F. Pantaleo, L. Pape, E. Perez, M. Peruzzi, A. Petrilli, G. Petrucciani, A. Pfeiffer, M. Pierini,

D. Piparo, M. Pitt, H. Qu, T. Quast, D. Rabady, A. Racz, G. Reales Gutiérrez, M. Rieger, M. Rovere, H. Sakulin, J. Salfeld-Nebgen, S. Scarfi, C. Schäfer, M. Selvaggi, A. Sharma, P. Silva, W. Snoeys, P. Sphicas[49], S. Summers, K. Tatar, V. R. Tavolaro, D. Treille, A. Tsirou, G. P. Van Onsem, J. Wanczyk[50], K. A. Wozniak, W. D. Zeuner

Paul Scherrer Institut, Villigen, Switzerland
L. Caminada[51], A. Ebrahimi, W. Erdmann, R. Horisberger, Q. Ingram, H. C. Kaestli, D. Kotlinski, M. Missiroli, T. Rohe

ETH Zurich-Institute for Particle Physics and Astrophysics (IPA), Zurich, Switzerland
K. Androsov[50], M. Backhaus, P. Berger, A. Calandri, N. Chernyavskaya, A. De Cosa, G. Dissertori, M. Dittmar, M. Donegà, C. Dorfer, F. Eble, K. Gedia, F. Glessgen, T. A. Gómez Espinosa, C. Grab, D. Hits, W. Lustermann, A.-M. Lyon, R. A. Manzoni, C. Martin Perez, M. T. Meinhard, F. Nessi-Tedaldi, J. Niedziela, F. Pauss, V. Perovic, S. Pigazzini, M. G. Ratti, M. Reichmann, C. Reissel, T. Reitenspiess, B. Ristic, D. Ruini, D. A. Sanz Becerra, M. Schönenberger, V. Stampf, J. Steggemann[50], R. Wallny, D. H. Zhu

Universität Zürich, Zurich, Switzerland
C. Amsler[52], P. Bärtschi, C. Botta, D. Brzhechko, M. F. Canelli, K. Cormier, A. De Wit, R. Del Burgo, J. K. Heikkilä, M. Huwiler, W. Jin, A. Jofrehei, B. Kilminster, S. Leontsinis, S. P. Liechti, A. Macchiolo, P. Meiring, V. M. Mikuni, U. Molinatti, I. Neutelings, A. Reimers, P. Robmann, S. Sanchez Cruz, K. Schweiger, Y. Takahashi

National Central University, Chung-Li, Taiwan
C. Adloff[53], C. M. Kuo, W. Lin, A. Roy, T. Sarkar[33], S. S. Yu

National Taiwan University (NTU), Taipei, Taiwan
L. Ceard, Y. Chao, K. F. Chen, P. H. Chen, W.-S. Hou, Y.y. Li, R.-S. Lu, E. Paganis, A. Psallidas, A. Steen, H.y. Wu, E. Yazgan, P.r. Yu

Department of Physics, Faculty of Science, Chulalongkorn University, Bangkok, Thailand
B. Asavapibhop, C. Asawatangtrakuldee, N. Srimanobhas

Physics Department, Science and Art Faculty, Çukurova University, Adana, Turkey
F. Boran, S. Damarseckin[54], Z. S. Demiroglu, F. Dolek, I. Dumanoglu[55], E. Eskut, Y. Guler, E. Gurpinar Guler[56], I. Hos[57], C. Isik, O. Kara, A. Kayis Topaksu, U. Kiminsu, G. Onengut, K. Ozdemir[58], A. Polatoz, A. E. Simsek, B. Tali[59], U. G. Tok, S. Turkcapar, I. S. Zorbakir, C. Zorbilmez

Physics Department, Middle East Technical University, Ankara, Turkey
B. Isildak[60], G. Karapinar[61], K. Ocalan[62], M. Yalvac[63]

Bogazici University, Istanbul, Turkey
B. Akgun, I. O. Atakisi, E. Gülmez, M. Kaya[64], O. Kaya[65], Ö. Özçelik, S. Tekten[66], E. A. Yetkin[67]

Istanbul Technical University, Istanbul, Turkey
A. Cakir, K. Cankocak[55], Y. Komurcu, S. Sen[68]

Istanbul University, Istanbul, Turkey
S. Cerci[59], B. Kaynak, S. Ozkorucuklu, D. Sunar Cerci[59]

Institute for Scintillation Materials of National Academy of Science of Ukraine, Kharkiv, Ukraine
B. Grynyov

National Science Centre, Kharkiv Institute of Physics and Technology, Kharkiv, Ukraine
L. Levchuk

University of Bristol, Bristol, UK
D. Anthony, E. Bhal, S. Bologna, J. J. Brooke, A. Bundock, E. Clement, D. Cussans, H. Flacher,

J. Goldstein, G. P. Heath, H. F. Heath, M.-L. Holmberg[69], L. Kreczko, B. Krikler, S. Paramesvaran, S. Seif El Nasr-Storey, V. J. Smith, N. Stylianou[70], K. Walkingshaw Pass, R. White

Rutherford Appleton Laboratory, Didcot, UK
K. W. Bell, A. Belyaev[71], C. Brew, R. M. Brown, D. J. A. Cockerill, C. Cooke, K. V. Ellis, K. Harder, S. Harper, J. Linacre, K. Manolopoulos, D. M. Newbold, E. Olaiya, D. Petyt, T. Reis, T. Schuh, C. H. Shepherd-Themistocleous, I. R. Tomalin, T. Williams

Imperial College, London, UK
R. Bainbridge, P. Bloch, S. Bonomally, J. Borg, S. Breeze, O. Buchmuller, V. Cepaitis, G. S. Chahal[72], D. Colling, P. Dauncey, G. Davies, M. Della Negra, S. Fayer, G. Fedi, G. Hall, M. H. Hassanshahi, G. Iles, J. Langford, L. Lyons, A.-M. Magnan, S. Malik, A. Martelli, D. G. Monk, J. Nash[73], M. Pesaresi, D. M. Raymond, A. Richards, A. Rose, E. Scott, C. Seez, A. Shtipliyski, A. Tapper, K. Uchida, T. Virdee[19], M. Vojinovic, N. Wardle, S. N. Webb, D. Winterbottom

Brunel University, Uxbridge, UK
K. Coldham, J. E. Cole, A. Khan, P. Kyberd, I. D. Reid, L. Teodorescu, S. Zahid

Baylor University, Waco, TX, USA
S. Abdullin, A. Brinkerhoff, B. Caraway, J. Dittmann, K. Hatakeyama, A. R. Kanuganti, B. McMaster, N. Pastika, M. Saunders, S. Sawant, C. Sutantawibul, J. Wilson

Catholic University of America, Washington, DC, USA
R. Bartek, A. Dominguez, R. Uniyal, A. M. Vargas Hernandez

The University of Alabama, Tuscaloosa, AL, USA
A. Buccilli, S. I. Cooper, D. Di Croce, S. V. Gleyzer, C. Henderson, C. U. Perez, P. Rumerio[74], C. West

Boston University, Boston, MA, USA
A. Akpinar, A. Albert, D. Arcaro, C. Cosby, Z. Demiragli, E. Fontanesi, D. Gastler, J. Rohlf, K. Salyer, D. Sperka, D. Spitzbart, I. Suarez, A. Tsatsos, S. Yuan, D. Zou

Brown University, Providence, RI, USA
G. Benelli, B. Burkle, X. Coubez[20], D. Cutts, M. Hadley, U. Heintz, J. M. Hogan[75], G. Landsberg, K. T. Lau, M. Lukasik, J. Luo, M. Narain, S. Sagir[76], E. Usai, W. Y. Wong, X. Yan, D. Yu, W. Zhang

University of California, Davis, Davis, CA, USA
J. Bonilla, C. Brainerd, R. Breedon, M. Calderon De La Barca Sanchez, M. Chertok, J. Conway, P. T. Cox, R. Erbacher, G. Haza, F. Jensen, O. Kukral, R. Lander, M. Mulhearn, D. Pellett, B. Regnery, D. Taylor, Y. Yao, F. Zhang

University of California, Los Angeles, CA, USA
M. Bachtis, R. Cousins, A. Datta, D. Hamilton, J. Hauser, M. Ignatenko, M. A. Iqbal, T. Lam, W. A. Nash, S. Regnard, D. Saltzberg, B. Stone, V. Valuev

University of California, Riverside, Riverside, CA, USA
K. Burt, Y. Chen, R. Clare, J. W. Gary, M. Gordon, G. Hanson, G. Karapostoli, O. R. Long, N. Manganelli, M. Olmedo Negrete, W. Si, S. Wimpenny, Y. Zhang

University of California, San Diego, La Jolla, CA, USA
J. G. Branson, P. Chang, S. Cittolin, S. Cooperstein, N. Deelen, D. Diaz, J. Duarte, R. Gerosa, L. Giannini, D. Gilbert, J. Guiang, R. Kansal, V. Krutelyov, R. Lee, J. Letts, M. Masciovecchio, S. May, M. Pieri, B. V. Sathia Narayanan, V. Sharma, M. Tadel, A. Vartak, F. Würthwein, Y. Xiang, A. Yagil

Department of Physics, University of California, Santa Barbara, Santa Barbara, CA, USA
N. Amin, C. Campagnari, M. Citron, A. Dorsett, V. Dutta, J. Incandela, M. Kilpatrick, J. Kim, B. Marsh, H. Mei, M. Oshiro, M. Quinnan, J. Richman, U. Sarica, F. Setti, J. Sheplock, D. Stuart, S. Wang

California Institute of Technology, Pasadena, CA, USA
A. Bornheim, O. Cerri, I. Dutta, J. M. Lawhorn, N. Lu, J. Mao, H. B. Newman, T. Q. Nguyen, M. Spiropulu, J. R. Vlimant, C. Wang, S. Xie, Z. Zhang, R. Y. Zhu

Carnegie Mellon University, Pittsburgh, PA, USA
J. Alison, S. An, M. B. Andrews, P. Bryant, T. Ferguson, A. Harilal, C. Liu, T. Mudholkar, M. Paulini, A. Sanchez, W. Terrill

University of Colorado Boulder, Boulder, CO, USA
J. P. Cumalat, W. T. Ford, A. Hassani, E. MacDonald, R. Patel, A. Perloff, C. Savard, K. Stenson, K. A. Ulmer, S. R. Wagner

Cornell University, Ithaca, NY, USA
J. Alexander, S. Bright-Thonney, Y. Cheng, D. J. Cranshaw, S. Hogan, J. Monroy, J. R. Patterson, D. Quach, J. Reichert, M. Reid, A. Ryd, W. Sun, J. Thom, P. Wittich, R. Zou

Fermi National Accelerator Laboratory, Batavia, IL, USA
M. Albrow, M. Alyari, G. Apollinari, A. Apresyan, A. Apyan, S. Banerjee, L. A. T. Bauerdick, D. Berry, J. Berryhill, P. C. Bhat, K. Burkett, J. N. Butler, A. Canepa, G. B. Cerati, H. W. K. Cheung, F. Chlebana, M. Cremonesi, K. F. Di Petrillo, V. D. Elvira, Y. Feng, J. Freeman, Z. Gecse, L. Gray, D. Green, S. Grünendahl, O. Gutsche, R. M. Harris, R. Heller, T. C. Herwig, J. Hirschauer, B. Jayatilaka, S. Jindariani, M. Johnson, U. Joshi, T. Klijnsma, B. Klima, K. H. M. Kwok, S. Lammel, D. Lincoln, R. Lipton, T. Liu, C. Madrid, K. Maeshima, C. Mantilla, D. Mason, P. McBride, P. Merkel, S. Mrenna, S. Nahn, J. Ngadiuba, V. O'Dell, V. Papadimitriou, K. Pedro, C. Pena[77], O. Prokofyev, F. Ravera, A. Reinsvold Hall, L. Ristori, B. Schneider, E. Sexton-Kennedy, N. Smith, A. Soha, W. J. Spalding, L. Spiegel, J. Strait, L. Taylor, S. Tkaczyk, N. V. Tran, L. Uplegger, E. W. Vaandering, H. A. Weber

University of Florida, Gainesville, FL, USA
D. Acosta, P. Avery, D. Bourilkov, L. Cadamuro, V. Cherepanov, F. Errico, R. D. Field, D. Guerrero, B. M. Joshi, M. Kim, E. Koenig, J. Konigsberg, A. Korytov, K. H. Lo, K. Matchev, N. Menendez, G. Mitselmakher, A. Muthirakalayil Madhu, N. Rawal, D. Rosenzweig, S. Rosenzweig, K. Shi, J. Sturdy, J. Wang, E. Yigitbasi, X. Zuo

Florida State University, Tallahassee, FL, USA
T. Adams, A. Askew, R. Habibullah, V. Hagopian, K. F. Johnson, R. Khurana, T. Kolberg, G. Martinez, H. Prosper, C. Schiber, O. Viazlo, R. Yohay, J. Zhang

Florida Institute of Technology, Melbourne, FL, USA
M. M. Baarmand, S. Butalla, T. Elkafrawy[78], M. Hohlmann, R. Kumar Verma, D. Noonan, M. Rahmani, F. Yumiceva

University of Illinois at Chicago (UIC), Chicago, IL, USA
M. R. Adams, H. Becerril Gonzalez, R. Cavanaugh, X. Chen, S. Dittmer, O. Evdokimov, C. E. Gerber, D. A. Hangal, D. J. Hofman, A. H. Merrit, C. Mills, G. Oh, T. Roy, S. Rudrabhatla, M. B. Tonjes, N. Varelas, J. Viinikainen, X. Wang, Z. Wu, Z. Ye

The University of Iowa, Iowa City, IA, USA
M. Alhusseini, K. Dilsiz[79], R. P. Gandrajula, O. K. Köseyan, J.-P. Merlo, A. Mestvirishvili[80], J. Nachtman, H. Ogul[81], Y. Onel, A. Penzo, C. Snyder, E. Tiras[82]

Johns Hopkins University, Baltimore, MD, USA
O. Amram, B. Blumenfeld, L. Corcodilos, J. Davis, M. Eminizer, A. V. Gritsan, S. Kyriacou, P. Maksimovic, J. Roskes, M. Swartz, T. Á. Vámi

The University of Kansas, Lawrence, KS, USA
A. Abreu, J. Anguiano, C. Baldenegro Barrera, P. Baringer, A. Bean, A. Bylinkin, Z. Flowers, T. Isidori, S. Khalil, J. King, G. Krintiras, A. Kropivnitskaya, M. Lazarovits, C. Lindsey, J. Marquez,

N. Minafra, M. Murray, M. Nickel, C. Rogan, C. Royon, R. Salvatico, S. Sanders, E. Schmitz, C. Smith, J. D. Tapia Takaki, Q. Wang, Z. Warner, J. Williams, G. Wilson

Kansas State University, Manhattan, KS, USA
S. Duric, A. Ivanov, K. Kaadze, D. Kim, Y. Maravin, T. Mitchell, A. Modak, K. Nam

Lawrence Livermore National Laboratory, Livermore, CA, USA
F. Rebassoo, D. Wright

University of Maryland, College Park, MD, USA
E. Adams, A. Baden, O. Baron, A. Belloni, S. C. Eno, N. J. Hadley, S. Jabeen, R. G. Kellogg, T. Koeth, A. C. Mignerey, S. Nabili, C. Palmer, M. Seidel, A. Skuja, L. Wang, K. Wong

Massachusetts Institute of Technology, Cambridge, MA, USA
D. Abercrombie, G. Andreassi, R. Bi, S. Brandt, W. Busza, I. A. Cali, Y. Chen, M. D'Alfonso, J. Eysermans, C. Freer, G. Gomez-Ceballos, M. Goncharov, P. Harris, M. Hu, M. Klute, D. Kovalskyi, J. Krupa, Y.-J. Lee, B. Maier, C. Mironov, C. Paus, D. Rankin, C. Roland, G. Roland, Z. Shi, G. S. F. Stephans, J. Wang, Z. Wang, B. Wyslouch

University of Minnesota, Minneapolis, MN, USA
R. M. Chatterjee, A. Evans, P. Hansen, J. Hiltbrand, Sh. Jain, M. Krohn, Y. Kubota, J. Mans, M. Revering, R. Rusack, R. Saradhy, N. Schroeder, N. Strobbe, M. A. Wadud

University of Nebraska-Lincoln, Lincoln, NE, USA
K. Bloom, M. Bryson, S. Chauhan, D. R. Claes, C. Fangmeier, L. Finco, F. Golf, C. Joo, I. Kravchenko, M. Musich, I. Reed, J. E. Siado, G. R. Snow†, W. Tabb, F. Yan, A. G. Zecchinelli

State University of New York at Buffalo, Buffalo, NY, USA
G. Agarwal, H. Bandyopadhyay, L. Hay, I. Iashvili, A. Kharchilava, C. McLean, D. Nguyen, J. Pekkanen, S. Rappoccio, A. Williams

Northeastern University, Boston, MA, USA
G. Alverson, E. Barberis, Y. Haddad, A. Hortiangtham, J. Li, G. Madigan, B. Marzocchi, D. M. Morse, V. Nguyen, T. Orimoto, A. Parker, L. Skinnari, A. Tishelman-Charny, T. Wamorkar, B. Wang, A. Wisecarver, D. Wood

Northwestern University, Evanston, IL, USA
S. Bhattacharya, J. Bueghly, Z. Chen, A. Gilbert, T. Gunter, K. A. Hahn, Y. Liu, N. Odell, M. H. Schmitt, M. Velasco

University of Notre Dame, Notre Dame, IN, USA
R. Band, R. Bucci, A. Das, N. Dev, R. Goldouzian, M. Hildreth, K. Hurtado Anampa, C. Jessop, K. Lannon, J. Lawrence, N. Loukas, L. Lutton, N. Marinelli, I. Mcalister, T. McCauley, C. Mcgrady, F. Meng, K. Mohrman, Y. Musienko[11], R. Ruchti, P. Siddireddy, A. Townsend, M. Wayne, A. Wightman, M. Wolf, M. Zarucki, L. Zygala

The Ohio State University, Columbus, OH, USA
B. Bylsma, B. Cardwell, L. S. Durkin, B. Francis, C. Hill, M. Nunez Ornelas, K. Wei, B. L. Winer, B. R. Yates

Princeton University, Princeton, NJ, USA
F. M. Addesa, B. Bonham, P. Das, G. Dezoort, P. Elmer, A. Frankenthal, B. Greenberg, N. Haubrich, S. Higginbotham, A. Kalogeropoulos, G. Kopp, S. Kwan, D. Lange, M. T. Lucchini, D. Marlow, K. Mei, I. Ojalvo, J. Olsen, D. Stickland, C. Tully

University of Puerto Rico, Mayaguez, PR, USA
S. Malik, S. Norberg

Purdue University, West Lafayette, IN, USA
A. S. Bakshi, V. E. Barnes, R. Chawla, S. Das, L. Gutay, M. Jones, A. W. Jung, S. Karmarkar, M. Liu,

G. Negro, N. Neumeister, G. Paspalaki, C. C. Peng, S. Piperov, A. Purohit, J. F. Schulte, M. Stojanovic, J. Thieman, F. Wang, R. Xiao, W. Xie

Purdue University Northwest, Hammond, IN, USA
J. Dolen, N. Parashar

Rice University, Houston, TX, USA
A. Baty, M. Decaro, S. Dildick, K. M. Ecklund, S. Freed, P. Gardner, F. J. M. Geurts, A. Kumar, W. Li, B. P. Padley, R. Redjimi, W. Shi, A. G. Stahl Leiton, S. Yang, L. Zhang, Y. Zhang

University of Rochester, Rochester, NY, USA
A. Bodek, P. de Barbaro, R. Demina, J. L. Dulemba, C. Fallon, T. Ferbel, M. Galanti, A. Garcia-Bellido, O. Hindrichs, A. Khukhunaishvili, E. Ranken, R. Taus

Rutgers, The State University of New Jersey, Piscataway, NJ, USA
B. Chiarito, J. P. Chou, A. Gandrakota, Y. Gershtein, E. Halkiadakis, A. Hart, M. Heindl, O. Karacheban[23], I. Laflotte, A. Lath, R. Montalvo, K. Nash, M. Osherson, S. Salur, S. Schnetzer, S. Somalwar, R. Stone, S. A. Thayil, S. Thomas, H. Wang

University of Tennessee, Knoxville, TN, USA
H. Acharya, A. G. Delannoy, S. Fiorendi, S. Spanier

Texas A&M University, College Station, TX, USA
O. Bouhali[83], M. Dalchenko, A. Delgado, R. Eusebi, J. Gilmore, T. Huang, T. Kamon[84], H. Kim, S. Luo, S. Malhotra, R. Mueller, D. Overton, D. Rathjens, A. Safonov

Texas Tech University, Lubbock, TX, USA
N. Akchurin, J. Damgov, V. Hegde, S. Kunori, K. Lamichhane, S. W. Lee, T. Mengke, S. Muthumuni, T. Peltola, I. Volobouev, Z. Wang, A. Whitbeck

Vanderbilt University, Nashville, TN, USA
E. Appelt, S. Greene, A. Gurrola, W. Johns, A. Melo, H. Ni, K. Padeken, F. Romeo, P. Sheldon, S. Tuo, J. Velkovska

University of Virginia, Charlottesville, VA, USA
M. W. Arenton, B. Cox, G. Cummings, J. Hakala, R. Hirosky, M. Joyce, A. Ledovskoy, A. Li, C. Neu, B. Tannenwald, S. White, E. Wolfe

Wayne State University, Detroit, MI, USA
N. Poudyal

University of Wisconsin-Madison, Madison, WI, USA
K. Black, T. Bose, C. Caillol, S. Dasu, I. De Bruyn, P. Everaerts, F. Fienga, C. Galloni, H. He, M. Herndon, A. Hervé, U. Hussain, A. Lanaro, A. Loeliger, R. Loveless, J. Madhusudanan Sreekala, A. Mallampalli, A. Mohammadi, D. Pinna, A. Savin, V. Shang, V. Sharma, W. H. Smith, D. Teague, S. Trembath-Reichert, W. Vetens

Authors affiliated with an institute or an international laboratory covered by a cooperation agreement with CERN, Geneva, Switzerland
S. Afanasiev, V. Andreev, Yu. Andreev, T. Aushev, M. Azarkin, A. Babaev, A. Belyaev, V. Blinov[85], E. Boos, V. Borshch, D. Budkouski, V. Bunichev, M. Chadeeva[85], A. Dermenev, T. Dimova[85], I. Dremin, M. Dubinin[77], L. Dudko, Y. Dydyshka, V. Epshteyn, G. Gavrilov, V. Gavrilov, S. Gninenko, V. Golovtcov, N. Golubev, I. Golutvin, I. Gorbunov, V. Ivanchenko, Y. Ivanov, V. Kachanov, L. Kardapoltsev[85], V. Karjavine, A. Karneyeu, V. Kim[85], M. Kirakosyan, D. Kirpichnikov, M. Kirsanov, V. Klyukhin, O. Kodolova[86], D. Konstantinov, V. Korenkov, A. Kozyrev[85], N. Krasnikov, E. Kuznetsova[87], A. Lanev, O. Lukina, N. Lychkovskaya, V. Makarenko[85], A. Malakhov, V. Matveev[85], V. Mossolov, V. Murzin, A. Nikitenko[88], S. Obraztsov, V. Okhotnikov, V. Oreshkin, I. Ovtin[85], V. Palichik, P. Parygin, A. Pashenkov, V. Perelygin, M. Perfilov, G. Pivovarov, V. Popov, E. Popova, M. Savina, V. Savrin, D. Seitova, D. Selivanova, V. Shalaev, S. Shmatov, S. Shulha, Y. Skovpen[85], S. Slabospitskii,

I. Smirnov, V. Smirnov, A. Snigirev, D. Sosnov, A. Spiridonov, A. Stepennov, V. Sulimov, E. Tcherniaev, A. Terkulov, O. Teryaev, D. Tlisov†, M. Toms, A. Toropin, L. Uvarov, A. Uzunian, E. Vlasov, S. Volkov, A. Vorobyev, N. Voytishin, B. S. Yuldashev[89], A. Zarubin, E. Zhemchugov[85], I. Zhizhin, A. Zhokin

† **Deceased**

1: Also at TU Wien, Vienna, Austria
2: Also at Institute of Basic and Applied Sciences, Faculty of Engineering, Arab Academy for Science, Technology and Maritime Transport, Alexandria, Egypt
3: Also at Université Libre de Bruxelles, Brussels, Belgium
4: Also at Universidade Estadual de Campinas, Campinas, Brazil
5: Also at Federal University of Rio Grande do Sul, Porto Alegre, Brazil
6: Also at University of Chinese Academy of Sciences, Beijing, China
7: Also at UFMS, Nova Andradina, Brazil
8: Also at Nanjing Normal University Department of Physics, Nanjing, China
9: Now at The University of Iowa, Iowa City, IA, USA
10: Also at University of Chinese Academy of Sciences, Beijing, China
11: Also at an institute or an international laboratory covered by a cooperation agreement with CERN, Geneva, Switzerland
12: Also at Helwan University, Cairo, Egypt
13: Now at Zewail City of Science and Technology, Zewail, Egypt
14: Now at British University in Egypt, Cairo, Egypt
15: Also at Purdue University, West Lafayette, IN, USA
16: Also at Université de Haute Alsace, Mulhouse, France
17: Also at Tbilisi State University, Tbilisi, Georgia
18: Also at Erzincan Binali Yildirim University, Erzincan, Turkey
19: Also at CERN, European Organization for Nuclear Research, Geneva, Switzerland
20: Also at III. Physikalisches Institut A, RWTH Aachen University, Aachen, Germany
21: Also at University of Hamburg, Hamburg, Germany
22: Also at Isfahan University of Technology, Isfahan, Iran
23: Also at Brandenburg University of Technology, Cottbus, Germany
24: Also at Physics Department, Faculty of Science, Assiut University, Assiut, Egypt
25: Also at Karoly Robert Campus, MATE Institute of Technology, Gyongyos, Hungary
26: Also at Institute of Physics, University of Debrecen, Debrecen, Hungary
27: Also at Institute of Nuclear Research ATOMKI, Debrecen, Hungary
28: Also at MTA-ELTE Lendület CMS Particle and Nuclear Physics Group, Eötvös Loránd University, Budapest, Hungary
29: Also at Wigner Research Centre for Physics, Budapest, Hungary
30: Also at G.H.G. Khalsa College, Ludhiana, Punjab, India
31: Also at Shoolini University, Solan, India
32: Also at University of Hyderabad, Hyderabad, India
33: Also at University of Visva-Bharati, Santiniketan, India
34: Also at Indian Institute of Technology (IIT), Mumbai, India
35: Also at IIT Bhubaneswar, Bhubaneswar, India
36: Also at Institute of Physics, Bhubaneswar, India
37: Also at Deutsches Elektronen-Synchrotron, Hamburg, Germany
38: Also at Sharif University of Technology, Tehran, Iran
39: Also at Department of Physics, University of Science and Technology of Mazandaran, Behshahr, Iran
40: Also at Italian National Agency for New Technologies, Energy and Sustainable Economic Development, Bologna, Italy
41: Also at Centro Siciliano di Fisica Nucleare e di Struttura Della Materia, Catania, Italy
42: Also at Università di Napoli 'Federico II', Naples, Italy
43: Also at Consiglio Nazionale delle Ricerche-Istituto Officina dei Materiali, Perugia, Italy
44: Also at Consejo Nacional de Ciencia y Tecnología, Mexico City, Mexico
45: Also at IRFU, CEA, Université Paris-Saclay, Gif-sur-Yvette, France
46: Also at Faculty of Physics, University of Belgrade, Belgrade, Serbia
47: Also at Trincomalee Campus, Eastern University, Sri Lanka, Nilaveli, Sri Lanka

48: Also at INFN Sezione di Pavia, Università di Pavia, Pavia, Italy
49: Also at National and Kapodistrian University of Athens, Athens, Greece
50: Also at Ecole Polytechnique Fédérale Lausanne, Lausanne, Switzerland
51: Also at Universität Zürich, Zurich, Switzerland
52: Also at Stefan Meyer Institute for Subatomic Physics, Vienna, Austria
53: Also at Laboratoire d'Annecy-le-Vieux de Physique des Particules, IN2P3-CNRS, Annecy-le-Vieux, France
54: Also at Şırnak University, Sirnak, Turkey
55: Also at Near East University, Research Center of Experimental Health Science, Mersin, Turkey
56: Also at Konya Technical University, Konya, Turkey
57: Also at Faculty of Engineering, Istanbul University-Cerrahpasa, Istanbul, Turkey
58: Also at Izmir Bakircay University, Izmir, Turkey
59: Also at Adiyaman University, Adiyaman, Turkey
60: Also at Yildiz Technical University, Istanbul, Turkey
61: Also at Izmir Institute of Technology, Izmir, Turkey
62: Also at Necmettin Erbakan University, Konya, Turkey
63: Also at Bozok Universitetesi Rektörlügü, Yozgat, Turkey
64: Also at Marmara University, Istanbul, Turkey
65: Also at Milli Savunma University, Istanbul, Turkey
66: Also at Kafkas University, Kars, Turkey
67: Also at Istanbul Bilgi University, Istanbul, Turkey
68: Also at Hacettepe University, Ankara, Turkey
69: Also at Rutherford Appleton Laboratory, Didcot, United Kingdom
70: Also at Vrije Universiteit Brussel, Brussels, Belgium
71: Also at School of Physics and Astronomy, University of Southampton, Southampton, UK
72: Also at IPPP Durham University, Durham, UK
73: Also at Monash University, Faculty of Science, Clayton, Australia
74: Also at Università di Torino, Turin, Italy
75: Also at Bethel University, St. Paul, MN, USA
76: Also at Karamanoğlu Mehmetbey University, Karaman, Turkey
77: Also at California Institute of Technology, Pasadena, CA, USA
78: Also at Ain Shams University, Cairo, Egypt
79: Also at Bingol University, Bingol, Turkey
80: Also at Georgian Technical University, Tbilisi, Georgia
81: Also at Sinop University, Sinop, Turkey
82: Also at Erciyes University, Kayseri, Turkey
83: Also at Texas A&M University at Qatar, Doha, Qatar
84: Also at Kyungpook National University, Daegu, Korea
85: Also at another institute or international laboratory covered by a cooperation agreement with CERN, Geneva, Switzerland
86: Also at Yerevan Physics Institute, Yerevan, Armenia
87: Also at University of Florida, Gainesville, FL, USA
88: Also at Imperial College, London, UK
89: Also at Institute of Nuclear Physics of the Uzbekistan Academy of Sciences, Tashkent, Uzbekistan